ANKARA YILDIRIM BEYAZIT UNIVERSITY

GRADUATE SCHOOL OF NATURAL AND APPLIED SCIENCES

IMPROVING STRENGTH OF RAIL STEEL AND INVESTIGATION OF MAIN MECHANICAL AND MICROSTRUCTURAL PROPERTIES

M.Sc. Thesis by

Abdulkadir KILIÇ

Department of Mechanical Engineering

August 2021

ANKARA

IMPROVING STRENGTH OF RAIL STEEL AND INVESTIGATION OF MAIN MECHANICAL AND MICROSTRUCTURAL PROPERTIES

A Thesis Submitted to

The Graduate School of Natural and Applied Sciences of

Ankara Yıldırım Beyazıt University

In Partial Fulfillment of the Requirements for the Degree of Master of Science in Mechanical Engineering, Department of Mechanical Engineering

by

Abdulkadir KILIÇ

August 2021

ANKARA

M.Sc. THESIS EXAMINATION RESULT FORM

We have read the thesis entitled **"IMPROVING STRENGTH OF RAIL STEEL AND INVESTIGATION OF MAIN MECHANICAL AND MICROSTRUCTURAL PROPERTIES"** completed by **ABDULKADİR KILIÇ** under the supervision of **ASSIST. PROF. DR. YASİN SARIKAVAK** and we certify that in our opinion it is fully adequate, in scope and in quality, as a thesis for the degree of Master of Science.

Assist. Prof. Dr. Yasin SARIKAVAK

Supervisor

Assist. Prof. Dr. Fatih GÖNCÜ

Jury Member

Prof. Dr. Ali Osman KURBAN

Jury Member

Prof. Dr. Sadettin ORHAN

Director

Graduate School of Natural and Applied Sciences

ETHICAL DECLARATION

I hereby declare that, in this thesis which has been prepared in accordance with the Thesis Writing Manual of Graduate School of Natural and Applied Sciences,

- All data, information and documents are obtained in the framework of academic and ethical rules,
- All information, documents and assessments are presented in accordance with scientific ethics and morals,
- All the materials that have been utilized are fully cited and referenced,
- No change has been made on the utilized materials,
- All the works presented are original,

and in any contrary case of above statements, I accept to renounce all my legal rights.

Date: **Signature:** …….

Name&Surname: …….

ACKNOWLEDGMENTS

I would like to express my sincere gratitude to my supervisor, Assist. Prof. Dr. Yasin SARIKAVAK for his guidance and practical suggestions.

I would like to thank Ankara Yıldırım Beyazıt University Scientific Research Projects Coordination Unit for providing financial support to the Project No: 2155. I would like to acknowledge the AYBU Metallurgical and Materials Engineering Department, which made use of its laboratory facilities, and the managers of TCDD, Railway Research, and Technology Center (DATEM), and especially researchers Önder AKGÜNLÜ and Ercan TEKİN for their support. I would also like to thank Uğur BARUT for his assistance in the microstructural investigation.

I would like to extend my deepest gratitude to Dr. Sercan BASİT for his invaluable contribution and fruitful discussions. İsmail BAYRAM needs a special mention on helping me with academic suggestion. I would like to thank my office colleague Burak Talha for his help in the organization of the thesis. I would also like to thank all the lathes, especially Hakan Tiryaki, who helped me with the challenging machining operations.

Finally, I must express my deep gratitude to my family, who have always supported me throughout my life and during the writing of this thesis. Finally, I must express my deep gratitude to my father Aslan KILIÇ, my mother Seniha Kılıç, my sister Büşra Fatma and my brother Bilal Said, who have always supported me throughout my life and during the writing of this thesis.

August 2021 **Abdulkadir KILIÇ**

IMPROVING STRENGTH OF RAIL STEEL AND INVESTIGATION OF MAIN MECHANICAL AND MICROSTRUCTURAL PROPERTIES

ABSTRACT

Rail transportation systems in Turkey are constantly developing as a result of the increase of demand in high-speed trains and heavy-loading transportation. As there are high contact pressures between the rail and the wheel, the components wear out rapidly according to the higher loads. To prevent these, it is desired to develop critical parts of rail systems with high wear resistance and strength values to extend their service life. For this purpose, methods such as increasing the carbon content in the rail composition, reducing the space between the lamellae in the pearlitic microstructure, and hardening the head of the rails have been studied. However, conducted studies have reached saturation and alternative microstructures such as bainitic microstructures have begun to be investigated all over the world.

In this study, it is aimed to obtain a bainitic microstructure by performing isothermal transformation in high carbon rail steel, which is frequently used in high-speed railway lines, instead of developing a new alloy. The combined high tensile strength and toughness by changing the microstructure is an important parameter to extend the service life of the components. To obtain different bainitic microstructures, various heat treatment processes conducted to the extracted specimens. In order to minimize the number of experiments, Taguchi experimental design method was used. After heat treatment processes, metallographic examination, hardness, impact, and tensile tests were carried out to clarify mechanical characteristics of the materials. In Taguchi method to determine the S/N ratios, obtained yield, and ultimate tensile stresses, hardness values, impact test results are used as an input parameter. In conclusion developed rail steels show improved mechanical properties than the conventional ones and the optimum parameters for heat treatment processes are clarified with the conducted.

Keywords: Rail Steel, Heat Treatment, Bainitic Microstructure, Mechanical Properties.

RAY ÇELİĞİ MUKAVEMETİNİ GELİŞTİRMEK VE ANA MEKANİK VE MİKROYAPI ÖZELLİKLERİNİN İNCELEMESİ

ÖZ

Türkiye'de raylı ulaşım sistemleri, yüksek hızlı tren hatlarının yaygınlaşması ve yüksek tonajda taşımacılığa olan talebin artması sonucu her geçen gün gelişmektedir. Ray ve teker arasında yüksek temas basınçları olduğunda sistem bileşenleri çabuk aşınmaktadır. Bunların önüne geçebilmek için raylı sistemlerin kritik parçalarının geliştirilerek hizmet ömürlerini uzatacak aşınma direnci ve mukavemet değerlerine sahip malzemeler geliştirilmek istenmektedir. Bu amaçla ray bileşimindeki karbon içeriğinin arttırılması, perlitik mikroyapıdaki lameller arasındaki boşluğun azaltılması ve rayların mantarının sertleştirilmesi gibi yöntemler çalışılmıştır. Ancak yapılan çalışmalar doygunluğa ulaşmış ve beynitik mikroyapılar gibi alternatifler dünya genelinde araştırılmaya başlanmıştır.

Yapılan çalışmada yeni bir alaşım oluşturmak yerine yüksek hızlı demiryolu hatlarında sıklıkla kullanılan yüksek karbonlu ray çeliğinde izotermal dönüşüm gerçekleştirilerek beynitik mikroyapı elde etmek amaçlanmıştır. Mikroyapı değiştirilerek çekme mukavemeti ve tokluğun yüksek olması bileşenlerin servis ömrünün artırılmasında önemli bir parametredir. Çıkarılan numunelere farklı beynitik mikroyapılar elde edebilmek için farklı ısıl işlemler uygulanmıştır. Yapılacak deney sayısını minimize etmek adına, Taguchi deney tasarım metodu kullanılmıştır. Isıl işlemlerden sonra, malzemenin mekanik özelliklerini açığa çıkarmak için metalografik inceleme, sertlik, darbe ve çekme deneyleri yapılmıştır. Taguchi metodunda Sinyal / Gürültü (S/N) oranlarını tespit edebilmek için, çekme testi sonucu elde edilen akma mukavemeti, uzama, sertlik değerleri, darbe testi sonuçları girdi olarak belirlenmiştir. Sonuç olarak geliştirilen ray çelikleri, geleneksel çeliklere göre daha iyi mekanik özellikler göstermekte ve yapılan ısıl işlem prosesleri ile optimum parametreler netleştirilmiştir.

Anahtar Kelimeler: Ray Çeliği**,** Isıl İşlem, Beynitik Mikroyapı, Mekanik Özellikler.

CONTENTS

M.Sc. THESIS EXAMINATION RESULT FORM ii
ETHICAL DECLARATION iii
ACKNOWLEDGMENTS iv
ABSTRACT v
ÖZ vi
NOMENCLATURE x
LIST OF TABLES xii
LIST OF FIGURES xiii
CHAPTER 1 - INTRODUCTION 1
CHAPTER 2 - LITERATURE SURVEY 4
2.1 Rail Steels 4
2.1.1 Rail Material Development Milestones 4
2.1.2 Chemical Composition 6
2.1.3 Classification of Steels 7
2.1.4 Bainitic Steels 7
2.1.5 Lower and Upper Bainite Microstructure 9
2.1.6 High Carbon Bainitic Steels 10
2.1.7 Bainitic Rail Steels 10
2.1.8 Bainite Transformation Studies 12
2.1.9 Effect of Retained Austenite (RA) on strength characteristics 14
2.1.10 Wear Resistance 14
2.1.11 Ausforming 16
2.1.12 Weldability 17
2.2 Taguchi Analysis 17
2.2.1 Robust Design 18
2.2.2 The Importance of Taguchi Method 19
2.2.3 Signal to Noise Ratios 20
2.2.4 Taguchi Lost Function 22
2.2.5 Analysis of Variance (ANOVA) 24
2.2.6 Gray Relational Optimization 26
CHAPTER 3 - MATERIALS and METHODS 28
3.1 Material Properties 28

3.2 Machining Operations 29
3.3 Heat Treatment 32
3.4 Taguchi Experimental Design 36
3.5 Hardness Test 37
3.6 Microstructural Characterization 38
3.7 Mechanical Tests 40
3.7.1 V-Notch Impact Test 40
3.7.2 Tensile Test 41
CHAPTER 4 - RESULTS and DISCUSSIONS 42
4.1 Mechanical Test Results 42
4.1.1 Spectral Analysis 42
4.1.2 Tensile Test 43
4.1.3 Impact Test 47
4.1.4 Hardness Test 48
4.1.5 Metallographic Examination 49
4.2 Results of Taguchi Analysis 55
4.2.1 S/N Ratios 55
4.2.1.1 Tensile Strength 55
4.2.1.2 Elongation 57
4.2.1.3 Impact Energy 58
4.2.1.4 Hardness 59
4.2.2 ANOVA 60
4.2.2.1 ANOVA for Tensile Strength 60
4.2.2.2 ANOVA for Elongation 60
4.2.2.3 ANOVA for Impact Strength 61
4.2.2.4 ANOVA for Hardness 61
4.2.3 Prediction 62
4.3 Gray Relational Analysis 65
4.3.1 Gray relational generation 65
4.3.2 Deviation Sequences 65
4.3.3 Gray Relational Coefficient 66
4.3.4 Gray relational grades 67
CHAPTER 5 - CONCLUSION 69

REFERENCES **72**
APPENDICES **77**
Appendix A: Optical micrographs 78
Appendix B-Tensile test results 88
CURRICULUM VITAE **97**

NOMENCLATURE

Subscripts

ºC	Celsius Degree
95 % CI	95% Confidence Interval
95 % PI	95% Predict Interval
A	Cross-sectional area, m2
$\mathbf{A_{cm}}$	Upper critical temperature for hypereutectoid steels
$\mathbf{A_{25}}$	Percentage Elongation (for 25mm gauge length)
$\boldsymbol{B_s}$	Bainite Start Temperature
GPa	Gigapascal
HB	Brinell Hardness
HV	Vickers Hardness
HRC	Rockwell Hardness
Pa	Pascal
$\mathbf{L_0}$	First length
$\mathbf{m_E}$	Modulus of Elasticity (Young's Modulus)
mm	Millimeter
MPa	Megapascal
$\boldsymbol{M_s}$	Martensite Start Temperature
$\mathbf{R_{p0.2}}$	Yield strength
$\mathbf{R_m}$	Tensile strength
µm	Micrometer

Acronyms

ANOVA	Analysis of Variance
ASTM	American Society for Testing and Materials
DF	Degree of freedom
HAZ	Heat Affected Zone
HSR	High Speed Rail
LPI	Logistics Performance Index
PTS	Predict Tensile Strength
RA	Retained Austenite
SS	Sum of Square
SEM	Scanning Electron Microscope
TRIP	Transformation induced plasticity
TTT	Time-Temperature-Transformation
UIC	International Union of Railways (UIC, French: Union international des chemins de fer)
WEDM	Wire Electrical Discharge Machining

LIST OF TABLES

Table 2.1 S/N ratio equations 20
Table 2.2 ANOVA Equations 25
Table 3.1 R260 rail steel mechanical properties 28
Table 3.2 Heat treatment parameters 32
Table 3.3 L_9 orthogonal array for heat treatment 36
Table 4.1 Spectral analysis result and standard rail composition 42
Table 4.2 Tensile test results 43
Table 4.3 Impact test results 47
Table 4.4 Result of the hardnesses. 48
Table 4.5 Total S/N Ratios for parameters 55
Table 4.6 Response Table for Signal to Noise Ratios 56
Table 4.7 Signal to Noise Ratios of elongation 57
Table 4.8 Signal to Noise Ratios of impact energy 58
Table 4.9 Signal to Noise Ratios of hardness 59
Table 4.10 ANOVA for Tensile Strength 60
Table 4.11 ANOVA for Elongation 60
Table 4.12 ANOVA for Impact Strength 61
Table 4.13 ANOVA for Hardness 61
Table 4.14 Predict values. 62
Table 4.15 Gray relational generation values 65
Table 4.16 Deviation Sequences 66
Table 4.17 Gray Relational Coefficient 66
Table 4.18 Gray relational grades with equal contribution. 67
Table 4.19 Gray relational grades with 10% elongation and 30% tensile strength, hardness and impact energy contribution. 68
Table 5.1 Optimum parameters for bainitic transformation 70

LIST OF FIGURES

Figure 2.1 Interaction effects. (a) Strong interaction. (b) No interaction..... 21

Figure 2.2 Quality loss function. (a) Traditional, (b) Taguchi. 23

Figure 2.3 Quality distribution in televisions produced by the same company (Sony) in different countries [53]..... 24

Figure 3.1 Rail head samples. 28

Figure 3.2 (a) Cutting surfaces. (b) Test specimen extracted regions. 29

Figure 3.3 Areas where it is recommended to extract tensile and impact test specimens according to EN 13674-1. 30

Figure 3.4 M10 cylindrical tensile test specimen dimensions-EN ISO 6892-1:200930

Figure 3.5 Charpy impact test specimen dimensions. 31

Figure 3.6 V notching device. 31

Figure 3.7 9 Prepared tensile and impact test specimens. 32

Figure 3.8 Applied heat treatment regime. 33

Figure 3.9 Schematic representation of bainitic transformation in time-temperature-transformation diagram for eutectoid steel: A, austenite; B, bainite; M, martensite; P, pearlite [65]. 34

Figure 3.10 Furnaces and salt baths used for heat treatment. 35

Figure 3.11 Hardness test regions 37

Figure 3.12 (a) Shimadzu HMV-G Vickers hardness tester, (b) Software that calculates the hardness from the trace diagonals left by the diamond tip. 38

Figure 3.13 Microstructure sample 38

Figure 3.14 (a) Grinding Machine, (b) Polishing Device. 39

Figure 3.15 (a) Nital etched sample, (b) Optical microscope. 39

Figure 3.16 Regions where tensile and impact test specimens were extracted. 40

Figure 3.17 (a) Impact test machine, (b) Tensile test machine 41

Figure 4.1 Stress-strain plot for austenitized specimens at 840 °C [(1)-A1B1C1, (6-A2B3C1), (8- A3B2C1] 44

Figure 4.2 Stress-strain plot for austenitized specimens at 860 °C [(3)- A1B3C3, (5)-A2B2C3), (7)- A3B1C3]..... 45

Figure 4.3 Stress-strain plot for austenitized specimens at 850 °C [(2)- A1B2C2, (4)-A2B1C2), (9)- A3B3C2]..... 46

Figure 4.4 The comparison chart of hardness versus impact energy values 48

Figure 4.5 Conventional R260 rail steel microstructure; (a) 500x, (b) 1000x. 50

Figure 4.6 Optical microscope images of (1)-A1B1C1 sample; (a) 500x, (b) 1000x. 50

Figure 4.7 Optical microscope images of (2)-A1B2C2 sample (a) 500x, (b) 1000.. 51

Figure 4.8 Optical microscope images of (3)-A1B3C3 sample; (a) 200x, (c) 500x. 51

Figure 4.9 Optical microscope images of (4)-A2B1C2 sample; (a) 200x, (b) 500x. 52

Figure 4.10 Optical microscope images of (5)-A2B2C3 sample; (a) 100x, (b) 200x. 52

Figure 4.11 Optical microscope images of (6)-A2B3C1 sample; (a) 500x, (b) 1000x. 53

Figure 4.12 Optical microscope images of (7)-A3B1C3 sample; (a) 100x, (b) 1000x 53

Figure 4.13 Optical microscope images of (8)-A3B2C1 sample; (a) 200x, (b) 500x. 54

Figure 4.14 Optical microscope images of (9)-A3B3C2 sample; (a) 200x, (c) 500x. 54

Figure 4.15 Main effects plot for S/N ratios of tensile strength..... 56

Figure 4.16 Main effects plot for S/N ratios of tensile elongation..... 57

Figure 4.17 Main effects plot for S/N ratios of Impact Energy. 58

Figure 4.18 Main effects plot for S/N ratios of hardness..... 59

Figure 4.19 Fitted line plot for tensile strength..... 63

Figure 4.20 Fitted line plot for elongation. 63

Figure 4.21 Fitted line plot for impact energy. 64

Figure 4.22 Fitted line plot for hardness. 64

Figure A.1 Conventional R260 rail steel microstructure; (a) 100x, (b) 500x, c) 1000x……..……..……...77

Figure A.2 Optical microscope images of (1)-A1B1C1 sample; (a) 200x, (b) 500x, c) 1000x-1, (d) 1000x-2…….…….78

Figure A.3 Optical microscope images of (2)-A1B2C2 sample; (a) 100x, (b) 200x, (c) 500x, (d) 1000. ……..……...79

Figure A.4 Optical microscope images of (3)-A1B3C3 sample; (a) 100x, (b) 200x, (c) 500x, (d) 1000. ……...…….…..…80

Figure A.5 Optical microscope images of (4)-A2B1C2 sample; (a) 100x, (b) 200x, (c) 500x, (d) 1000x. ……...……...…81

Figure A.6 Optical microscope images of (5)-A2B2C3 sample; (a) 100x, (b) 200x, (c) 500x, (d) 1000x. ……...……...….82

Figure A.7 Optical microscope images of (6)-A2B3C1 sample; (a) 100x, (b) 200x, (c) 500x, (d) 1000x. ……...……...….83

Figure A.8 Optical microscope images of (7)-A3B1C3 sample; (a) 100x, (b) 200x, (c) 500x, (d) 1000x. ……..……...……...……84

Figure A.9 Optical microscope images of (8)-A3B2C1 sample; (a) 100x, (b) 200x, (c) 500x, (d) 1000x. ……...……...….85

Figure A.10 Optical microscope images of (9)-A3B3C2 sample; (a) 100x, (b) 200x, (c) 500x, (d) 1000x. ……...……....86

Figure B.1 Tensile test result of A1B1C1. ……...……..…..……87

Figure B.2 Tensile test result of A1B2C2. ……...…….....88

Figure B.3 Tensile test result of A1B3C3. ……...……...….89

Figure B.4 Tensile test result of A2B1C2. ……...…….……...90

Figure B.5 Tensile test result of A2B2C3. ……91

Figure B.6 Tensile test result of A2B3C1. ……....92

Figure B.7 Tensile test result of A3B1C3. ……...…….93

Figure B.8 Tensile test result of A3B2C1. ……..…...……....94

Figure B.9 Tensile test result of A3B3C2. ……..…..…..…95

CHAPTER 1

INTRODUCTION

Logistics activities gained importance with increase in global trade and demand for mobility. Thus, alternative transportation modes and multimode transportation frequently preferred for feasible and reliable transportation capability both for passenger and freight. Passenger transportation with high-speed trains increase day by day, where it is relatively safe and more economic than highway transportation. In this context, reducing the density on highways and balanced demands for transportation is one of the main goals of managements and governments. Logistics centers are established by making rail-port connections all over the world to reach these goals. Railway transportation is more sustainable in terms of the environment with its low carbon emissions, as well as less energy costs. In the world, many countries increase their investments to railways, where rail transportation will be an important component in terms of freight and passenger.

In Turkey highway transportation stands out as 89% while 3.9% of the freights is transported by railway and only 1% of the passengers are transported by rail systems [1]. However, in Europe, 28% of freight transport and 6.7% of passenger transport are carried out by rail system [2]. According to the LPI (Logistics Performance Index) ranking, while Turkey was 27th in 2012, it dropped to 47th in 2018 in terms of logistics success [2]. In the 2023 vision of Turkey, it is aimed to increase the railway percentage from 3.9% to 15% [3]. After this decline in success, more attention was drawn to this issue in future plans. In the planned projects, reducing transportation costs in freight corridors and building logistics centers integrated with railways are the target activities. In addition to heavy haul freight transportation, the railways highly preferred for passenger transportation as well. Turkey intends to build 6000 km high speed railway (HSR) by 2023 [4].

In this context, when the railway works in the world are examined, it is seen that developed countries invest at least as much as Turkey. China, Spain, Japan, Germany

shown as the leader countries in railways investments. Recently countries such as Turkey, Iran, and India have also begun to focus on this issue. Germany is the leading country in the mass production of railways, Japan also has advanced rail material development studies [5].

Rail transportation systems, which are among the most reliable mode of transportation, improves the quality of life. Railway administrations desires to increase the speeds, however comfort and safety issues become important factors to be considered. In Turkey, the importance of railway transportation will continue to increase in future to reduce the density on the highways and to provide cost-effective, high-speed, and sustainable transportation. In this scope, enhancing the service life of rail system components is among the main goals of manufacturers and managements. Due to friction and contact high wear values on the wheel/rail interfaces emerged the development of alternative rail and wheel materials. Furthermore, cyclic loadings cause fatigue fractures and discontinuities in the system components.

Principally, the infrastructure service life in rail transportation is calculated as 40 years [6]. On the other hand, rails change every 20 to 25 years on the straight road, and every 2-3 years in places where wear is loud such as narrow curved railways, switches, and frogs [6]. Approximately 30% of the railway in Turkey are constructed with narrow bends [7]. Therefore, the maintenance costs constitute a serious burden. In the National Science and Technology Policy Strategy report prepared by TUBITAK (The Scientific and Technological Research Council of Turkey), attention is drawn to this issue and the necessity of increasing technological competence is mentioned [3].

In the study, after austempering of raw rail steel, isothermal transformation was carried out in salt bath at different temperatures. The experiments to be carried out were followed by the Taguchi method and the ANOVA analysis method. In this context, considering the studies in the literature, Isothermal Transformation Temperature, Isothermal Transformation Time, Austenitization Temperature were determined as parameters.

Tensile, impact and metallographic examination and hardness samples were extracted from the obtained steels from the regions specified in the EN 13674-1 standard [8]. Tensile and impact tests were applied to the extracted samples in accordance with international standards [9-10]. Mechanical properties such as impact energy, tensile strength, fracture toughness have been studied in detail. The data obtained are presented in 3 different sections of the results section. In the first part, the results of the mechanical tests are included. The second part covers Taguchi, ANOVA, and regression analysis. Finally, Gray Relational Analysis is included in the optimization section where all the results are evaluated together.

CHAPTER 2

LITERATURE SURVEY

2.1 Rail Steels

2.1.1 Rail Material Development Milestones

The quality of rail steel material has greatly increased with recent developments. Resistance to wear, plastic deformation, and crack propagation has increased significantly. However, as the forces on the rail in heavy hauls increase, the formation of unexpected cracks on the tracks stands out as the most critical problem. Dynamic forces in high-speed train lines also pose hazards in terms of fatigue and crack propagation.

In the early periods, very high hardness of cast iron rails was used. However, brittle fractures were observed in these rails due to low toughness and discontinuities in the inner surface. The rails produced by the iron-casting method were replaced by the steel rails produced by Henry Bessemer for the first time in 1856. After determining the correlation between wear resistance and hardness, the carbon content in the rail composition was increased to increase the hardness. With the studies on the composition of the steel and alloying elements, the hardness has been increased and the service life has been extended.

Although the hardness of martensite obtained by rapid cooling is very high, since brittle fractures are observed, pearlitic steels obtained by slow cooling rates and high in ductility are generally preferred in rail production. The most important factor in this preference is to wear resistance, hence high hardness. However, as hard as the rails are required, toughness and ductility are also needed to prevent brittle fractures and increase impact resistance. In order to increase the hardness without losing too much ductility, the lamellar structure of pearlite was used and the interlamellar distance was reduced. After these developments, head-hardened rails were produced.

In this method, high hardness is obtained by rapidly cooling the head part of the rail, while the bulk material remains ductile [7].

For many years, pearlitic rails have been the most preferred rail type in the rail steel production and development industry. The carbon content has increased day by day in order to obtain pearlitic and hyper-eutectoid structures. First, ferrite-pearlite mixed rails with 0.5% carbon content, known as grade 700, were obtained. To increase the hardness and wear resistance, it was necessary to obtain a 100% pearlitic structure. 100% pearlite is provided in Grade-900 class steels with carbon content up to 0.75% [6]. Grade 900 was a suitable structure for general applications with its tensile strength of 900 MPa. However, greater strength is required in heavy-haul freight, narrow bends, and rough terrain [11].

Previous developments were achieved only by changing the composition of the material. However, it has been revealed that the strength value of Grade-900 can be increased under specified conditions with continuous cooling [11]. The microstructure of pearlitic steel consists of cementite and ferrite lamellae, and the mechanical properties get better as the thickness of these lamellas decreases. The microstructure can be changed by varying the rate of carbon diffusion with different cooling rates. A decrease in primary austenite grain size increases toughness [12].

The mechanical properties of pearlitic steel have been improved with studies on wear resistance. In these improvements, the lamellar structure of pearlitic steel was generally used. It has been found that the smaller the interlamellar space, the harder and more wear-resistant the material. However, there is a practical limit to this space, and this limit has been reached with wear-resistant rails [13]. With the studies carried out, it has been revealed that the development of the mechanical properties of the pearlitic rails, especially the strength, has reached the saturation point [13]. The interlamellar spacing of pearlite cannot be completely reduced, as the high carbon content required to produce purely pearlitic steel is associated with low weldability [13].

Except for special applications, martensite is an undesirable phase because brittle fractures with high hardness occur. While the whole mass is desired to have high toughness, the surface is required to be hard for wear resistance. With head-hardened rails, ductility is maintained in the mass, while high strength and rigidity can be achieved on the contacting head surface. However, beyond this hardening, microstructure studies continued. In this context, studies have focused on steels with martensitic and bainitic microstructures. Many studies have reviewed the potential of bainitic microstructure as a good alternative to the pearlite phase [13-14].

Bhadeshia et al have made a new development in high strength bainitic rail steels. They suppressed the formation of cementite and formed a carbide-free bainitic alloy with silicon. With this development, ferrite plates separated by austenite zones were obtained. This mixed structure is an important step towards the use of bainitic rails, with its superior mechanical properties [15].

2.1.2 Chemical Composition

In the 19th century, rails were produced with high Potassium (0.085) and Silicon (0.075) content and low carbon ratio (0.50-0.65). The new generation rail steel produced in 2013 contains carbon in the 0.74-0.86 band, while low Phosphorus (0.020) and Silicon (0.02) ratios are used. Phosphorus and Silicon content has been reduced as it has been found to provide low ductility. Silicon was considered necessary for molten steel deoxidation, and its rate increased in new types of rails. Silicon contributes to solid solution strengthening. Vanadium, on the other hand, contributes to the hardening of ferrite by precipitation in pearlite [16].

Molybdenum and boron element contribution exhibit triggering behavior on bainitic transformation. Wear resistance is associated with strength and B_s (bainite starting temperature). The addition of nickel, chromium, and manganese lowers the bainite start temperature and also increases the strength without any appreciable decrease in ductility values [17].

2.1.3 Classification of Steels

Classification of steel is made based on carbon content. Steels are divided into three subgroups according to the amount of carbon: Low Carbon Steels (carbon less than 0.25%), Medium Carbon Steels (between 0.25%-0.55% carbon), and High Carbon Steels (more than 0.55% carbon). Steels with a carbon content higher than 0.8%, which are also used as rail materials, are called hypereutectoid steel [18]. In addition, steels are classified according to the amount of alloy. If the alloying elements are higher than 5%, they are called high alloy steels, otherwise low alloy steels. Another classification is based on the phase transformation capability of the steel. These classifications of steel are associated with weldability. The chemical composition of the steel plays an important role in the phase transformations, the microstructure of the welded heat-affected zone (HAZ), and grain sizes.

2.1.4 Bainitic Steels

Bainite was first viewed under an optical microscope by Davenport and Bain. This microstructure was named "bainite" in honor of Edgar C. Bain after his death by his friends. The temperature range required for bainite formation is defined as below the pearlite nose and above the M_s (martensite start temperature) [18]. Showing a tougher feature at the same hardness value, bainite combined the hardness of martensite with the ductility of pearlite [28]. Bainitic steels show a toughness as a result of the fine microstructure between high carbon thin austenite layers and the ferrite layers. These transform into martensite by absorbing energy under strain [3]. During the formation of martensite, carbon atoms do not have time to diffuse due to rapid cooling and remain as interstitial atoms, which creates a supersaturated structure with carbon [19].

The toughness of bainitic steels is due to the high carbon thin austenite layers between the bainitic ferrite layers and their fine microstructure. These transform into martensite by absorbing energy under deformation. In addition, steels with high toughness are more resistant to fracture and wear particle production. The wear

properties of steels are not easy to predict and changes in microstructure have a significant impact on wear even at the same hardness level [13].

It has been determined that steels with bainitic microstructure perform better than pearlitic steels in terms of tensile strength, yield strength, elongation, fracture toughness, and impact energy absorption properties [20-21]. In addition, the retained austenite (RA) content is very stable in bainitic structures. No further transformation occurs with a cooling effect or minor deformations [13].

In general, bainitic steels have tensile strength values of 800-1200 MPa, while in some studies, nano-structured bainite and super bainite structures with a tensile strength of 2500 MPa have been presented using carbide-free bainite lath and RA. In order to follow commercial developments in bainitic steels, a project called Nanobain is being carried out in Europe [22].

In the study of M.Ö. Faruk and K. Volkan on nano-bainitic steels, it was revealed that bainitic microstructure can be obtained by austenitizing at 900°C for 30 minutes and then isothermal holding at 200°C. Increasing the austenitization temperature decreased the bainite formation temperature in high carbon and low alloy steels. The highest bainite volume ratio was obtained as a result of austenitization at 980°C [18].

Q. Liu et.al., examining the effect of temperature gradient on the microstructure of high carbon silicon-rich steel, revealed that the austenitization temperature should be at least 100 °C higher than A_{cm} for bainite structure to have a more uniform composition. In the experiments, the amount of bainite is almost the same in O_x and O_y gradients. There is no distribution according to orientation. However, it was observed that the bainite content increased as the thickness decreased in the O_z direction. In the study, samples of different thicknesses were subjected to heat treatment under the same conditions. As a result, a high cooling temperature gradient was obtained in the thickness direction at 2mm thickness. Thus, the bainite-martensite ratio increased up to 3 times [23].

Recent studies have shown that bainite has better rolling-sliding wear resistance than pearlitic microstructure. Especially low carbon bainite, particularly carbide-free

microstructures, show very good wear resistance [24]. In addition, bainite's high toughness is an advantage over pearlite [3]. Bhadeshia et.al. has a patent study for the production of carbide-free bainitic steel that is resistant to rolling contact fatigue. Steels obtained by natural or accelerated cooling during rolling require a thin layer of austenite blocks for good toughness. It has been shown that this can be achieved with a good steel composition and heat treatment [25]. According to the strengthening mechanism of bainite described by Bhadeshia, yield strength depends on the dissolution of interstitial atoms, carbon content, dislocation density, and bainitic ferrite thickness [25].

J. Tian et.al. applied 4 different isothermal heat treatments on low carbon bainitic steel, below or above the martensite start temperature (M_s). The specimens, which were heated at 5 °C per second in order to obtain a complete austenite structure, were austenitized at 1000 °C for 900s (15 minutes). Afterward, the specimens were held at 430,400,350,330 °C for 30 minutes for bainite precipitation to cool at 30 °C per second. As a result, although the finer microstructure was observed below the martensite start temperature, the optimum mechanical properties were observed at 400 °C [26].

Mechanical properties are improved with heat treatments and changes in microstructure and studies are still ongoing [27]. Studies on bainitic steels have paved the way for its use in rail and wheel [28].

2.1.5 Lower and Upper Bainite Microstructure

Pearlitic steel gets its strength from its fine grain structure. But there is a limit to the production of very fine grain structures. In addition, dislocations also increase the strength of this structure. Obtaining bainitic microstructure is highly dependent on chemical composition and transformation parameters. Although the bainitic microstructure has many varieties, it is divided into two main categories: upper bainite and lower bainite. These structures are classified according to whether the carbides are in the ferrite or in the region between the ferrites [29]. The mechanical properties of the lower and upper bainite differ as well as their appearance. Lower

bainite has an appearance similar to tempered acicular martensite. On the other hand, the upper bainite has a feather-like structure. While the lower bainite has higher strength and hardness, the toughness and ductility properties of the upper bainite stand out [30]. M. Tu et. al., in 2007, investigated the mechanical properties and microstructure of lower bainite and JIS SK5 tempered martensite steel. At the same hardness, lower bainite had superior toughness and ductility values, while yield strength was lower than martensite. Fracture surfaces were also examined in the study, and a correlation was established between the bainite sheaf and the size of the fracture [31].

2.1.6 High Carbon Bainitic Steels

High carbon steels are among the steels with the highest hardness and strength. The carbon content is increased to impart wear resistance. However, the rail steel must also be resistant to brittle fractures. For this, studies are carried out to take advantage of the toughness of the bainitic microstructure. Many studies have been carried out on bainitic steels to date and continue to be done intensively. In the light of these studies on high and low carbon steels, more studies are needed on the transformation mechanisms of high carbon pearlitic steel to bainitic microstructure. Studies in the literature for bainitic steels focuses special alloy compositions and low carbon contents. However, high carbon bainitic steels are still not fully discovered yet [32]. There is very limited research on this subject [11,33-34]. For this reason, the development of bainitic steel from common and frequently used high carbon steels in current operating condition is an important topic for this microstructure to be applicable.

2.1.7 Bainitic Rail Steels

Studies for the use of bainitic microstructure in new generation rail steels date back to 1987 [32]. While bainitic and pearlitic steels show equal wear resistance at 200-230 HV hardness, bainitic steels have much better wear values at higher hardnesses.

In addition, bainitic steel outperforms pearlitic steel at all high contact pressures [35]. Bainitic steels provide a tensile strength of up to 1400 MPa without a decrease in fracture toughness, as well as ductility of 15-18 percent, showing that they are an important alternative for rail steels [36]. The first bainitic rail is a carbide-containing mixture of pearlite and bainite and is superior to normal pearlitic rails in wear, toughness, and rolling contact fatigue properties. Bhadeshia et al. made a new development in high-strength bainitic rail steels. They formed an alloy with silicon by suppressing cementite formation in carbide-free bainitic microstructure [11]. Bainitic rails have a soft transfer layer while maintaining high mass rigidity. The absence of brittle cementite parts contributes to rolling contact resistance. While the cementite particles provide hardness, they also give brittleness. The fact that pearlite colonies are bicrystal makes this situation dangerous. This situation is related to the size of the colony rather than the distance between the lamellae [15].

Tempered bainitic rail steels are being explored as alternatives for high speed or heavy-haul fright lines as they have 10% higher yield strength, 5 times higher impact toughness, better heat damage resistance [37]. In the study of K. Wang in 2016, the heat treatment behaviors of bainitic rail steels were examined in terms of microstructure transformations, and their mechanical properties were investigated by tensile, impact tests, and SEM. The steel with the highest strength and ductility was obtained by tempering at 280 °C [38].

In the study numbered [30], changes in the microstructure such as impact energy and wear resistance were investigated after different heat treatments. After 1 hour of austenitization at 860 °C, the sample was held in a salt bath at 400 °C for 25 minutes. The other specimen was held at 300 °C for 200 minutes. As a result, it has been determined that the heat treatment applied to bainite increases the wear resistance, especially in long friction paths. In structures with lower bainite, the amount of wear is less than 2 times compared to pearlite. While bainitic microstructure showed the best impact resistance, structures with lower bainite showed the best abrasion resistance.

F. Çakır and O. N. Çelik, in their study based on 4 different steels, determined that the parameter, which was austenitized at 860 °C, followed by 25 minutes at 400 °C and 3 hours at 300 °C, was determined as optimum. Impact tests were applied to the samples obtained. The impact toughness of the samples obtained from upper bainite was 2.5 times higher than the reference sample, and 1.5 times higher in lower bainite [30].

While crack propagation occurs in 220,000 cycles in traditional pearlitic premium rails, there is a crack-free structure even in 1 million cycles in new generation bainitic rails [39]. In the study [33], the mechanical properties of the rails of 2 different compositions produced by the Rolls-Rolls company were evaluated. All measured hardnesses are at least 370 and 390 HV. Test studies have been started in Poland, as it has a hardness value equal to or higher than conventional rails that are heat-treated, providing a cost advantage. Currently, British Steel has commercialized bainitic steels as a commercial product [40]. There are also completed bainitic rail routes in England, France, and Switzerland [41].

The data obtained show that bainitic steels exhibit a tougher mechanical property with the same hardness. Studies have shown that bainite is a potential rail material candidate. In this context, many rail steels were produced, and trial lines were established in Japan and Germany.

2.1.8 Bainite Transformation Studies

In the study of Garcia-Mateo and G. Caballero, the material was homogenized at 1200 °C for 2 days and left to cool slowly at room temperature to prevent martensite transformation. 30 minutes before austenitization at 900 °C, heat treatment was carried out at 200, 250, 300 °C and cooled to room temperature with water. As a result, it was determined that the transformation to martensite under strain should be neither too high nor too low to get the most out of the TRIP effect. The mechanical properties of the high carbon silicon-rich bainitic microstructure obtained at 200-300 °C were tested. The resulting microstructure is a combination of tensile properties that has not been achieved before in bainitic steels [42].

In a study on steels with high carbon and low alloy content, by D. Kong et.al. were revealed that the austenitization temperature was very effective on the bainitic transformation kinetics. As the austenitization temperature increases up to 980 °C, the time required for isothermal transformation decreases. After austenitization at 980 °C, bainite sheaves tend to transform. As a result, the high volume bainite was obtained at 980 °C. 810 HV hardness was achieved. In addition, the relationship between the hardness values obtained by isothermal transformation at 250 °C for 20 minutes and the austenitization temperature is explained. The increase in hardness was considered to be associated with carbon precipitation at the dislocations [34]. In another study by D. Kong et.al. on high carbon steels, bainite was performed at 200 °C. As a result, it has been determined that the bainite phase has a low transition ability to the lattice structure of austenite. In addition, there are inconsistencies in the sliding mechanism with the mechanism explaining the martensite phase [43].

In the study of Min Zhu et.al., it was heated to 1250 °C in 210 minutes in continuous casting slots. Then it was applied for 200 minutes tempering at 300, 350, 400, 450, 500 °C degrees. It was then brought to room temperature by continuous cooling with air (approximately 0.8 °C/s). As a result, the manufacture of rail material with high strength and high toughness above 1500 MPa has been achieved [21].

In another study, the wear properties of metastable austenite and nanostructured bainite were compared. High carbon (1.21%) steel is first austenitized and then allowed to cool rapidly. In another heat treatment, it was austenitized and hold isothermal at 250 °C for 8 hours. As a result, it was found that one of the strongest reasons for the wear of steel is the RA volume ratio [44].

In the study of Z. Öztürk, austenitized high carbon R260 steel at 850 °C and low carbon 32CrB4 steel at 880 °C. Then, the samples were held slightly above the martensite starting temperature for isothermal transformation. While the bainitic structure is mostly formed at the grain boundaries, most of the microstructure has martensitic grains [19].

2.1.9 Effect of Retained Austenite (RA) on strength characteristics

Strength is generally provided by fine-scale ferrite plates (strong phase), while ductility is mostly controlled by RA (soft phase) [11,45]. In the study of M. Zhu et.al., it was determined by microstructural analyzes that RA plays an important role in toughness. In addition, it has been revealed that thin-film RA has a positive effect on the propagation of fracture due to rolling contact fatigue [21]. In K. Wang et. al.'s study on the effect of RA on mechanical properties, steels were tempered at 250, 280, 320, 350 °C for 4 hours. As a result, it has been revealed that film RA prevents the formation and propagation of micro-fractures in bainitic and martensitic structures due to the TRIP effect [27]. According to Dong et al. observed the positive effect of RA on RCF in some high alloy steels [35]. Austenite blocks have been found to be detrimental to toughness. The solution is to reduce size or increase stability to avoid martensitic microstructure [15]. The presence of austenite can be made more stable by avoiding carbide precipitation at room temperature [32]. Tempering is done to allow carbon diffusion from martensite to retained austenite and RA becomes more stable [38]. There are two types of RA. The first is film RA, the other one is block RA. Comparing these two, film RA is more stable. This is an advantage in terms of mechanical properties. Block RA has low carbon content and exhibits more ductile behavior under load with TRIP effect. Film RA has a high carbon content and has high stability. In the study, which was applied as 800, 850, 900, 950, 1000 cooling temperatures to determine the RA ratio in different carbon dissolutions, it was concluded that the RA ratio was directly proportional to the temperature, and after 850 °C, bainite formations were observed [44].

2.1.10 Wear Resistance

Bolton and Clayton divided wear into regimes as Type I, Type II, and Type III. While I is the least wear, III is the highest wear value and II is considered as critical wear [46]. Many studies have been done on wear resistance. Clayton et.al. compared bainitic and pearlitic rails with 9 different compositions under the same conditions and determined that the chromium content had a significant effect on wear. Previous studies have accepted that the bainitic rail wears faster than the pearlitic rail. In this

study, the possibility of a new generation rail in terms of wear resistance of the bainitic microstructure was investigated. A load of at least 60 kgf is required to obtain high wear regime. For this purpose, tests were carried out with a pin-on-disc wear tester with a constant sliding speed and a load range of 75-150 kgf [17].

In addition, these values are provided with 0.7 percent C content in pearlite versus only 0.2 percent C in bainite. Low C means toughness, ductility, and weldability [32].R. Devanathan and P. Clayton studied bainitic steel of 3 different chemical compositions. Different carbon-containing microstructures were obtained by continuous cooling from the austenite formation range. As a result, bainitic steel with 0.04 carbon content shows better wear performance at all contact pressures than high hardness pearlitic steel. Granular bainite, the lowest carbon, showed the best performance with 29 HRC hardness. Bainitic steels, which can compete with pearlitic rail with a hardness of 33 HRC, can be a successful candidate at high contact pressures [35].

Pearlite has good wear resistance due to the microstructure of fine lamellar carbides and ferrite. Under shear wear, microstructure improvements occur by positioning on the surface in the direction of shear as a result of deformation and breaking of the cementite layer. The soft ferrite is compressed during this process and the near-surface cementite volume ratio increases, resulting in a harder and wear-resistant surface [13].

In the study of N. Jin and P. Clayton, the effect of alloying 5 low carbon steels with nickel, chromium, and silicon on the wear performance is observed. Three different types of bainite were identified as granular, carbide-free, and lower bainite. In general, as the carbon ratio and ferrite lath volume ratio increase, the hardness also increases.

The highest wear resistance was obtained in J1 steel, and acicular martensite, bainitic ferrite, and in borders RA structures have appeared in the microstructure. Residual austenite structures in the border regions [47].

Shipway et al. (1997) performed wear tests on bainitic, martensitic, and normalized microstructures using the pin-on-disc method. The best wear resistance was seen in the carbide-free upper bainite microstructure with less martensite. In addition, this structure showed higher toughness than the structure with more martensite content. They concluded that good wear resistance is attributed to RA and high-fine bainitic microstructure, which prevents microfractures and deformation of wear particles [48].

In the study of C. Pitt, rolling-sliding wear tests were carried out in the laboratory environment and the reasons that increase the wear resistance of real rails were investigated. Bainitic rail and conventional rail (pearlitic) were compared under the same conditions. For this purpose, it was heat-treated at 250 and 350 °C. It was observed that the related heat treatment increased the tensile stress value [13].

2.1.11 Ausforming

1900 MPa tensile and 24 percent elongation were obtained by ausforming. With this method, nanostructured bainitic steel with high toughness was obtained. With high strength and excellent ductility, bainitic steels, which show acceptable wear resistance, have paved the way for their application in the defense, automobile, and rail industries. In the study, it was revealed that ausforming at 300 °C reduces the isothermal transformation time. In addition, it has a positive effect on mechanical properties with finer RA in the microstructure [25].

In another study on steel with 5 different compositions of medium carbon, 3 different ausforming routes were determined. The volume ratios from the obtained microstructure images were found by image processing methods. 60% bainite was obtained. Carbide-free steels are the most studied multi-phase steel in the last 10 years. In this study, it was shown that the wear resistance of steel does not depend only on hardness. At the same time, the microstructural properties are also visibly effective [45].

2.1.12 Weldability

High-carbon steels converted from extremely thin bainite plates embedded in a carbon-enriched matrix are used commercially in the manufacture of engineering parts. Low weldability reduces the usage areas of steels with high carbon content. However, the weldability of high carbon rail steels in current mass production is feasible. There are 2 types of welding methods applied without difficulty: Alumina thermite welding and flush butt welding. It is necessary to prevent the austenitized rail formed by high temperature from transforming into martensite with rapid cooling during welding. A method that enables the reproduction of bainitic ferrite and RA mixture is reported by K. Fang et.al. Micro cracks are easily formed due to martensite formed by high carbon and heat input in the traditional welding method. To avoid these cracks, the reheating process is designed. The weld is kept in the bainite form by holding it in the oven at 250 °C without falling below 300 °C [49].

2.2 Taguchi Analysis

Considering the parameters in the literature, an experimental design can be applied with the Taguchi method to perform the optimum heat treatment conditions for improved mechanical properties. While developing a product or process in experimental design, output parameters and factors affecting output are evaluated together. By determining the optimum manufacturing parameters of the product, the variability that may occur in production and service conditions is reduced, thus minimizing defect in production and sensitivity to environmental factors, results with time and cost saving.

There are controllable parameters and uncontrollable parameters in experimental design. Controllable parameters are called design variables, and uncontrollable ones are called the noise factors [50-51].

The effect of uncontrollable factors on output is usually not easily calculated. For this reason, it is aimed to determine the parameter that affects the output the most in the experimental design, and even to calculate how much each parameter affects the output.

2.2.1 Robust Design

In robust design, it is the basic principle to increase the quality by reducing the effect caused by the parameters without neglecting them. The method has two major tools.

Orthogonal arrays as a new mathematical tool that allows working with multiple design parameters simultaneously, and the Signal-to-Noise factor, an advanced measure of quality.

It was put forward by Ronald Fisher, who worked on agricultural practices in the 1920s, and later elaborated with the ANOVA (Analysis of Variance) method. Adding many innovations to the experimental design method developed by Fisher, Taguchi laid the foundations of Robust design as a result of his work as a development manager at Nippon Telephone company. In 1960, Japan proved the validity of its method by completing the telephone-telegraph system in a short period of 4 years. The concept of experimental design came to the fore again in the 1980s with the increasing competition in the manufacturing sector. The method, the foundations of which were laid before but remained in theory, was used in manufacturing applications as a result of the studies carried out to achieve Japanese quality.

Experimental design is done to determine the optimum result by reducing the effect of factors that cannot be controlled with the least experiment. By performing analysis of variance with the help of signal-to-noise ratios, the number of experiments to be done is reduced, thus providing time and cost benefits [52].

The effect of each parameter on the output can be observed individually by keeping the other parameters constant. However, the interaction of factors also referred to as simultaneous analysis, is ignored. Trying all combinations is also not feasible in terms of cost and time. In addition, statistical methods such as ANOVA should be used to evaluate the errors in the experiments.

The following steps are applied in the Taguchi method:

- Identifying factors and interactions,
- Determining factor levels,
- Choosing the appropriate orthogonal array,
- Placing the appropriate factors in the columns,
- Conducting the experiments,
- Analyzing the results,
- Performing validation experiments,

In data analysis, S/N ratios are used to control the variability of the response, while ANOVA (Analysis of Variance) is applied for statistical reliability.

2.2.2 The Importance of Taguchi Method

The Taguchi method is important in terms of calculating the percentage of effect of controlled parameters by showing minimum sensitivity to uncontrollable factors. The first example of the robust design was applied by Phadke in the "Window photolithography" application in the USA [53]. Here, Taguchi's strengths and positive impact on cost are understood. In a polysilicon deposition application with a surface defect of 10 to 5000, the surface defect was reduced between 0 and 10 by making 18 experiments. The scrap rate has been reduced. In the project named Router Bit Life-Improvement, it was applied for optimum values in terms of reliability and life improvement of the guide inserts by making minimal experiments. After seeing the success of these applications, many companies in the automotive sector, under the leadership of the American Supplier Institute and Ford Motor Company, made quality and cost improvements based on Robust Design.

In the study [54] which accepts cutting speed, depth of cut, and feed rate as control parameters, the effect of cutting force and surface roughness in the drilling of AISI 1050 material was investigated by Taguchi experimental design method and optimal cutting parameters were determined. With the Taguchi L9 orthogonal experimental

design, 18 experiments were performed instead of 54 experiments, and the test results were obtained in a short time and optimum values were reached.

In Y.H. Cheny et.al.'s study, the optimization of Photomask, which is widely used in LCD construction, for various designs using the Taguchi method is discussed. As a result, the effect of processing linewidth of these 5 parameters was examined. L16 orthogonal array was used in the experiments [55].

In the study of N. Tosun et al., it was aimed to optimize the kerf (cutting width) and material removal rate (MRR) outputs by optimizing the WEDM operation processing parameters with the Taguchi method. L18 orthogonal array is used with 3 levels of 4 parameters [50].

2.2.3 Signal to Noise Ratios

In solving the problems in the application, the signal/noise ratio is calculated differently depending on the type of target. There are 3 common S/N ratio calculations (see Eq 1.1a-c) as summarized in Table 1.1.

Table 2.1 S/N ratio equations

Goal	S/N formula	Desired y Value	Equation
Smaller is better	$S/N\ Ratio = -10\log\frac{1}{N}\sum_{i=1}^{N} {y_i}^2$	Zero	1.1a
Larger is better	$S/N\ Ratio = -10\log\frac{1}{N}\sum_{i=1}^{N}\frac{1}{{y_i}^2}$	Limitless	1.1b
Nominal is better	$S/N\ Ratio = 10\log\sum_{i=1}^{N}\frac{\bar{y}^2}{S^2}$	Target Value	1.1c

The y_i in the formulas is the response obtained from the i[th] experiment and N represents the number of tests. In all 3 cases, a high S/N ratio is desired. The level of freedom of a factor is one less than the level of that factor, see Eq. 1.2 [56].

$$\nu_A = k_A - 1 \tag{1.2}$$

The sum of the degrees of freedom of each factor separately gives the total degrees of freedom, Eq. 1.3

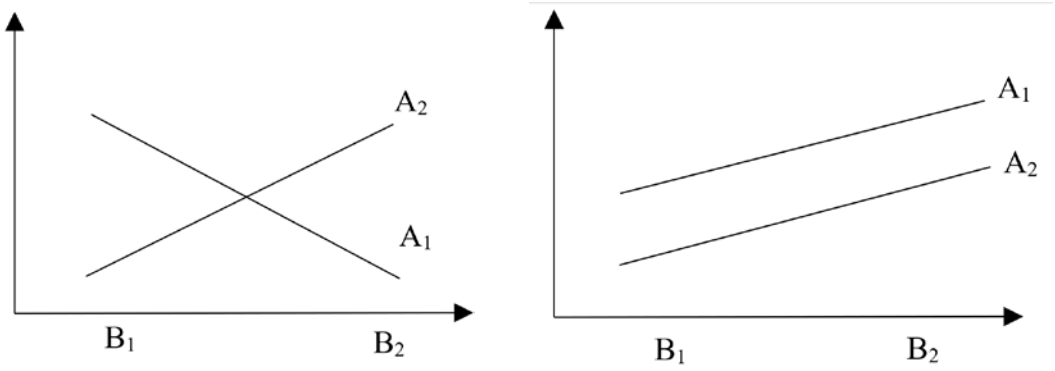
$$\nu_T = N - 1 = \nu_A + \nu_B + \nu_C + \nu_e \tag{1.3}$$

The total degrees of freedom of the factors are considered in the selection of the orthogonal sequence. As can be seen in Eq. 1.3, one more of the total degrees of freedom is desired to be equal to the number of trials [52].

In addition to the individual effects of the factors, the interactions between the factors are also determined. These interactions are called interaction effects. In such a case, the degrees of freedom for interaction; are the product of the degrees of freedom of the interacting factors, Eq. 2.4. The weak and strong interactions are shown in Figure 2.1. The mode of interaction is determined by whether the two-factor responses are parallel or not [56].

$$\nu_{AxB} = (\nu_A)(\nu_B) \tag{2.4}$$

Where (k_A =Number of levels of factor A, ν_A = Degree of freedom of factor A, ν_B = Degree of freedom of factor B, ν_C = Degree of freedom of factor C, ν_{AxB} = Degree of freedom of interaction A to B, ν_e = Degree of freedom of error.)



(a) **(b)**

Figure 2.1 Interaction effects. (a) Strong interaction. (b) No interaction

2.2.4 Taguchi Lost Function

Although quality is generally seen as checking whether the product is within the specified parameter ranges, how much it deviates from the target value is also an important factor. In the traditional loss function, the loss is either complete or zero. Traditional and Taguchi loss functions are shown in Figure 2.2. While the vertical axis represents the material loss, the horizontal axis shows the amount of deviation from the desired value. In cases where the product is within the control limits, how close or far it is from the target can be calculated with the Taguchi loss function. With this new understanding of quality, it can be calculated with the help of Eq 1.5, assuming that the amount of deviation affects the quality on a square scale [53].

$$L(y) = k(y - t)^2 \tag{1.5}$$

where t is the target value, y is the measured value, and k is a coefficient that converts the deviation amount to the accepted currency [57]. Engineering specifications should not be misunderstood. Not every product within the tolerance is considered correct. Loss of quality should be thought of as a quadratic function rather than a step function, see Figure 1.3a. Because in case of quality loss, it is necessary to calculate how much the products within tolerance reduce the quality.

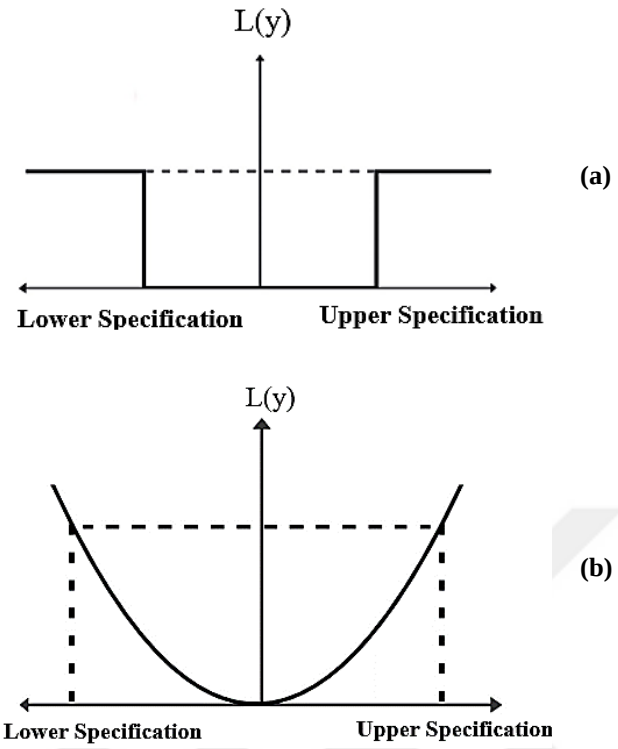


Figure 2.2 Quality loss function. (a) Traditional, (b) Taguchi.

In general, if the products within the tolerance are too far from the mean, the quality will decrease. With Taguchi, deviations from the target can be minimized to reduce variance even within acceptable values. The best example of this is Sony-Japan and Sony-USA production difference, Figure 2.3.

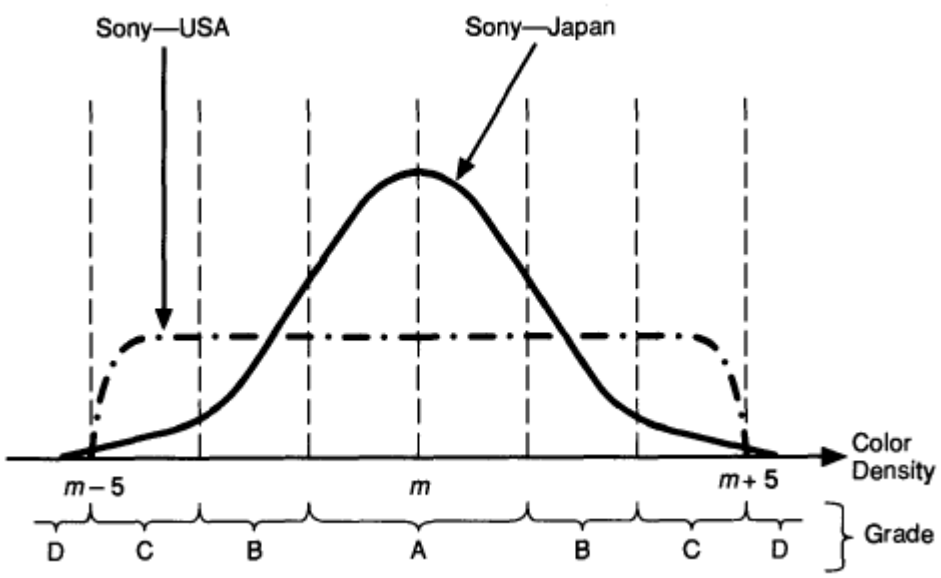


Figure 2.3 Quality distribution in televisions produced by the same company (Sony) in different countries [53].

2.2.5 Analysis of Variance (ANOVA)

Analysis of variance is performed to determine how much the results deviate from the target value and to test the statistical reliability of the experiments. This test is also called the F-test because of Ficher. With ANOVA, it is determined which parameter is effective as a percentage. The S/N ratios calculated for each experiment with the larger is the best characteristic (Table 1.1- 1.1b) are given in the section of Results and Discussions.

$$S^2 = \frac{1}{(r-1)} \sum_{i=1}^{r} (y_i - \bar{y})^2 \tag{1.6}$$

Here r is the number of experiments, y_i is the i^{th} test result, $\bar{y}$ is the mean of the experiments. The positive square root of the expression is calculated as the standard deviation (S) by Eq. 1.6. $\bar{y}$ is calculated with the following formula.

$$\bar{y} = \frac{1}{n}\sum_{i=1}^{n} y_i \tag{1.7}$$

The effect of each parameter on all levels is calculated. For this, the average of the S/N ratios of the levels is taken. For example, for Level 2 of the austenitization temperature parameter, the average of the S/N ratios of the 2,4 and 9th Experiments is taken. In addition, the average of the S/N ratio of all experiments is calculated. The necessary formulas for all these calculations are given in Table 2.2 [52,58-59].

Table 2.2 ANOVA Equations

Description	**Equation**
Sum of squares of factor A	$SS_A = \left[\sum_{i=1}^{k_A}\left(\frac{{A_i}^2}{n_{A_i}}\right)\right] - \frac{T^2}{N}$
Sum of squares of error	$SS_e = \sum_{j=1}^{k_A}\sum_{i=1}^{n_{A_i}}\left(y_{i-}A_j\right)^2$
Sum of squares of all data	$SS_T = \left[\sum_{i=1}^{N}(y_i)^2\right] - \frac{T^2}{N}$
	$SS_T = SS_A + SS_B + SS_C + SS_e$
Variance of A	$V_A = \frac{SS_A}{\nu_A}$
Variance of error	$V_e = \frac{SS_e}{\nu_e}$
F value of A	$F_A = \frac{V_A}{\nu_A}$
The expected value of the sum of squares of A	$SS_A{}' = SS_A - (V_A)(V_e)$
Contribution percentage of A	$P_A = \frac{SS_A{}'}{SS_T} x100$
T = Sum of all experiments N = Total number of experiments k_A =Number of levels of factor A n_{A_i} = A_i number of experiments at ith level ν_A = Degree of freedom of A	

2.2.6 Gray Relational Optimization

Different experiments with the same parameters are applied to test the mechanical properties of a material. Multi-objective optimization methods have been developed to evaluate these different experimental results together. This method has been used in many different areas in the literature, such as determining machining parameters on turning, removal rate and kerf in WEDM, and even osmosis parameters [50, 60-63]. In this study, the gray relational analysis method, which is a multi-objective optimization tool, will be used. The method is based on the logic of positioning all responses between 0 and 1. To do this, using Eq. 1.9 or Eq. 1.10, all responses are normalized to obtain gray relational generation values. Here, there are two different normalizations according to the contribution of the responses to the design. Eq. 1.10 represents the "lower is better" approach, while Eq. 1.9 represents the "larger is better". The series of experimental responses with length N is as follows, Eq. 1.8 [63].

$$x_i = (x_i(1), x_i(2), \dots, x_i(N)) \tag{1.8}$$

$$x^*{}_i(k) = \frac{x_i(k) - \min x_i(k)}{max\, x_i(k) - min\, x_i(k)} \tag{1.9}$$

$$x^*{}_i(k) = \frac{\max x_i(k) - x_i(k) +}{max\, x_i(k) - min\, x_i(k)} \tag{1.10}$$

Then deviation sequence values are calculated using Eq. 1.11 [62].

$$\Delta_{0i}(k) = |x_0(k) - x_i(k)| \tag{1.11}$$

By placing these values in Eq. 1.12, Gray Relational Coefficients are found. Here, the value of ζ has been determined as 0.5, considering the engineering approach and other studies [50,60,62]. The Δ_{min} and Δ_{max} values are 0 and 1, respectively.

$$\xi_i(k) = \frac{\Delta_{min} + \xi\Delta_{max}}{\Delta_{0i}(k) + \xi\Delta_{max}} \tag{1.12}$$

Lastly, the final value called Gray Relational grade is found by Eq. 1.13. This value ensures that all results of the relevant experimental parameter are evaluated on the same scale. While the parameter with the highest value is determined as optimum, grades close to this value indicate acceptable parameters [61].

$$\alpha_k = \frac{1}{n}\sum_{i=1}^{n} Y_i(k) \tag{1.13}$$

CHAPTER 3

MATERIALS and METHODS

High carbon rail steel with R260 quality have pearlitic microstructure. Extracted rail heads, can be seen in Figure 3.1. The heat treatment process applied to the extracted rail samples. Steel with bainitic microstructure was obtained by isothermal transformation in a salt bath at different temperatures. The performed operations are explained in the following sections.



Figure 3.1 Rail head samples.

3.1 Material Properties

The mechanical properties of the rail steel samples are given in Table 3.1.

Table 3.1 R260 rail steel mechanical properties

Material Properties Hardness (HV)	**Yield strength (MPa)**	**Tensile strength (MPa)**	**Ductility (%)**	**Fracture Toughness (MPa.m 1/2)**	**Hardness (HV)**
R260-EN 13674-1	-	≥ 880	≥10	26	260-300

Spectral analysis is the test performed by measuring the intensity or polarization of light to determine the type of material. Material test results with Spectromax device are presented in the results section.

3.2 Machining Operations

Test specimens were extracted with the help of turning and milling machines in the machining workshop from raw rail steel. Sectioned rails, cut surfaces and extracted specimens for mechanical tests and microstructural analysis can be seen in Figure 3.2.

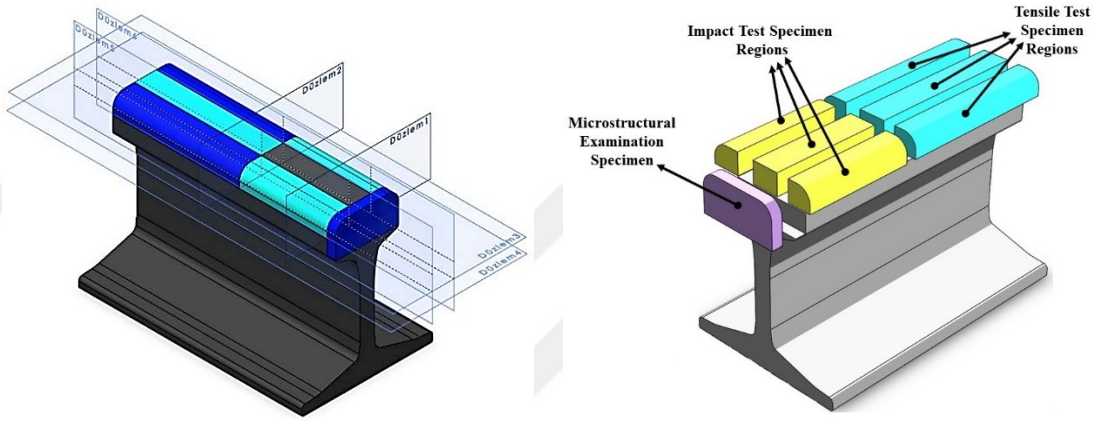


Figure 3.2 (a) Cutting surfaces. (b) Test specimen extracted regions.

Specimens for experimental analysis were extracted from the obtained parts with the help of turning and milling machines. The specimens were heat treated after they were extracted from the rail head for mechanical tests. Since the hardness of the sample is very high, they were processed with special diamond tools. It was machined and threaded in a single pass so that the tensile axis was kept concentric. After threading, tapping was performed. Tensile and impact test specimens from the regions specified in the EN 13674-1 standard (see Figure 3.3) were machined in accordance with the geometry in Figure 3.4 and Figure 3.5 [8].

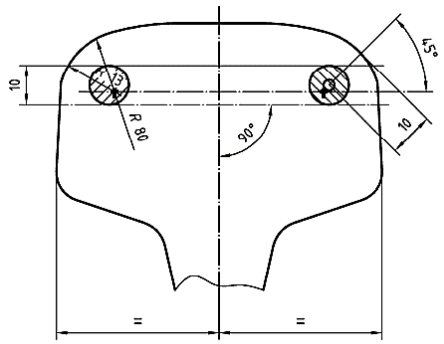


Figure 3.3 Areas where it is recommended to extract tensile and impact test specimens according to EN 13674-1.

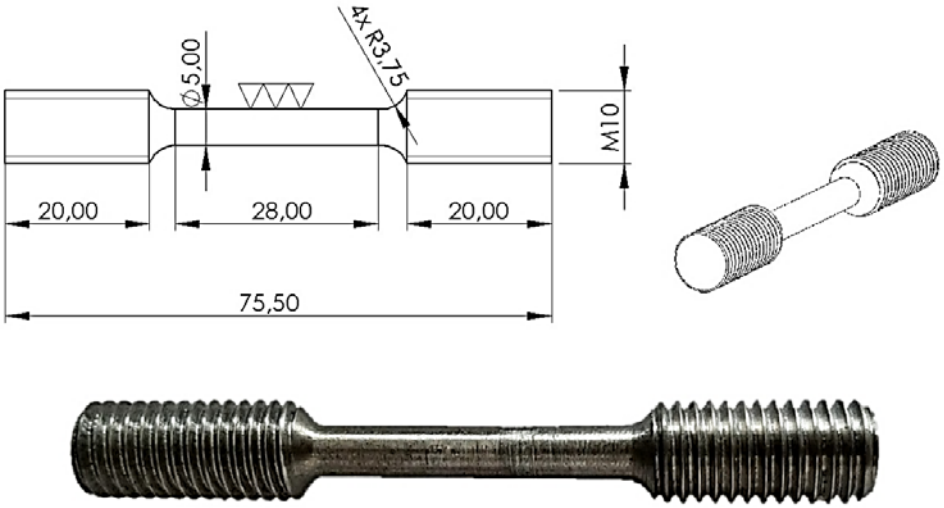


Figure 3.4 M10 cylindrical tensile test specimen dimensions-EN ISO 6892-1 :2009

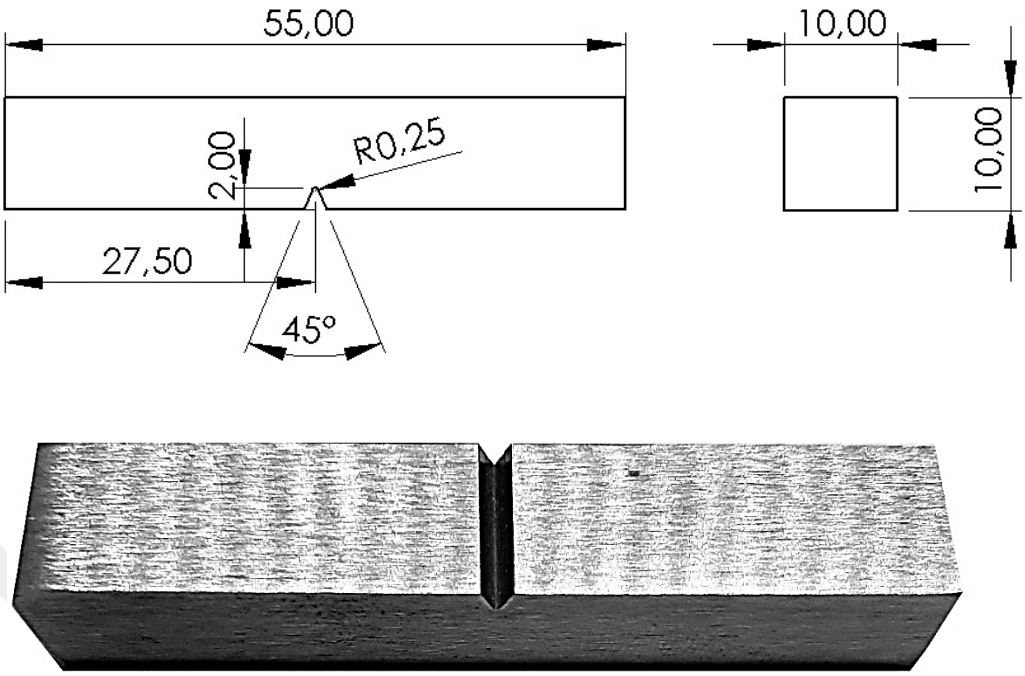


Figure 3.5 Charpy impact test specimen dimensions.

The notches of the impact test specimen were made following the standards in the V notching device, Figure 3.6. Obtained specimens are shown in Figure 3.7.



Figure 3.6 V notching device.

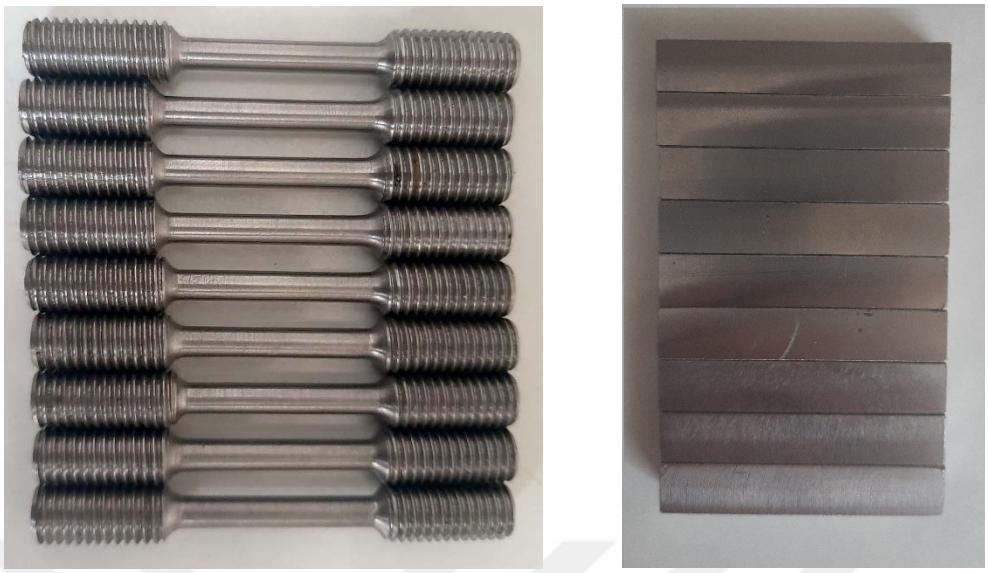


Figure 3.7 9 Prepared tensile and impact test specimens.

3.3 Heat Treatment

The obtained specimens were taken to the austenitizing temperature in a furnace with a capacity of 900 °C for austempering and hold for a while. Then, bainitic microstructure steel was obtained by isothermal transformation at different temperatures in a salt bath. AS-140 tempering salt was used in the salt bath. The applied heat treatment is shown in Figure 3.8. In this context, isothermal transformation temperature, isothermal transformation time, austenitizing temperature were determined as parameters, Table 3.2

Table 3.2 Heat treatment parameters

Parameters	Level 1	Level 2	Level 3
Isothermal Transformation Temperature (°C)	200	250	300
Isothermal Transformation Time (hour)	2	3	4
Austenitizing Temperature (°C)	840	850	860

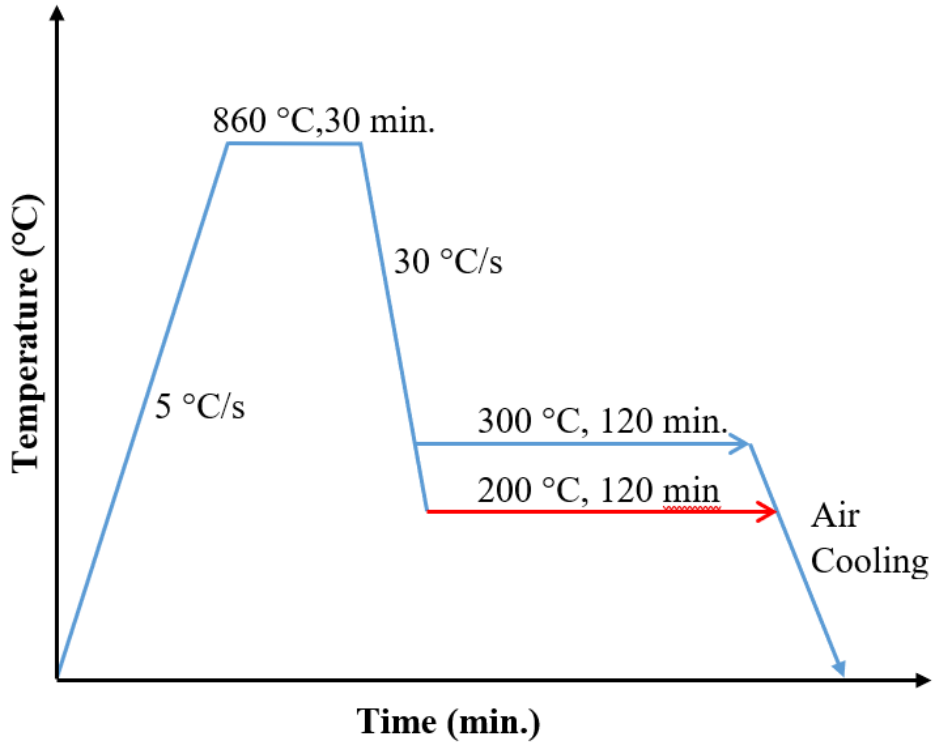


Figure 3.8 Applied heat treatment regime.

These parameters were chosen considering the studies in the literature. In the time-temperature-transformation diagrams drawn for high carbon steels, the time and temperature values required to obtain lower bainite and upper bainite are given [64]. The bainitic transformation in the time-temperature-transformation diagram for eutectoid steel is shown schematically in Figure 3.9.

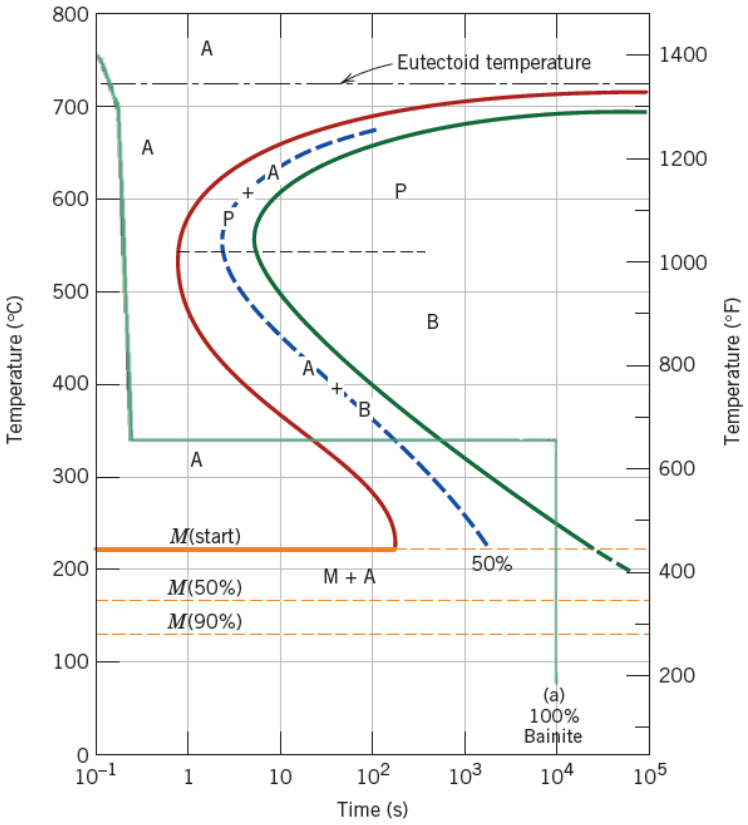


Figure 3.9 Schematic representation of bainitic transformation in time-temperature-transformation diagram for eutectoid steel: A, austenite; B, bainite; M, martensite; P, pearlite [65].

In the first experiments, values between 200 and 400 °C at the bainite margin were tried. New parameters were determined by updating where deemed appropriate.



(a) Preheat Furnace



(b) Austenitizing Furnace



(c) Salt Bath (up to 500 °C)



(**d)** Salt Bath (after 500 °)

Figure 3.10 Furnaces and salt baths used for heat treatment.

After the specimens were tied with different wire mesh to match each, they were first heated in the preheating furnace in Figure 3.10a to prevent residual stresses. Then, it was hold in the austenitizing furnace for 30 minutes at the austenitizing temperature in accordance with Table 3.2. Then, it was hold in the salt bath in Figure 3.10c during the isothermal transformation period and then left to cool in air.

3.4 Taguchi Experimental Design

In line with all these data, parameters were used as level and mechanical properties were used to determine the optimum value as noise data. The variables were determined as austenitization temperature, isothermal transformation temperature and isothermal transformation time for control parameters.

The rolling mill temperature of the rails produced in Turkey is generally at the level of 950 °C. Therefore, this value was considered in the austenitization temperature variables. In order to minimize the number of experiments to be performed, the Taguchi experimental design method was used. In this context, Taguchi L9 design was found to be suitable for the parameters in Table 3.3.

Signal/Noise ratios were calculated by ANOVA method using impact toughness, hardness values, and yield -rupture points values obtained as a result of the tensile test. Minitab software was used in these calculations and the data obtained are presented in the section of Results.

Table 3.3 L_9 orthogonal array for heat treatment

Experimental Set	Variables	A (Transformation Temperature) (°C)	B (Transformation Time) (hour)	C (Austenitizing Temperature) (°C)
1	A1B1C1	1 (200)	1 (2hr)	1 (840)
2	A1B2C2	1 (200)	2 (3hr)	2 (850)
3	A1B3C3	1 (200)	3 (4hr)	3 (860)
4	A2B1C2	2 (250)	1 (2hr)	2 (850)
5	A2B2C3	2 (250)	2 (3hr)	3 (860)
6	A2B3C1	2 (250)	3 (4hr)	1 (840)
7	A3B1C3	3 (300)	1 (2hr)	3 (860)
8	A3B2C1	3 (300)	2 (3hr)	1 (840)
9	A3B3C2	3 (300)	3 (4hr)	2 (850)

3.5 Hardness Test

Hardness measurements were made from 3 different points shown in Figure 3.11. For this purpose, the samples were first grinded with a grade of 200, 400, 600, 800, 1200 grid abrasive papers respectively. Then specimens polished with 3 µ and 1 µ diamond polishers, respectively.

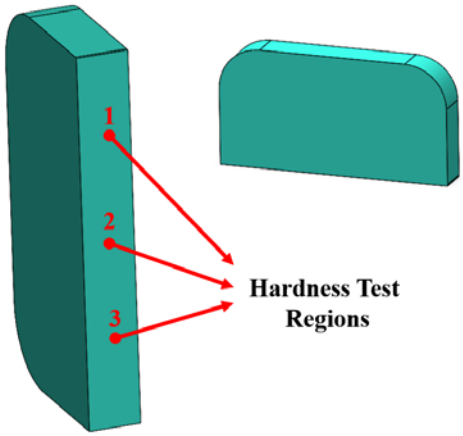
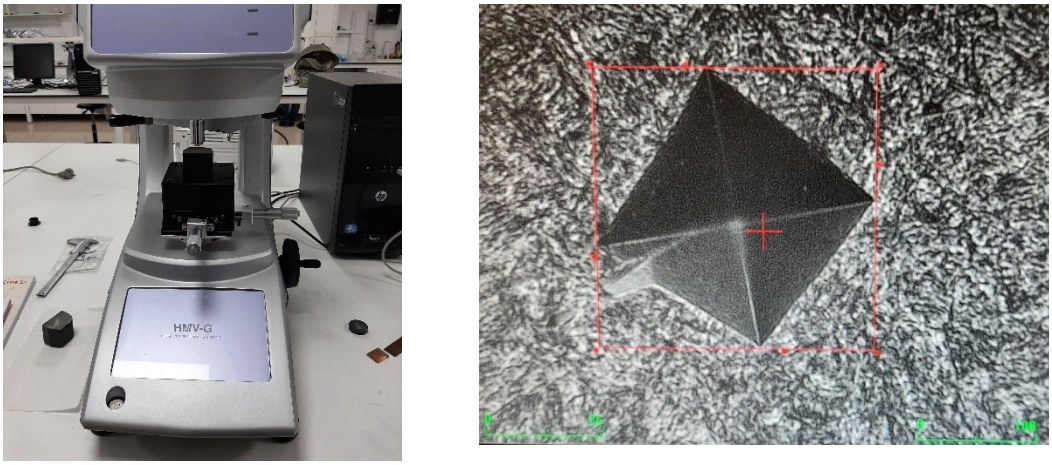


Figure 3.11 Hardness test regions

Hardness testing was performed with the Shimadzu HMV-G Vickers microhardness device, (see, Figure 3.12a). The hardnesses are obtained by the software (see Figure 3.12b) that calculates the hardness from the trace diagonals left by the diamond tip. The tests were carried out using the HV2 method, holding the 9.807 N force for 10 seconds.



(a) **(b)**

Figure 3.12 (a) Shimadzu HMV-G Vickers hardness tester, (b) Software that calculates the hardness from the trace diagonals left by the diamond tip.

3.6 Microstructural Characterization

Microstructural characterizations were performed after grinding, polishing, and etching processes. For each heat treatment applied sample, the 72x51x10 mm sized specimens prepared for metallographic examination as shown in Figure 3.13.

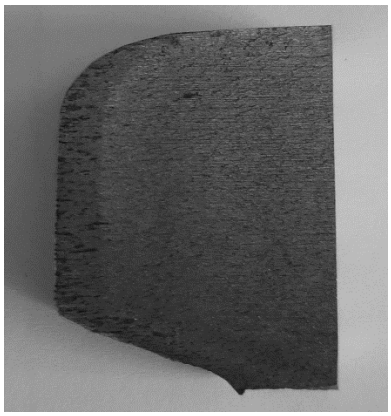


Figure 3.13 Microstructure sample

Since the samples are in sizes that can be easily held by hand, the mounting process was not considered necessary. In this context, it was grinded with 240, 320, 400, 600, 800, 1000, 1200 grinding papers underwater with a Metkon grinding device. Then, it

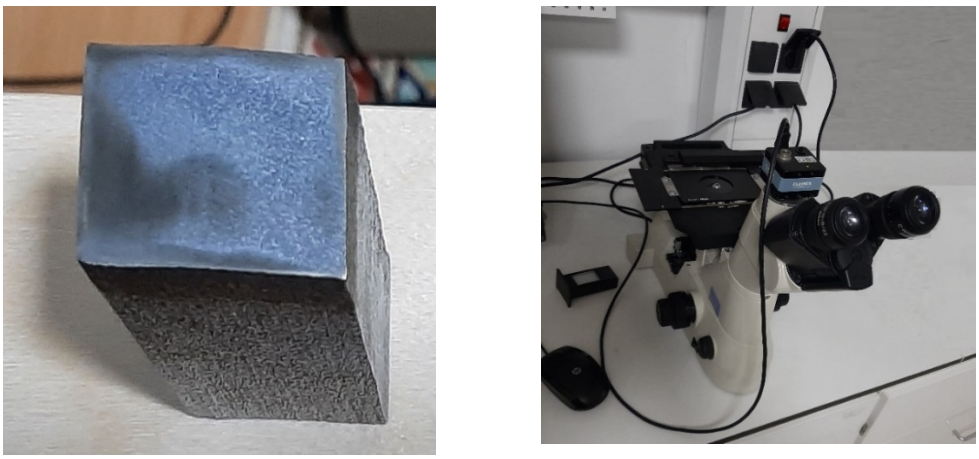
was polished with 3 and 1 µ diamond suspensions, respectively, with a Presi polishing device, Figure 3.14.



(a) **(b)**

Figure 3.14 (a) Grinding Machine, (b) Polishing Device.

It was then etched with 3% Nital at room temperature for 7 seconds. The etched raw sample can be seen in Figure 2.15. Microstructure images of all etched samples were taken with Nikon optical microscope, which allows image recording with Clemex software integration. Images obtained at 50x, 100x, 200x, 500x, 1000x magnifications are presented in the results section.



(a) **(b)**

Figure 3.15 (a) Nital etched sample, (b) Optical microscope.

3.7 Mechanical Tests

Tensile and impact tests were applied to the specimens in accordance with international standards. Tensile and impact test specimens for each parameter were extracted from the regions specified in 13674-1 as shown in Figure 3.16. The main reason for this is that the material reaches very high hardness values after heat treatment.Then, tensile and v-notch impact tests were carried out according to the boundary conditions stated in the standards.

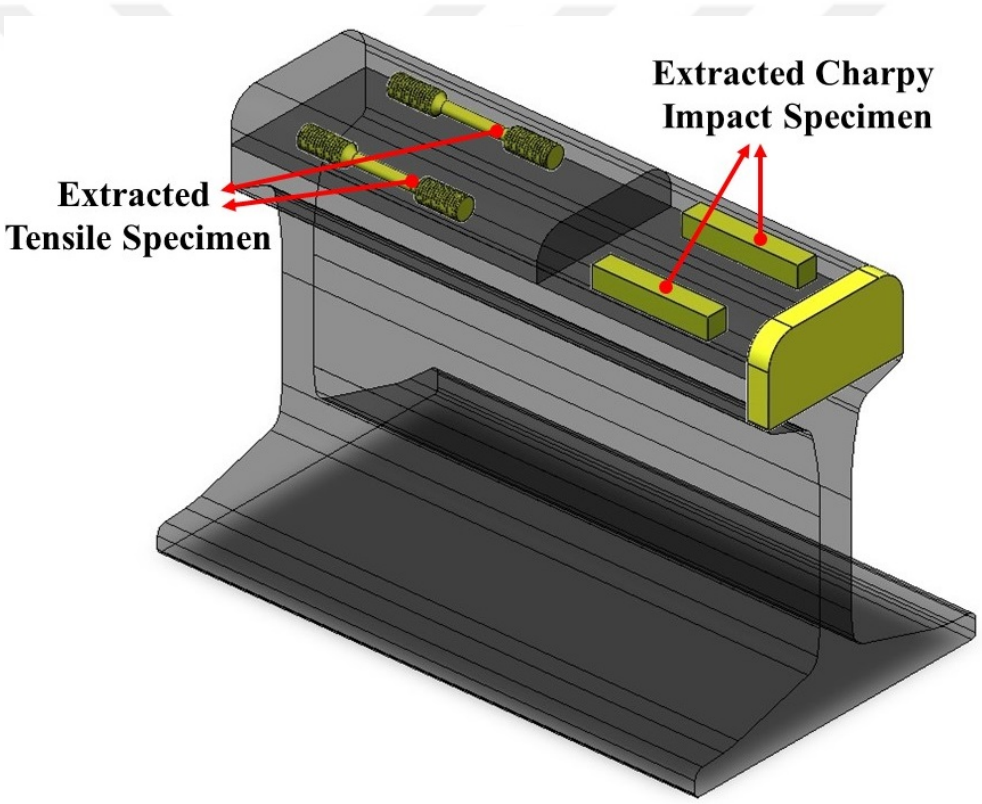
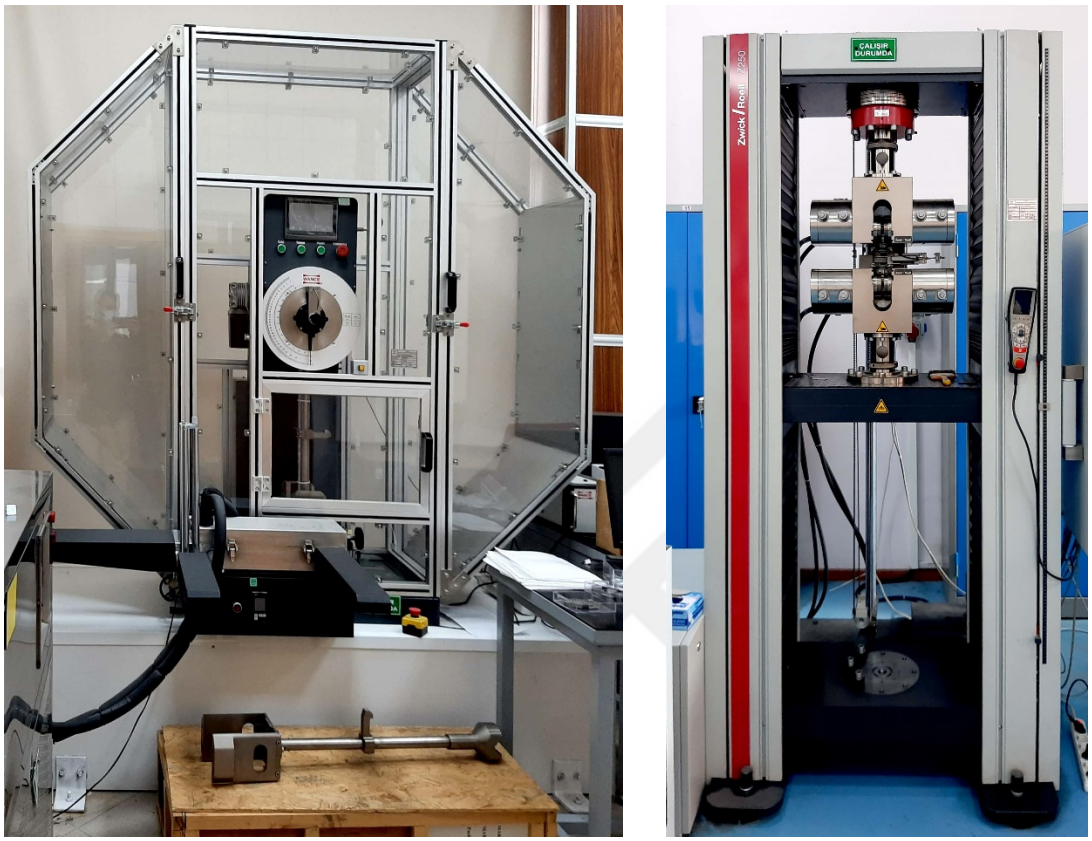


Figure 3.16 Regions where tensile and impact test specimens were extracted.

3.7.1 V-Notch Impact Test

Mechanical properties such as impact energy, tensile strength, breaking point, fracture toughness have been studied in detail. The notch impact tests were

performed according to ISO 14556:2000 Steel-Charpy V-notch pendulum impact test standard on the WANCE PIT 452G-4 model, shown in Figure 3.17a [9].



(a) **(b)**

Figure 3.17 (a) Impact test machine, (b) Tensile test machine

3.7.2 Tensile Test

The tensile test was carried out on a Zwick-Roell Z250 model tensile device with high precision and strength with a mechanical extensometer, Figure 3.17b. The tests were carried out according to TS EN ISO 6892-1 Metallic Materials-Tension Test (Method B). In tests performed at ambient temperature, the preload is 5 MPa and the test rate is 0.006/s [10]. The data obtained are presented in the results section.

CHAPTER 4

RESULTS and DISCUSSIONS

The results will be presented in 3 parts. In the first part, mechanical test results will be presented with tables and graphs, in the second part, Taguchi analysis and ANOVA analysis results and graphics. In the last part, the result of gray relational analysis calculation will be presented.

4.1 Mechanical Test Results

Test samples were heat treated after machining. Thus, residual stresses are eliminated caused by machining operations. Since the rail geometry was formed by the rolling method, the orientation of the grain structures according to the directions could not be determined. However, it is assumed that the effect of machining is not very significant for mechanical properties.

4.1.1 Spectral Analysis

Material characterization was performed as a preliminary study to determine the chemical composition of the material, Table 4.1. It was confirmed that the steel was high carbon steel similar to 1070 steel.

Table 4.1 Spectral analysis result and standard rail composition

	C (%)	**Si (%)**	**Mn (%)**	**P (%)**	**S (%)**	**Cr (%)**	**Ni (%)**	**Al (%)**	**V (%)**
Test	0,69	0,329	1,006	0,066	0,001	0,084	0,0625	0,0010	0,0050
EN 13674-1	0,60-0,82	0,13 - 0,60	0,65 - 1,25	0,030 (max)	0,030 (max)	≤0,15	0,06	0,04 (max)	0,030 (max)

4.1.2 Tensile Test

Table 4.2 Tensile test results

Experimental Set	Tensile Strength (MPa)	Elongation (%)
Standard	880	10
1	1053	13
2	1079	16
3	993	16,5
4	1043	13
5	994	13,5
6	995	14
7	1005	16
8	1023	15
9	1034	13

A1B2C2 specimen exhibits the highest tensile strength with a value of 1079 MPa. It is also among the highest elongations with 16 %. Apart from this, the A1B1C1 specimen also shows high mechanical properties with a tensile value of 1053 MPa.

Stress-strain plots are given in 3 different groups according to the austenitization temperature, see Figure 4.1, Figure 4.2, Figure 4.3.

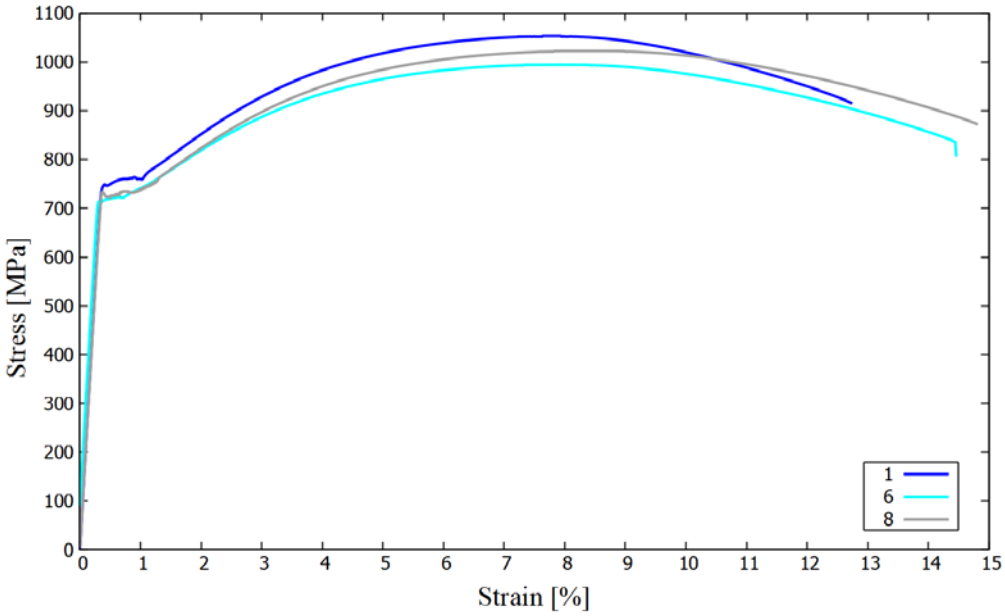


Figure 4.1 Stress-strain plot for austenitized specimens at 840 °C [(1)-A1B1C1, (6- A2B3C1), (8-A3B2C1]

When the graphs are examined, the highest values in terms of tensile strength were obtained at 850 °C. However, ductility and elongation values vary according to the isothermal transformation temperature. The lowest tensile strength was obtained at 860 °C.

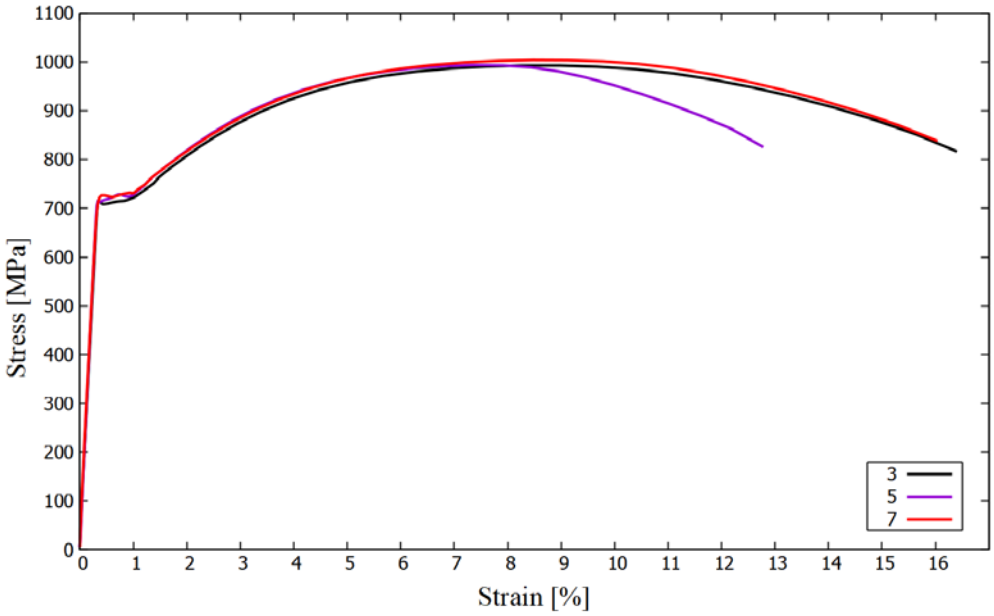


Figure 4.2 Stress-strain plot for austenitized specimens at 860 °C [(3)- A1B3C3, (5)- A2B2C3), (7)- A3B1C3]

Experiment sets (3)- A1B3C3 and (7)- A3B1C3 show very close tensile strength and elongation, while (5)- A2B2C3 set has lower elongation. (5)- A2B2C3 is the sample with the lowest toughness among all samples with 13.5% elongation and 8.62 joules of impact energy. In addition, it does not perform well with a tensile of 994 MPa.

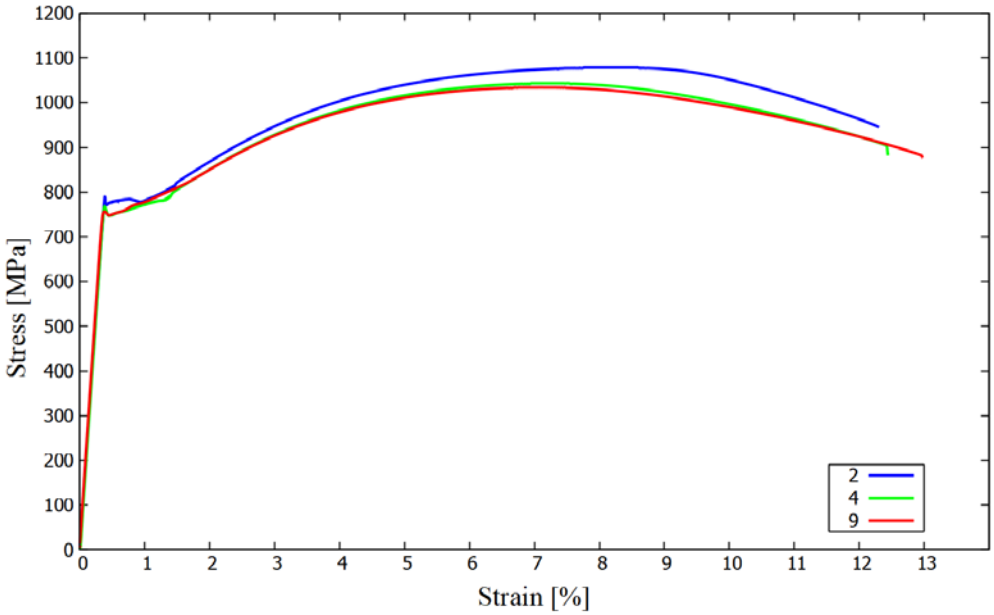


Figure 4.3 Stress-strain plot for austenitized specimens at 850 °C [(2)- A1B2C2, (4)- A2B1C2), (9)- A3B3C2]

4.1.3 Impact Test

According to the impact test data presented in Table 4.3 the impact energy increased significantly. Particularly, samples 3, 6, and 7 showed high toughness properties. The steels obtained were considered to be upper bainite. These results are consistent with the data obtained in F.H. Çakır's study [30].

Table 4.3 Impact test results

Experimental Set	Impact Energy (Joule)	Impact Strength (kJ/m^2)
Standard	4	-
1	10	1.250
2	9.99	1.249
3	13.3	1.663
4	9.57	1.196
5	8.62	1.078
6	14.3	1.788
7	15.7	1.963
8	11.6	1.450
9	10.3	1.287

4.1.4 Hardness Test

It was determined that the ductility increment of the samples did not decrease with the bainitic transformation. All hardness test results presented in Table 4.4 were higher than the values recommended by the standards.

Table 4.4 Result of the hardnesses.

Experimental Set	Measurement 1	Measurement 2	Measurement 3	Average
Standard				280
1	329	344	315	329
2	335	322	332	330
3	300	297	317	305
4	323	340	300	321
5	323	332	295	317
6	303	309	307	306
7	274	271	280	275
8	315	321	337	324
9	312	340	328	327

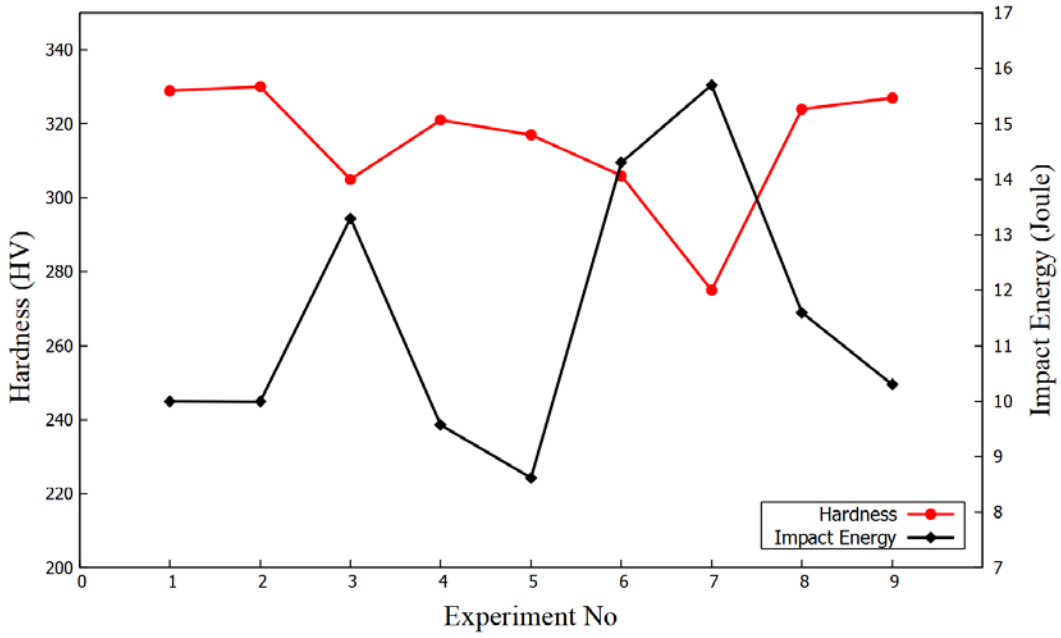


Figure 4.4 The comparison chart of hardness versus impact energy values

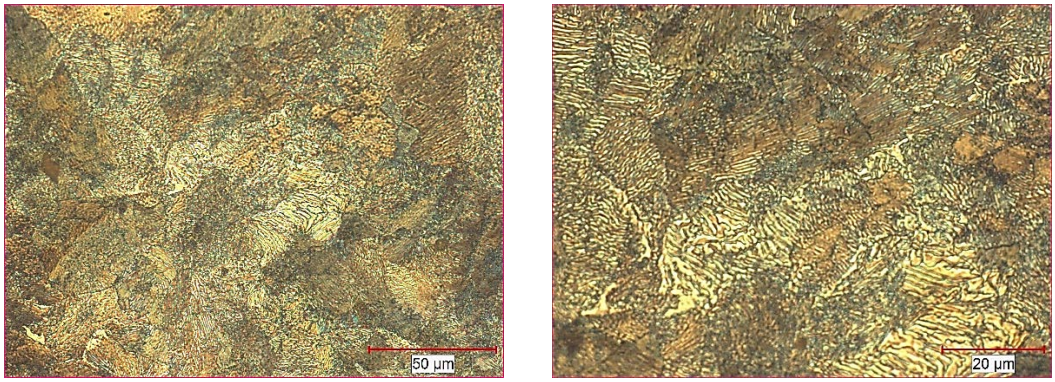
4.1.5 Metallographic Examination

In the ASTM Metallography and Microstructures handbook, it is stated that the feathery structure is less common in high carbon bainitic steels, and the feathery structure will become more pronounced as the carbon content decreases [66]. Although the properties of bainitic steels are observed in the obtained samples, the feathery structure is not evident in some samples due to the high carbon content. While it is not visible in some samples due to the low bainite ratio, the samples need to be imaged with an SEM.

When the microstructure images were examined, it was observed that the raw pearlitic R260 samples transformed into the bainitic microstructure. In a great majority of samples, it is clearly seen that the lamellar structure has transformed to a feathery structure, which is the typical bainitic microstructure appearance. As mentioned above, it is necessary to take images with SEM for more precise images. When the images taken with 100x and 200x magnification were examined, it was evaluated that the bainitic structure was highly homogeneously distributed, and the martensitic structure was in a smaller amount but still in a homogeneous distribution.

Fine lattice bainitic ferrite and a small amount of martensite structure are observed in the samples subjected to isothermal heat treatment. In the literature, dark feathery grains are generally interpreted as bainite. In addition, it has been stated that there are light-colored small acicular martensite grains among the grains that have completed the bainitic transformation [42, 45].

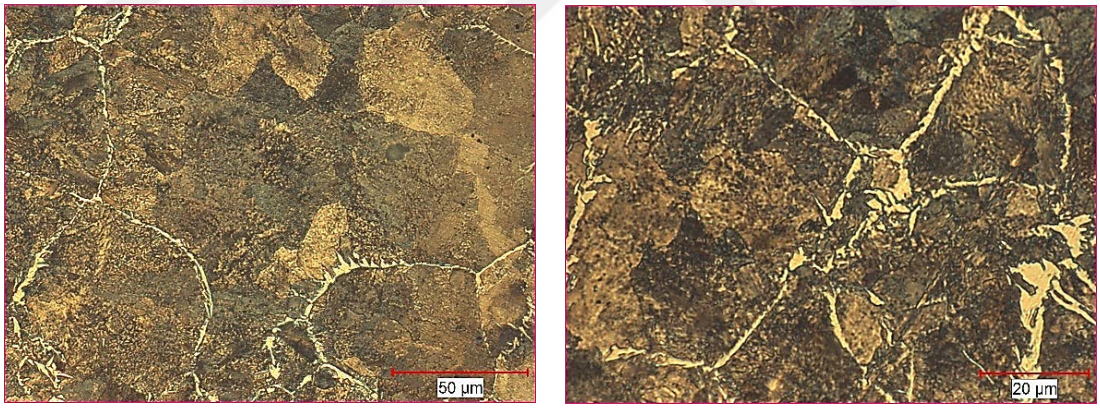
When the images obtained examined with the optical microscope, (see Figure 4.5-Figure 4.14) it was evaluated that they were very similar to the bainitic microstructure images obtained in the studies of G. Mateo et. al. and O. Haiko et. al. [45, 67].



(a) **(b)**

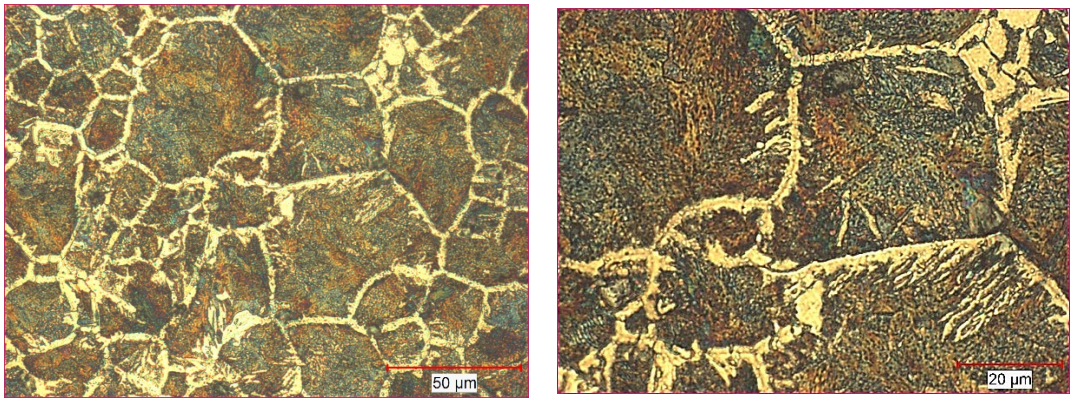
Figure 4.5 Conventional R260 rail steel microstructure; (a) 500x, (b) 1000x.

The lamellar structure of pearlitic steel, whose microstructure was examined before heat treatment, is clearly seen in Figure 4.5. This microstructure, known as fine pearlite, which shows good mechanical properties as a result of its fine-grained microstructure.



(a) **(b)**

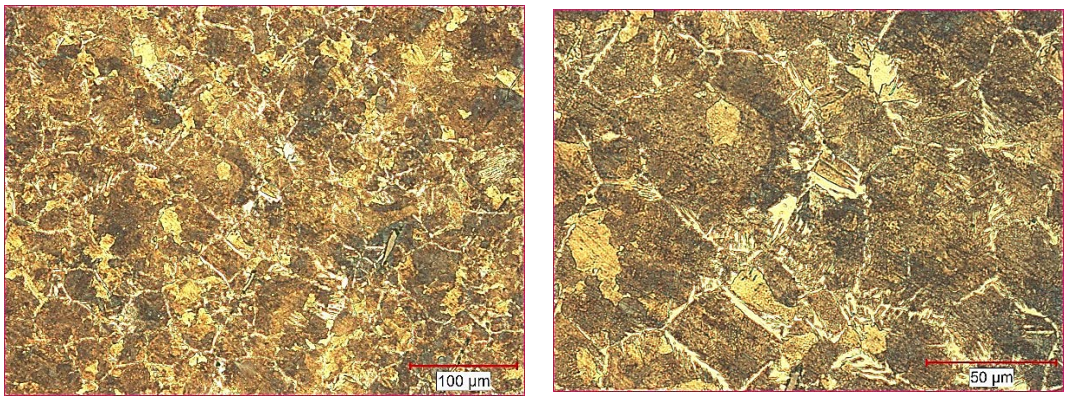
Figure 4.6 Optical microscope images of (1)-A1B1C1 sample; (a) 500x, (b) 1000x.



(a) **(b)**

Figure 4.7 Optical microscope images of (2)-A1B2C2 sample (a) 500x, (b) 1000.

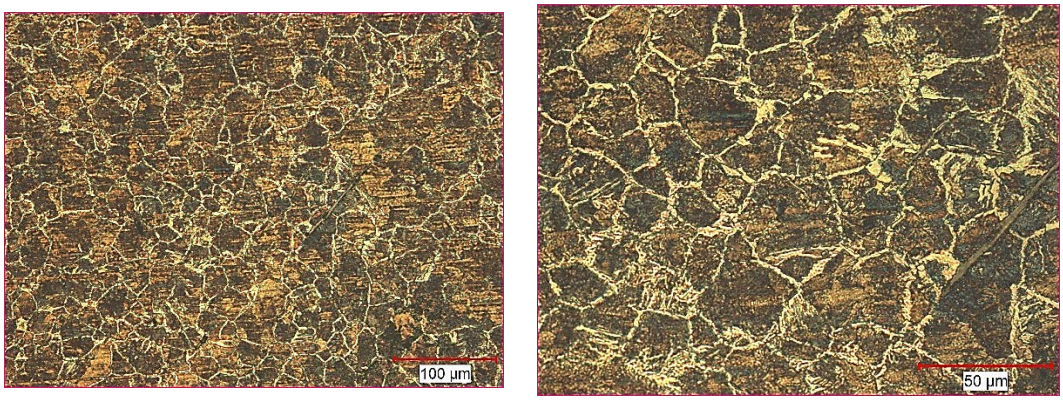
The highest tensile strength obtained for the samples A1B1C1-(Experimental Set 1) and A1B2C2-(Experimental Set 2) where high mechanical properties are consistent with the observed microstructures, see Figure 4.6 and Figure 4.7. Dark feathery structures are known to be bainitic. In addition, the samples in these two parameters are the 2 highest parameters in terms of hardness. Observation of bainitic and local martensitic structures explains the hardness and high tensile strength.



(a) **(b)**

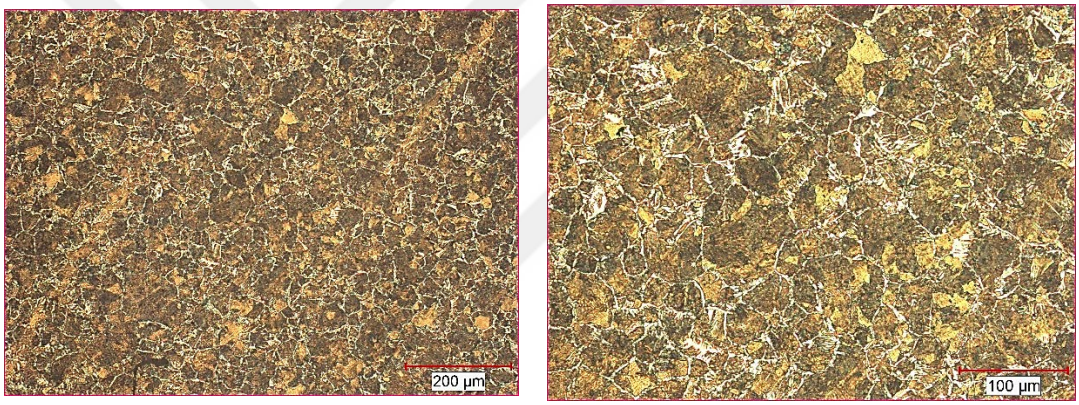
Figure 4.8 Optical microscope images of (3)-A1B3C3 sample; (a) 200x, (c) 500x.

In Figure 4.8, A1B3C3-(Experimental Set 3) specimen has higher values for ductility and impact energy, although its tensile and hardness values are low due to the high RA ratio, indicating applicable parameters.



(a) **(b)**

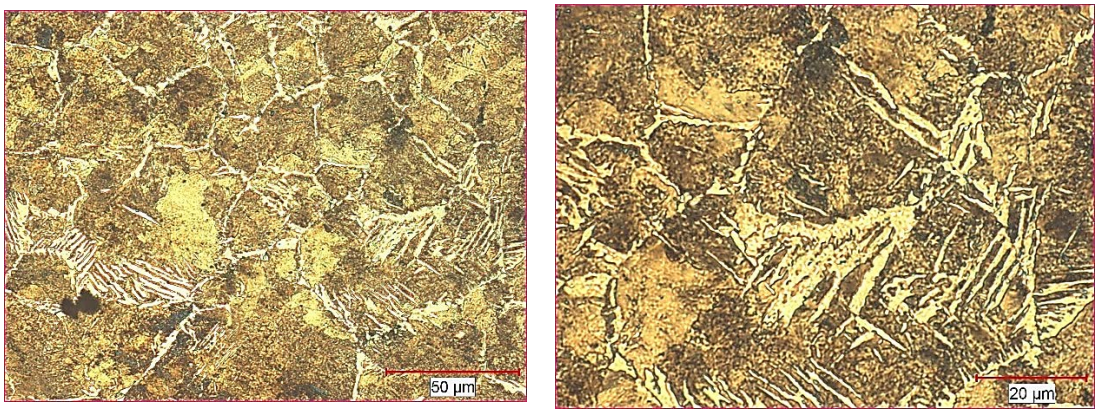
Figure 4.9 Optical microscope images of (4)-A2B1C2 sample; (a) 200x, (b) 500x.



(a) **(b)**

Figure 4.10 Optical microscope images of (5)-A2B2C3 sample; (a) 100x, (b) 200x.

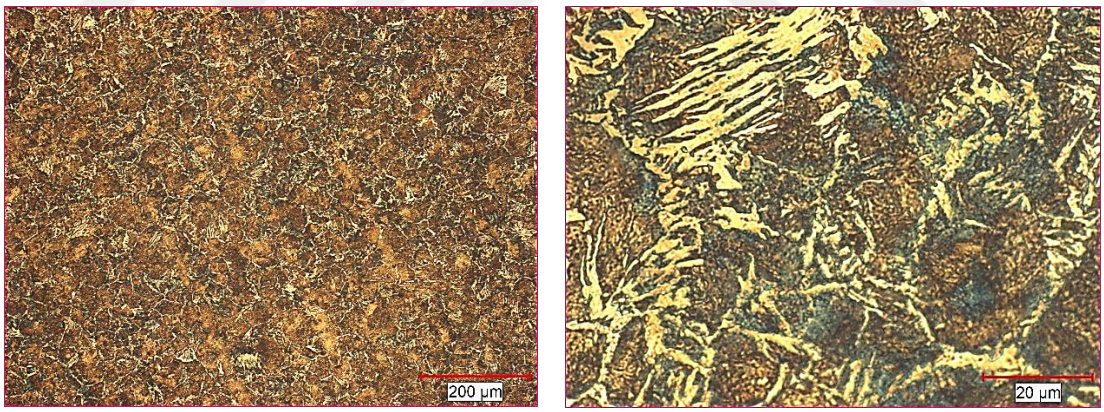
In Figure 4.9 and Figure 4.10 for the experiments A2B1C2-(Experimental Set 4) and A2B2C3-(Experimental Set 5) results show brittle properties due to the martensite structure that can be easily noticed. Acicular grains, which are very light in color compared to other phases, are defined as martensite. In these two parameters, while high hardness and tensile strength are observed as a result of these structural properties, they are not preferred due to low ductility and toughness values.



(a) **(b)**

Figure 4.11 Optical microscope images of (6)-A2B3C1 sample; (a) 500x, (b) 1000x.

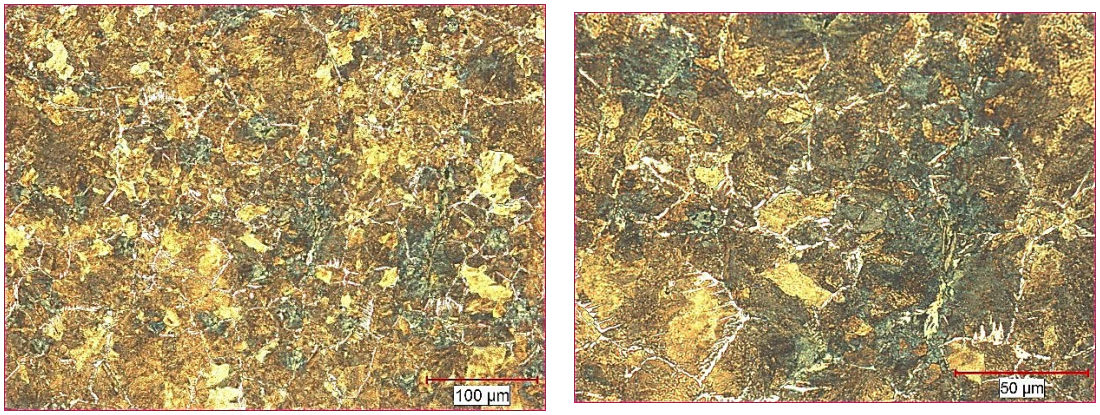
In Figure 4.11, A2B3C1-(Experimental Set 6) sample has lower tensile strength and hardness values compared to the other experimental results. The main reason for this can be explained by the relatively low bainite ratio. The high amount of RA, whose relationship with toughness has been explained by various studies, explains the value of 14.3 as impact energy, see Figure 4.11, [15, 45].



(a) **(b)**

Figure 4.12 Optical microscope images of (7)-A3B1C3 sample; (a) 100x, (b) 1000x

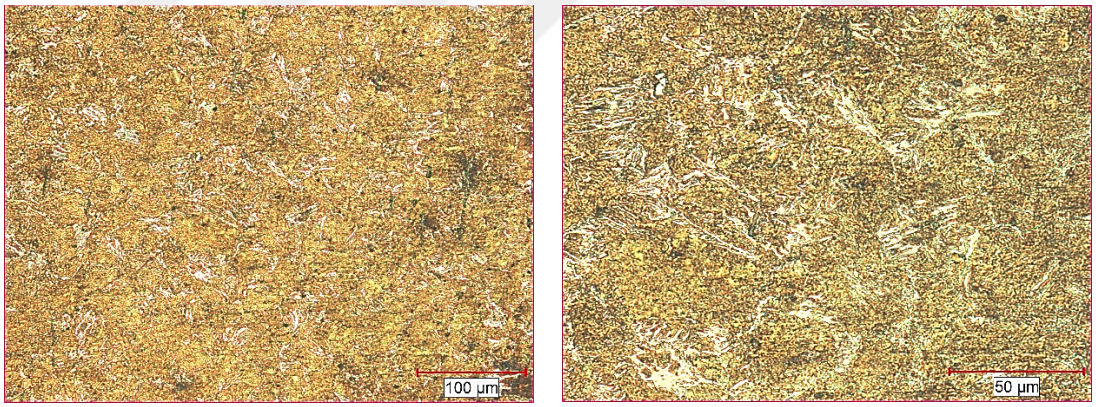
The thin film RA structure, which gives ductility, is homogeneously distributed in the A3B1C3-(Experimental Set 7) sample as seen in its optical image in Figure 4.12. This light-colored grain structure explains the elongation (16%) and high impact energy (15.7 Joule). The fact that the ductility of this sample is so high explains that it is 9th as hardness and 6th as tensile with obtained values of 275 HV and 1005 MPa, see Figure 4.12.



(a) **(b)**

Figure 4.13 Optical microscope images of (8)-A3B2C1 sample; (a) 200x, (b) 500x.

A3B2C1-(Experimental Set 8) sample is approximately 4th in all test results. It exhibits near-optimal mechanical properties in all tests. The main reason for this can be shown as the density of the bainitic structure and the less and homogeneous distribution of the martensitic structure, which is clearly seen in Figure 4.13.



(a) **(b)**

Figure 4.14 Optical microscope images of (9)-A3B3C2 sample; (a) 200x, (c) 500x.

The sample A3B3C2-(Experimental Set 9), on the other hand, exhibits high tensile and hardness properties while having low impact resistance due to the intense presence of light-colored acicular martensite grain structure, see Figure 4.14.

4.2 Results of Taguchi Analysis

Taguchi experimental design was processed with the parameters determined in Table 3.3 (L9 orthogonal array for Heat Treatment Processes)) by using Minitab software. S/N ratios calculated using Eq. 1.1ab and other ANOVA terms were obtained with the help of this software. The results obtained will be presented separately according to each experimental parameter. Since the properties that should be high in the rail material were tested, the 'Larger is better' approach was used in the entire design.

4.2.1 S/N Ratios

The total S/N ratios of each parameter for 9 different parameters are presented in Table 3.5.

Table 4.5 Total S/N Ratios for parameters

Experimental Set	Variables	A	B	C	S/N for Tensile Strength	S/N for Elongation	S/N for Impact Energy	S/N for Hardnesses
1	ABC	1	1	1	60.45	22.28	20.00	50.34
2	A1B2C2	1	2	2	60.66	24.08	19.99	50.37
3	A1B3C3	1	3	3	59.94	24.35	22.48	49.69
4	A2B1C2	2	1	2	60.37	22.28	19.62	50.13
5	A2B2C3	2	2	3	59.95	22.61	18.71	50.02
6	A2B3C1	2	3	1	59.96	22.92	23.11	49.71
7	A3B1C3	3	1	3	60.04	24.08	23.92	48.79
8	A3B2C1	3	2	1	60.20	23.52	21.29	50.21
9	A3B3C2	3	3	2	60.29	22.28	20.26	50.29

A: Transformation Temperature, B: Transformation Time, C: Austenitizing Temperature

In addition, response table and main effects of plot will be presented to reveal the effect of each parameter level on the response.

4.2.1.1 Tensile Strength

Tensile strength S/N ratios are in the Table 4.6. As a result of the analysis, 2 hours isothermal transformation at 200 °C after austenitization at 850 °C were determined as the optimum parameters in terms of tensile strength. According to main effects

plots of tensile strength, it has been revealed that the most effective factor for tensile strength is the isothermal transformation temperature, see Figure 4.15.

Table 4.6 Response Table for Signal to Noise Ratios

Level	Isothermal Transformation Temperature	Isothermal Transformation Time	Austenitizing Temperature
1	60,35	60,29	60,20
2	60,09	60,27	60,44
3	60,18	60,06	59,98
Rank	2	3	1

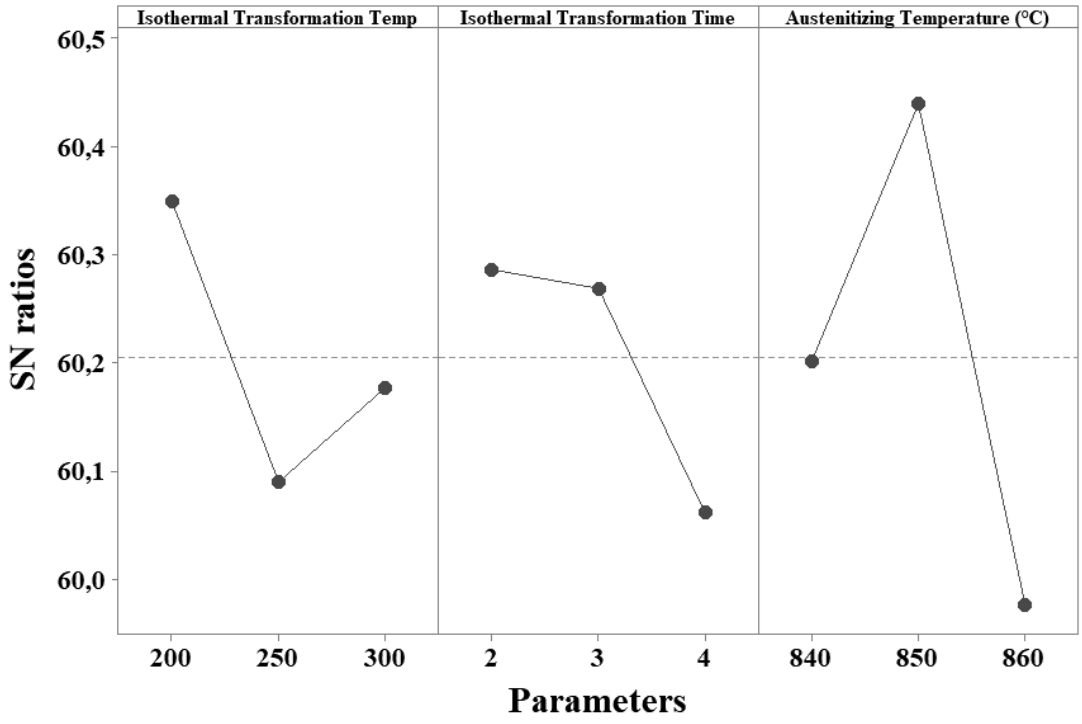


Figure 4.15 Main effects plot for S/N ratios of tensile strength.

4.2.1.2 Elongation

S/N ratios for elongation are presented in the Table 4.7. It is easily noticed that the isothermal transformation temperature is very effective, while the isothermal transformation time is at a relatively lower level. In terms of elongation, there was no difference between austenitization at 840 °C and 850 °C degrees, but a significant increase occurred at 860 °C levels, see Figure 4.16. As a result of the analysis, isothermal transformation parameters at 200 °C for 3 hours after austenitization at 860 °C were determined as optimum in terms of elongation.

Table 4.7 Signal to Noise Ratios of elongation

Level	Isothermal Transformation Temperature	Isothermal Transformation Time	Austenitizing Temperature (°C)
1	23,57	22,88	22,91
2	22,60	23,40	22,88
3	23,29	23,18	23,68
Rank	1	3	2

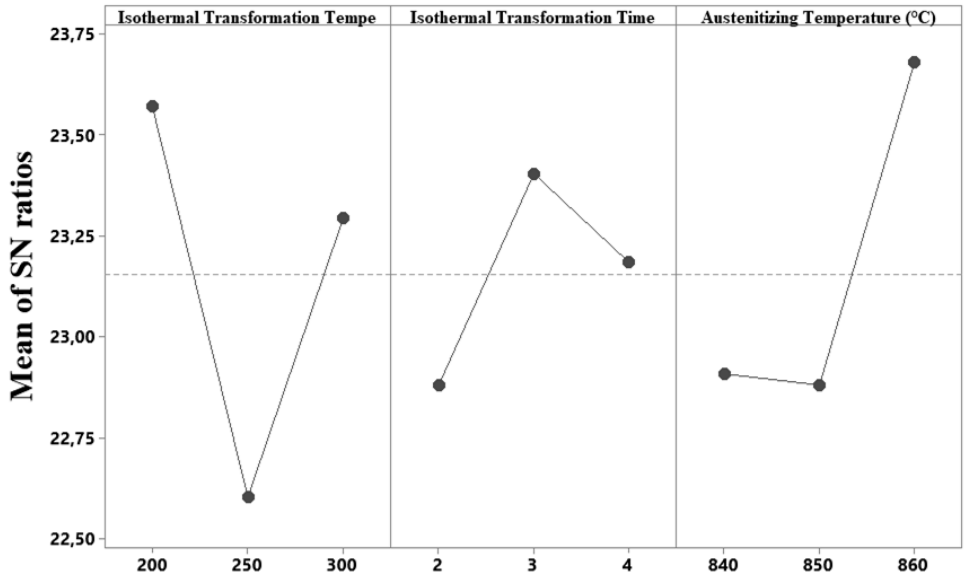


Figure 4.16 Main effects plot for S/N ratios of tensile elongation.

4.2.1.3 Impact Energy

Impact energy S/N ratios are in the Table 4.8. It is understood from the Figure 4.17 that all 3 parameters are effective in terms of impact energy. The main plots show that austenitization at 850 ℃, 2 hours at 200 ℃ isothermal transformation parameters are optimum in terms of impact energy.

Table 4.8 Signal to Noise Ratios of impact energy

Level	Isothermal Transformation Temperature	Isothermal Transformation Time	Austenitizing Temperature (°C)
1	20,82	21,18	21,47
2	20,48	20,00	19,96
3	21,82	21,95	21,70
Rank	3	1	2

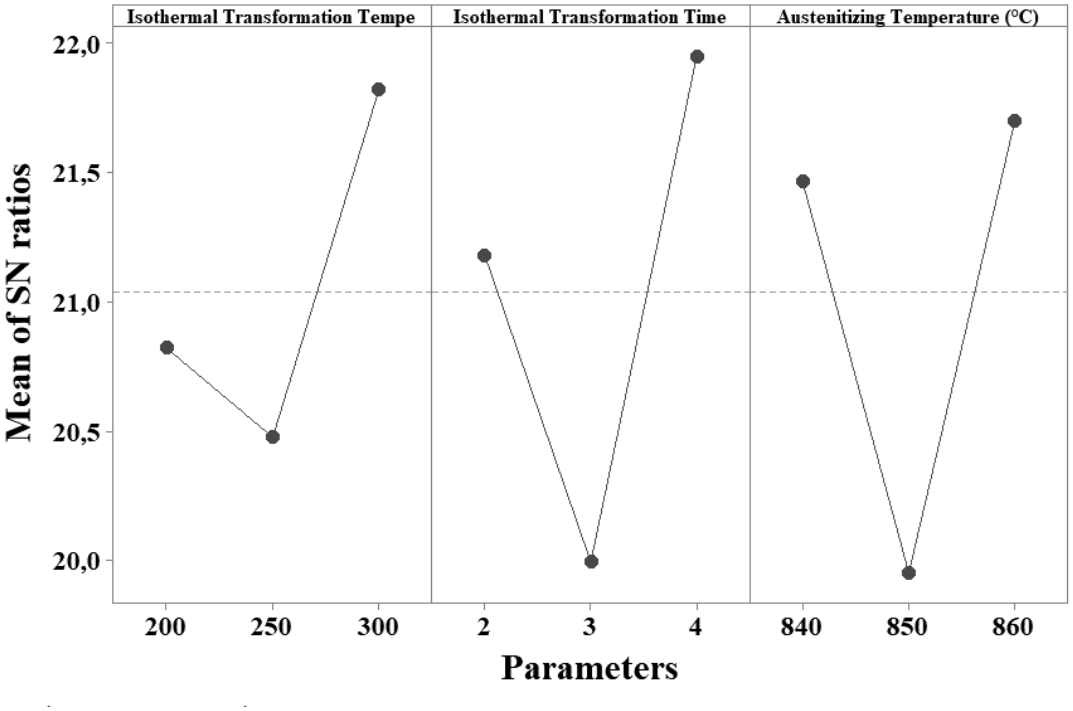


Figure 4.17 Main effects plot for S/N ratios of Impact Energy.

4.2.1.4 Hardness

Hardness S/N ratios are in the Table 4.9. The high hardness of the martensitic microstructure is achieved as a result of rapid cooling to low temperatures. This is clearly noticeable in Figure 4.18. As the isothermal transformation temperature decreases, the S/N ratio increases in direct proportion. Afterward high austenitizing temperatures have a negative effect on hardness. The lowest S/N ratio was obtained at 860 °C. It is understood from the main effects' plots that the austenitization temperature at 860 °C and the isothermal transformation parameters at 200 °C for 3 hours are optimum in terms of hardness.

Table 4.9 Signal to Noise Ratios of hardness

Level	Isothermal Transformation Temperature	Isothermal Transformation Time	Austenitizing Temperature (°C)
1	50,13	49,75	50,09
2	49,96	50,20	50,26
3	49,76	49,90	49,50
Rank	3	2	1

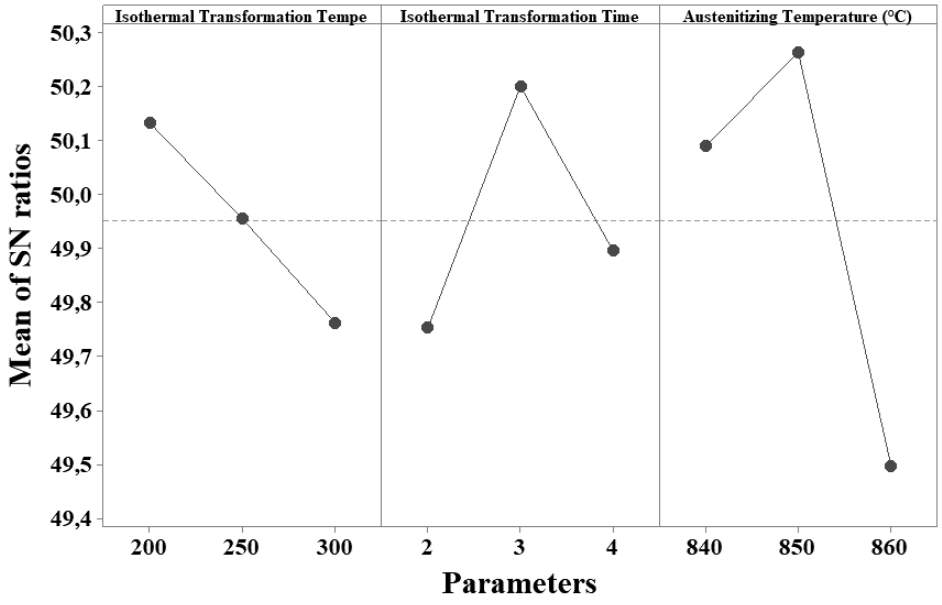


Figure 4.18 Main effects plot for S/N ratios of hardness.

4.2.2 ANOVA

4.2.2.1 ANOVA for Tensile Strength

Table 4.10 ANOVA for Tensile Strength

Parameters	DF	SS	Contribution	MS	F	P
Isothermal Transformation Temperature	2	1502,00	20,32%	751,00	15,22	0,062
Isothermal Transformation Time	2	1304,67	17,65%	652,33	13,22	0,070
Austenitizing Temperature (°C)	2	4484,67	60,69%	2242,33	45,45	0,022
Error	2	98,67	1,34%	49,33		
Total	8	7390,00	100,00%			

DF: Degree of freedom, SS: Sum of squares, MS: Mean square

4.2.2.2 ANOVA for Elongation

Table 4.11 ANOVA for Elongation

Parameters	DF	SS	Contribution	MS	F	P
Isothermal Transformation Temperature	2	4,389	26,25%	2,1944	0,57	0,638
Isothermal Transformation Time	2	1,056	6,31%	0,5278	0,14	0,880
Austenitizing Temperature (°C)	2	3,556	21,26%	1,7778	0,46	0,685
Error	2	7,722	46,18%	3,8611		
Total	8	16,722	100,00%			

DF: Degree of freedom, SS: Sum of squares, MS: Mean Square

4.2.2.3 ANOVA for Impact Strength

Table 4.12 ANOVA for Impact Strength

Parameters	DF	SS	Contribution	MS	F	P
Isothermal Transformation Temperature	2	5,036	10,78%	2,518	0,25	0,802
Isothermal Transformation Time	2	10,184	21,80%	5,092	0,50	0,667
Austenitizing Temperature (°C)	2	11,073	23,70%	5,537	0,54	0,648
Error	2	20,424	43,72%	10,212		
Total	8	46,718	100,00%			

DF: Degree of freedom, SS: Sum of squares, MS: Mean square

4.2.2.4 ANOVA for Hardness

Table 4.13 ANOVA for Hardness

Parameters	DF	SS	Contribution	MS	F	P
Isothermal Transformation Temperature	2	240,9	9,76%	120,4	0,37	0,731
Isothermal Transformation Time	2	374,9	15,20%	187,4	0,57	0,636
Austenitizing Temperature (°C)	2	1196,2	48,49%	598,1	1,83	0,354
Error	2	654,9	26,55%	327,4		
Total	8	2466,9	100,00%			

DF: Degree of freedom, SS: Sum of squares, MS: Mean square

4.2.3 Prediction

Predict values were obtained with the Taguchi analysis and presented in Table 4.14.

Table 4.14 Predict values.

Experimental Set	Variables	A	B	C	Predict Tensile Strength	Predict Elongation	Predict Impact Energy	Predict Hardness
1	ABC	1	1	1	1050,33	22.28	20.00	50.34
2	A1B2C2	1	2	2	1077,00	24.08	19.99	50.37
3	A1B3C3	1	3	3	997,67	24.35	22.48	49.69
4	A2B1C2	2	1	2	1047,67	22.28	19.62	50.13
5	A2B2C3	2	2	3	991,33	22.61	18.71	50.02
6	A2B3C1	2	3	1	993,00	22.92	23.11	49.71
7	A3B1C3	3	1	3	1003,00	24.08	23.92	48.79
8	A3B2C1	3	2	1	1027,67	23.52	21.29	50.21
9	A3B3C2	3	3	2	1031,33	22.28	20.26	50.29

A: Transformation Temperature, B: Transformation Time, C: Austenitizing Temperature

Regression analysis was performed with the obtained data. The graphs in Figure 4.19-22 were obtained by performing polynomial quadratic regression analysis with 95% confidence on these values. While CI in the graphs is the confidence interval, PI represents the predict interval. As a result, it was determined that the fit assigned to the impact, hardness and tensile strength values was reliable since all values were within the confidence interval. However, more data is needed for elongation.

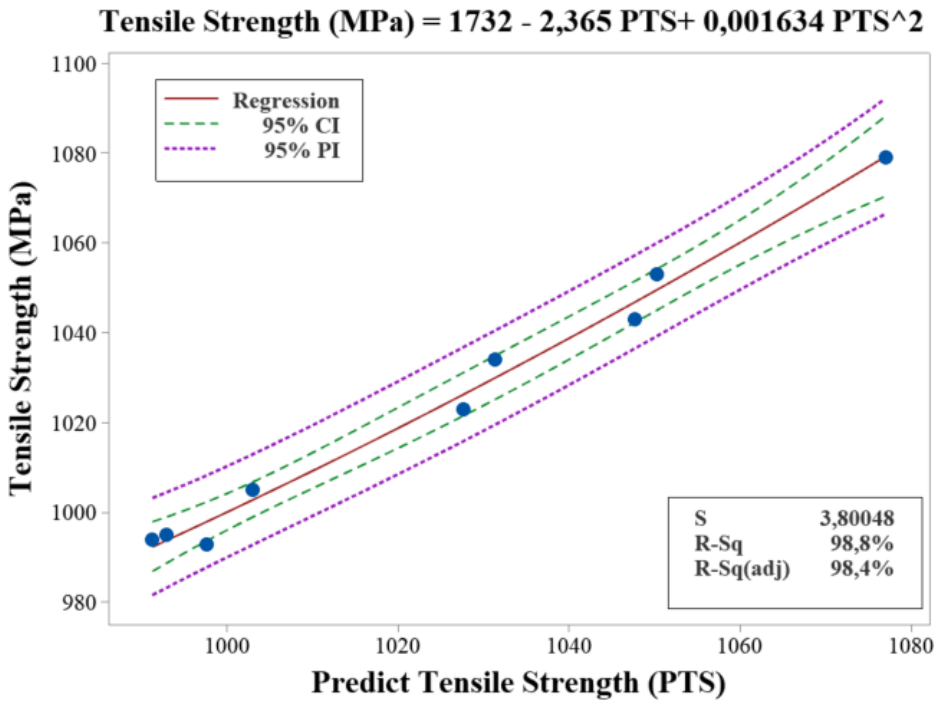


Figure 4.19 Fitted line plot for tensile strength.

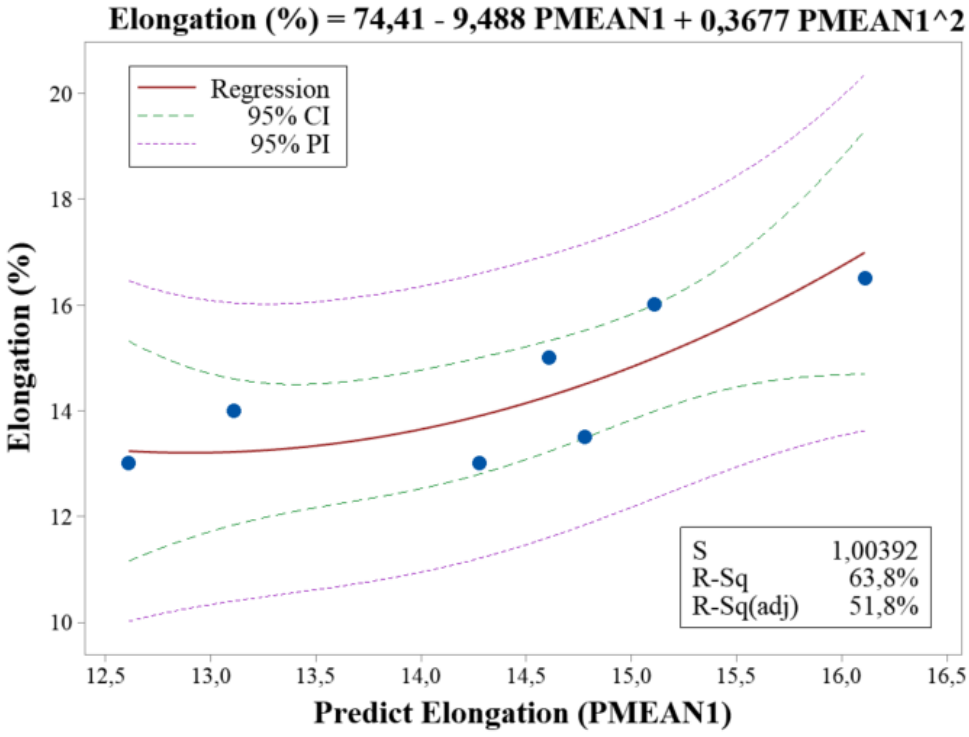


Figure 4.20 Fitted line plot for elongation.

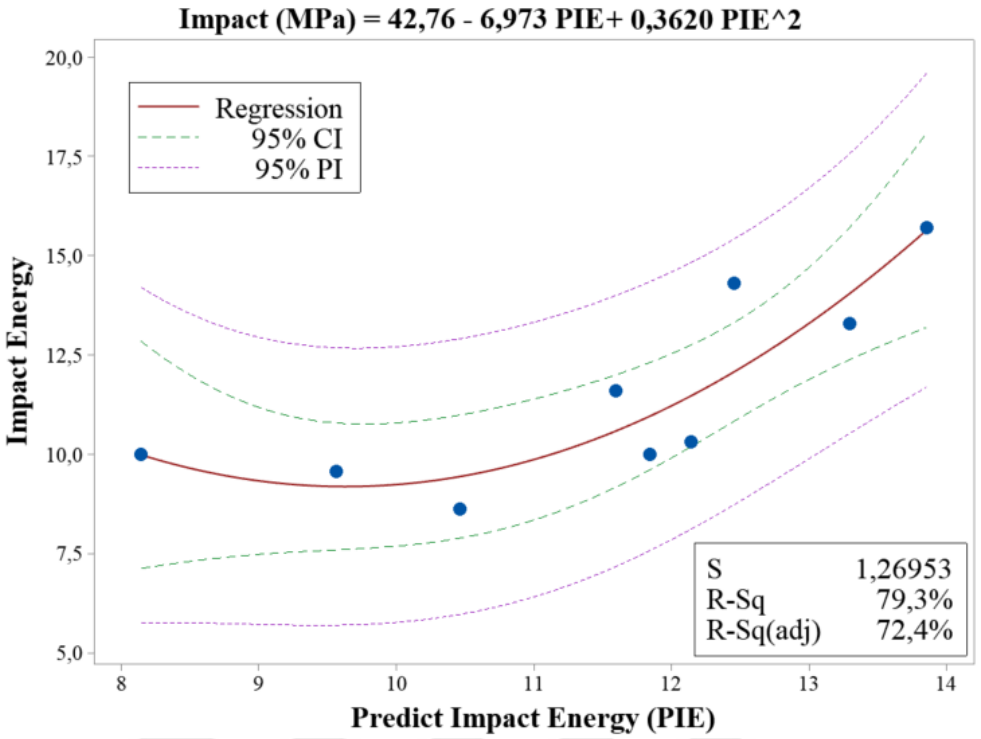


Figure 4.21 Fitted line plot for impact energy.

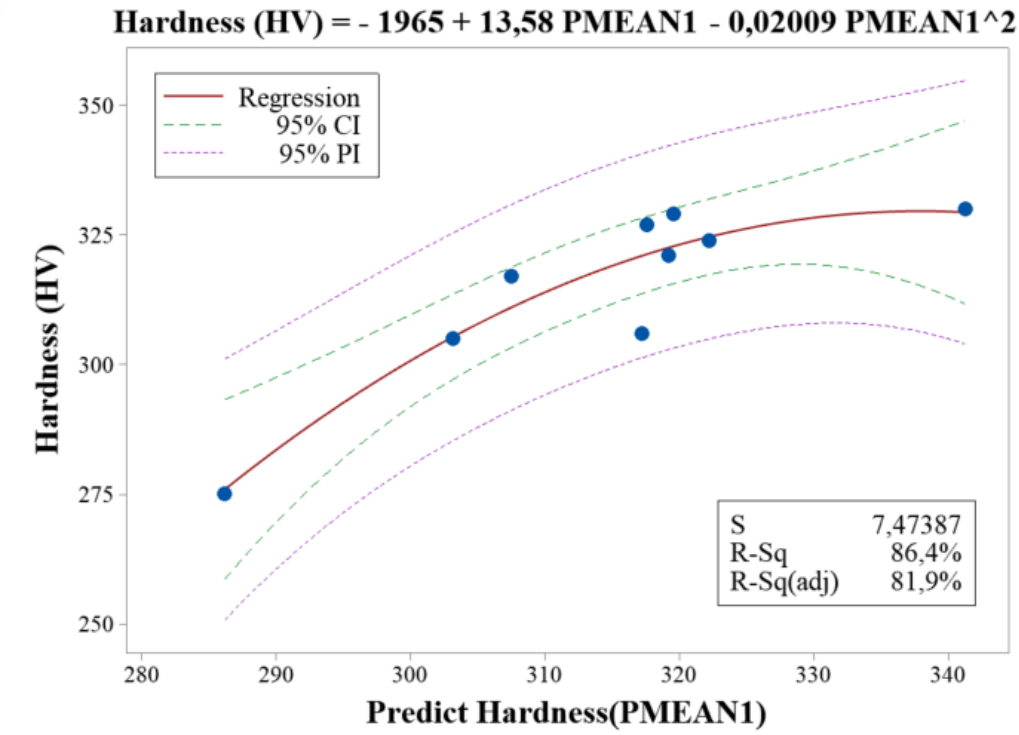


Figure 4.22 Fitted line plot for hardness.

4.3 Gray Relational Analysis

Gray relational analysis was performed using tensile, elongation, impact and hardness test results. The calculation made for the A1B1C1 sample is given below in detail. It was calculated in the same sample for each value and the other results are presented in the tables. The $x_i(k)$ value is taken as $x_t(1)$ as the result of the first tensile test result.

4.3.1 Gray relational generation

The Gray relational generation value was calculated using eq.1.9.

$$x^*_t(1) = \frac{x_t(1) - \min x_t(1)}{max\, x_t(1) - min\, x_t(1)} = \frac{1053 - 993}{1079 - 993} = 0{,}698$$

The same procedure was applied to all results, see Table 4.15.

Table 4.15 Gray relational generation values

Experimental Set	Tensile	Elongation	Impact	Hardness
1	0.698	0.000	0.195	0.982
2	1.000	0.857	0.194	1.000
3	0.000	1.000	0.661	0.545
4	0.581	0.000	0.134	0.836
5	0.012	0.143	0.000	0.764
6	0.023	0.286	0.802	0.564
7	0.140	0.857	1.000	0.000
8	0.349	0.571	0.421	0.891
9	0.477	0.000	0.237	0.945

4.3.2 Deviation Sequences

Then deviation sequence values were calculated using Eq. 1.11 and other results in Table 3.16

$$\Delta_{0t}(1) = |1 - 0{,}698)| = 0{,}302$$

Table 4.16 Deviation Sequences

Experimental Set	Tensile	Elongation	Impact	Hardness
1	0.302	1.000	0.805	0.018
2	0.000	0.143	0.806	0.000
3	1.000	0.000	0.339	0.455
4	0.419	1.000	0.866	0.164
5	0.988	0.857	1.000	0.236
6	0.977	0.714	0.198	0.436
7	0.860	0.143	0.000	1.000
8	0.651	0.429	0.579	0.109
9	0.523	1.000	0.763	0.055

4.3.3 Gray Relational Coefficient

By placing these values in Eq. 1.12, Gray Relational Coefficients were found, see Table 4.17.

$$\xi_t(1) = \frac{\Delta_{min} + \xi\Delta_{max}}{\Delta_{0t}(1) + \xi\Delta_{max}} = \frac{0 + (0{,}5)(1)}{0{,}302 + (0{,}5)(1)} = 0{,}623$$

Table 4.17 Gray Relational Coefficient

Experimental Set	Tensile	Elongation	Impact	Hardness
1	0.623	0.333	0.383	0.965
2	1.000	0.778	0.383	1.000
3	0.333	1.000	0.596	0.524
4	0.544	0.333	0.366	0.753
5	0.336	0.368	0.333	0.679
6	0.339	0.412	0.717	0.534
7	0.368	0.778	1.000	0.333
8	0.434	0.538	0.463	0.821
9	0.489	0.333	0.396	0.902

Finally Gray Relational grade was found by Eq. 1.13.

$$\alpha_1 = \frac{1}{n}\sum_{k=i}^{n} Y_i(k) = \frac{1}{4}\sum_{k=1}^{4} Y_1(k) = Y_1(1)+Y_2(k) + Y_3(k) + Y_4(k)$$

4.3.4 Gray relational grades

After calculating Gray relational grades, the optimum value is found by ranking.

Table 4.18 Gray relational grades with equal contribution.

#	Variables	A	B	C	Tensile	Elong.	Impact	Hardness	Gray Relational Grade	RANK
	ABC	°C	hr	°C	(MPa)	(%)	Joule	HV		
1	A1B1C1	200	2	1	1053	13	10	329	0.576	4
2	A1B2C2	200	2	2	1079	16	9.99	330	0.790	1
3	A1B3C3	200	3	3	993	16.5	13.3	305	0.613	3
4	A2B1C2	250	1	2	1043	13	9.57	321	0.499	8
5	A2B2C3	250	2	3	994	13.5	8.62	317	0.429	9
6	A2B3C1	250	3	1	995	14	14.3	306	0.500	7
7	A3B1C3	300	1	3	1005	16	15.7	275	0.620	2
8	A3B2C1	300	2	1	1023	15	11.6	324	0.564	5
9	A3B3C2	300	3	2	1034	13	10.3	327	0.530	6

A: Transformation Temperature, B: Transformation Time, C: Austenitizing Temperature

Since the R-sq value was low (63.8%) in the regression analysis, it was decided to determine new gray relational grades by reducing the contribution rate of elongation. A new gray relational analysis was performed with 10% elongation, while the contribution ratios were determined as 30% for tensile strength, hardness and impact energy results. Results are presented in Table 4.19.

Table 4.19 Gray relational grades with 10% elongation and 30% tensile strength, hardness and impact energy contribution.

#	Variables	A	B	C	Tensile	Elong.	Impact	Hardness	Gray Relational Grade	RANK
	ABC	°C	hr	°C	(MPa)	(%)	Joule	HV		
1	A1B1C1	200	2	1	1053	13	10	329	0.625	2
2	A1B2C2	200	2	2	1079	16	9.99	330	0.793	1
3	A1B3C3	200	3	3	993	16.5	13.3	305	0.536	6
4	A2B1C2	250	1	2	1043	13	9.57	321	0.532	7
5	A2B2C3	250	2	3	994	13.5	8.62	317	0.441	9
6	A2B3C1	250	3	1	995	14	14.3	306	0.518	8
7	A3B1C3	300	1	3	1005	16	15.7	275	0.588	3
8	A3B2C1	300	2	1	1023	15	11.6	324	0.569	4
9	A3B3C2	300	3	2	1034	13	10.3	327	0.569	5

A: Transformation Temperature, B: Transformation Time, C: Austenitizing Temperature

As a result of the new analysis, it was determined that the optimum value remained the same as 1, while a small change in the other parameters stood out.

CHAPTER 5

CONCLUSION

In this thesis, heat treatments applied to the existing pearlitic rail steel, which is in mass production and widely used in high-speed train lines to improve mechanical properties the lower bainite and upper bainite microstructures were obtained with isothermal transformations. Mechanical properties of the heat-treated samples were investigated in terms of tensile strength, impact resistance and hardness. Taguchi method used for experimental design to analyze optimum boundary conditions.

This study shows that bainitic rail steels have harder structure and improved mechanical properties than conventional pearlitic steels. Important results have been obtained that shows pearlitic rail can be replaced in the near future by bainitic steels because of its higher strength and toughness values.

Recently, it is expected that bainitic steels, which are one of the most researched topics in the steel industry, will continue to be researched more due to its superior properties such as ultra-high strength, toughness, and elongation. This study which explores understanding the most suitable structure by applying different heat treatment variables and investigates microstructure and mechanical properties, experimentally and statistically. As can be seen in the experimental results, significant improvements in mechanical properties have been achieved compared to conventional rail steels, and these results provide concrete data for future studies to develop the research in different ways. Table 5.1 summarizes the optimum parameters according to Taguchi and Grey relational analysis.

Table 5.1 Optimum parameters for bainitic transformation

Method	Target	Optimum parameters	ANOVA Contribution
Taguchi Analysis	Tensile Strength	A1B2C2	Austenitizing Temperature
	Elongation	A1B3B3	Isothermal Transformation Temperature
	Impact Energy	A3B3C3	Isothermal Transformation Temperature
	Hardness	A1B3C2	Austenitizing Temperature
Gray Relational Analysis	Overall	A1B2C2	

According to the obtained results below conclusions can be drawn:

- The tensile strength value, which was 880 MPa in the standards, was at least 10 percent higher than the standard in all conducted parameters.
- Toughness, which is the main feature of the bainitic structure, increased in all specimens. In standard R260 steel, the impact energy of 4 Joules was improved 2-to 3 times higher.
- Elongation varied between 13-16%.
- Considering that the hardness decreases as the ductility increases, the obtained hardness values are higher than the standards, with an average of 300 HV.

- According to Gray relational analysis, A1B2C2 was determined as the optimum parameter. In Table 5.1, optimum levels according to Taguchi analysis are indicated for each response, ANOVA analysis determined how much the parameters affect the response.
- The highest tensile strength was measured as 1079 MPa in the specimen (A1B2C2) which was austenitized at 850°C and then hold to isothermal transformation at 200°C for 2 hours. The impact energy of the same parameter is 9.99 Joules, and the hardness value is 330 HV. It was determined that the optimum parameter was A1B2C2 levels, with the highest percentage elongation of 16%.

In future studies, the fatigue and wear resistance of this microstructure can be investigated. In addition, how the effect of microstructure on toughness changes with the orientation of bainite sheaves can be examined by electron backscattering. International standards (EN, ISO, JIS, AREMA) have been prepared based on pearlitic steels. With the study, promising results were obtained for the new specifications to be prepared. Further studies can be conducted on the stability of the RA by changing the chemical composition and bainitic transformation cooling rates. Ausforming facilities can be searched for shortening the bainitic isothermal transformation time.

REFERENCES

[1] TCDD Taşımacılık, “TCDD 2018 İstatistik Yıllığı Özeti,” ANKARA, 2018.

[2] C. Bozkurt, “Türkiye ve G8 Ülkelerinin Lojistik Performans Endeksine Göre Karşılaştırılması,” *İşletme ve İktisat Çalışmaları Derg.*, vol. 7, no. 2, pp. 107–117, 2019.

[3] TUBITAK, “Ulusal Bilim ve Teknoloji Politikaları 2003-2023 Strateji Belgesi,” *Tubitak*, vol. 44, no. SUPPL. 1, pp. 2–3, 2010.

[4] İ. Pektaş, “Türkiye’de Raylı Ulaşım Sistemlerinin Gelişimi,” pp. 81–82, 2016.

[5] UTİKAD, “Dünya Demir Ağlarla Örülüyor.” [Online]. Available: https://www.utikad.org.tr/Detay/Sektor-Haberleri/10852/dunya-demir-aglarla-oruluyor. [Accessed: 03-Jan-2021].

[6] H. Koymatçık, “R260 Kalite Rayların Optimum Mantar Sertleştirme Parametrelerinin Belirlenmesi ve Mekanik Özelliklerinin İncelenmesi,” Karabük Üniversitesi, 2012.

[7] Ömer ONAT, “Mantarı Sertleştirilmiş R260 Kalite Rayların Aşınma Özelliklerinin İncelenmesi,” *Karabük Üniversitesi Fen Bilim. Enstitüsü*, vol. 66, no. 3, pp. 37–39, 2012.

[8] E. Standard, “EN 13674-1-Railway Applications,” 2003.

[9] ISO, “ISO 14556:2000-Charpy V-notch pendulum impact test- Instrumented test method,” 2000.

[10] T. Standard, “Turkish Standart TS EN ISO 6892-1,” vol. 1, no. 112, 2010.

[11] A. Ray, “Niobium microalloyed rail steels,” University of Cambridge, 2017.

[12] W. Heller, R. Schweitzer, and L. Weber, “Modern developments in rail steel metallurgy and production,” *Can. Metall. Q.*, vol. 21, no. 1, pp. 3–15, 1982, doi: 10.1179/cmq.1982.21.1.3.

[13] C. E. Pitt, “Wear and microstructure relationships in carbide-free bainitic rail steel,” 1999.

[14] A. S. P. Folgarait, *Technical Steel Research*, no. 7210. 2001.

[15] H. K. D. H. Bhadeshia *et al.*, “Novel Steels for Rails,” pp. 1–7, 2002.

[16] B. Bramfitt and F. Fletcher, “A Perspective on the Manufacture of Modern-Day High-Strength Steel Rail,” *Arema*, pp. 171–193, 2013.

[17] P. Clayton, K. J. Sawley, P. J. Bolton, and G. M. Pell, “Wear Behavior of Bainitic Steels,” *Wear*, vol. 120, no. 1987, pp. 199–220, 1999.

[18] Ö. F. Murathan and V. Kılıçlı, “Nano Beynitik Çelikler,” *J. Polytech.*, vol. 19, no. 2, pp. 115–128, 2016.

[19] Z. Öztürk, “An Investigation of Bainitic Transformation in Low Carbon Alloy and High Carbon Railway Steels,” 2018.

[20] H. Yokoyama and S. Mitao, “High Strength Bainitic Steel Rails for Heavy Haul Railways with Superior Damage Resistance,” 2001.

[21] M. Zhu, G. Xu, M. Zhou, Q. Yuan, J. Tian, and H. Hu, “Effects of tempering on the microstructure and properties of a high-strength bainite rail steel with good toughness,” *Metals (Basel).*, vol. 8, no. 7, 2018, doi: 10.3390/met8070484.

[22] B. Buchmayr, “Critical assessment 22: Bainitic forging steels,” *Mater. Sci. Technol. (United Kingdom)*, vol. 32, no. 6, pp. 517–522, 2016, doi: 10.1080/02670836.2015.1114272.

[23] Q. Liu, X. Zhao, X. Zhang, and H. Wang, “Effect of cooling temperature field on formation of shelf-like bainite in high carbon silicon steel,” *Mater. Sci. Eng. A*, vol. 720, pp. 176–179, 2018, doi: 10.1016/j.msea.2018.02.061.

[24] L. C. Chang, “Bainite Transformation and Novel Bainitic Rail Steels,” University of Cambridge, 1995.

[25] H. Guo, Q. Li, Y. Fan, and X. Feng, “Bainite transformation behavior, microstructural feature and mechanical properties of nanostructured bainitic steel subjected to ausforming with different strain,” *J. Mater. Res. Technol.*, vol. 9, no. 4, pp. 9206–9218, 2020, doi: 10.1016/j.jmrt.2020.06.063.

[26] J. Tian, G. Xu, M. Zhou, and H. Hu, “Refined Bainite Microstructure and Mechanical Properties of a High-Strength Low-Carbon Bainitic Steel Treated by Austempering Below and Above MS,” *Steel Res. Int.*, vol. 89, no. 4, pp. 1–10, 2018, doi: 10.1002/srin.201700469.

[27] K. K. Wang, Z. L. Tan, G. H. Gao, X. L. Gui, and B. Z. Bai, “Effect of retained austenite stability on mechanical properties of bainitic rail steel,” *Adv. Mater. Res.*, vol. 1004–1005, pp. 198–202, 2014, doi: 10.4028/www.scientific.net/AMR.1004-1005.198.

[28] J.J.Kalker, D.F. Cannon, and O. Orringer, *Rail Quality and Maintenance for Modern Railway Operation*, vol. 51, no. 1. 2018.

[29] H. A. Aglan, Z. Y. Liu, M. F. Hassan, and M. Fateh, “Mechanical and fracture behavior of bainitic rail steel,” *J. Mater. Process. Technol.*, vol. 151, no. 1-3 SPEC. ISS., pp. 268–274, 2004, doi: 10.1016/j.jmatprotec.2004.04.073.

[30] F. H. Çakir and O. N. Çelik, “Effect of Isothermal Bainitic Quenching on Rail Steel Impact Strength and Wear Resistance,” *Met. Sci. Heat Treat.*, vol. 59, no. 5–6, pp. 289–293, 2017, doi: 10.1007/s11041-017-0144-7.

[31] M. Y. Tu, C. A. Hsu, W. H. Wang, and Y. F. Hsu, “Comparison of microstructure and mechanical behavior of lower bainite and tempered martensite in JIS SK5 steel,” *Mater. Chem. Phys.*, vol. 107, no. 2–3, pp. 418–425, 2008, doi: 10.1016/j.matchemphys.2007.08.017.

[32] N. J. P.Clayton, R.Devanathan, “A Review of Bainitic Steels For Wheel/Rail Contact,” in *Rail Quality and Maintenance for Modem Railway Operation*, 1993, no. 6, pp. 41–51.

[33] J. Pacyna, “The microstructure and properties of the new bainitic rail steels,” *J. Achiev. Mater. Manuf. Eng.*, vol. 28, no. 1, pp. 19–22, 2008.

[34] D. Kong, Q. Liu, and L. Yuan, “Effect of Austenitizing Temperature on Formation of Hard Bainite,” *Met. Sci. Heat Treat.*, vol. 56, no. 7–8, pp. 444–448, 2014, doi: 10.1007/s11041-014-9779-9.

[35] R. Devanathan and P. Clayton, “Rolling-sliding wear behavior of three bainitic steels,” *Wear*, vol. 151, no. 2, pp. 255–267, 1991, doi: 10.1016/0043-1648(91)90253-Q.

[36] I. Hlavatý, M. Sigmund, L. Krejčí, and P. Mohyla, “The Bainitic Steels for Rails Applications,” *Mater. Eng.*, vol. 16, no. 4, pp. 44–50, 2009.

[37] J. Zhu *et al.*, “Effect of tempering temperature on microstructure and mechanical properties of bainitic railway wheel steel with thermal damage resistance by alloy design,” *Metals (Basel).*, vol. 10, no. 9, pp. 1–13, 2020, doi: 10.3390/met10091221.

[38] K. Wang, Z. Tan, G. Gao, X. Gui, R. D. K. Misra, and B. Bai, “Ultrahigh strength-toughness combination in Bainitic rail steel: The determining role of austenite stability during tempering,” *Mater. Sci. Eng. A*, vol. 662, pp. 162–168, 2016, doi: 10.1016/j.msea.2016.03.043.

[39] J. K. Yates, “Innovation in Rail Steel,” *Science in Parliament*, 1997. [Online]. Available: http://www.phase-trans.msm.cam.ac.uk/parliament.html. [Accessed: 04-Jul-2021].

[40] British Steel, “Bainitic Low Fatigue.” [Online]. Available: https://britishsteel.co.uk/what-we-do/rail/flat-bottomed-vignole-rail/bainitic-low-fatigue-blf/.

[41] H. K. D. H. Bhadesh, “High Performance Bainitic Steels,” 2005.

[42] C. García-Mateo and F. G. Caballero, “The Role of Retained Austenite on Tensile Properties of Steels with Bainitic Microstructures,” *Mater. Trans.*, vol.

46, no. 8, pp. 1839–1846, 2005, doi: 10.2320/matertrans.46.1839.

[43] D. Kong, Q. S. Liu, and Z. J. Dong, “Bainite Growth Behavior at Early Stage of Transformation in a High Carbon Silicon-Containing Steel,” *J. Iron Steel Res. Int.*, vol. 20, no. 3, pp. 45–49, 2013, doi: 10.1016/S1006-706X(13)60068-0.

[44] V. G. Efremenko *et al.*, “Two-body abrasion resistance of high-carbon high-silicon steel: Metastable austenite vs nanostructured bainite,” *Wear*, vol. 418–419, pp. 24–35, 2019, doi: 10.1016/j.wear.2018.11.003.

[45] O. Haiko, P. Kaikkonen, M. Somani, K. Valtonen, and J. Kömi, “Characteristics of Carbide-Free Medium-Carbon Bainitic Steels In High-Stress Abrasive Wear Conditions,” *Wear*, vol. 456–457, p. 203386, 2020, doi: 10.1016/j.wear.2020.203386.

[46] P. J. Bolton and P. Clayton, “Rolling-sliding wear damage in rail and tyre steels,” *Wear*, vol. 93, no. 2, pp. 145–165, Jan. 1984, doi: 10.1016/0043-1648(84)90066-8.

[47] N. Jin and P. Clayton, “Effect of microstructure on rolling/sliding wear of low carbon bainitic steels,” *Wear*, vol. 202, no. 2, pp. 202–207, Jan. 1997, doi: 10.15290/bb.2015.07.16.

[48] P. H. Shipway, S. J. Wood, and A. H. Dent, “The hardness and sliding wear behaviour of a bainitic steel,” vol. 204, 1997.

[49] K. Fang, J. G. Yang, X. S. Liu, K. J. Song, H. Y. Fang, and H. K. D. H. Bhadeshia, “Regeneration technique for welding nanostructured bainite,” *Mater. Des.*, vol. 50, pp. 38–43, 2013, doi: 10.1016/j.matdes.2013.02.019.

[50] N. Tosun, C. Cogun, and G. Tosun, “A study on kerf and material removal rate in wire electrical discharge machining based on Taguchi method,” *J. Mater. Process. Technol.*, vol. 152, no. 3, pp. 316–322, 2004, doi: 10.1016/j.jmatprotec.2004.04.373.

[51] Ö. Hasgül, “Ürün ve Süreçlerin Geliştirilmesinde Deney Tasarımı: Gıda Sektöründe Bir Uygulama,” pp. 42–67.

[52] D. Taylan, “Taguchi Deney Tasarımı Uygulaması,” Süleyman Demirel Üniversitesi, 2009.

[53] M. S. Phadke, *Engineering Using Robust Design*, 10th ed. New Jersey: P T R Prentice-Hall, 1989.

[54] G. Meral, M. Sarikaya, and H. Dilipak, “Delme işlemlerinde kesme parametrelerinin Taguchi yöntemiyle optimizasyonu The optimization of cutting of parameters in drilling processes by Taguchi method,” vol. 27, no. 4, pp. 332–338.

[55] Y. H. Chen, S. C. Tam, W. L. Chen, and H. Y. Zheng, “Application of the Taguchi method in the optimization of laser micro-engraving of photomasks,” *Int. J. Mater. Prod. Technol.*, vol. 11, no. 3–4, pp. 333–344, 1996, doi: 10.1504/IJMPT.1996.036336.

[56] D. C. Montgomery, *Design and Analysis of Experiment*, 7.th. Arizona: John Wiley & Sons.

[57] M. Şirvancı, *Kalite İçin Deney Tasarımı Taguçi Yaklaşımı*. Literatür Yayıncılık, 1997.

[58] F. Işık, “Taguchi Metodu ve Bir Uygulama tez.pdf.” 2000.

[59] S. Tasgetiren, “Kalite İçin Deney Tasarımı,” no. February 2009, 2014.

[60] E. Nas and N. A. Ozbek, “Optimization the Machining Parameters in Turning of Hardened Hot Work Tool Steel Using Cryogenically Treated Tools,” *Surf. Rev. Lett.*, 2019, doi: 10.1142/S0218625X19501774.

[61] E. YILMAZ and F. GÜNGÖR, “Gri İlişkisel Analiz Yöntemine Göre Farklı Sertliklerde Optimum Takım Tutucusunun Belirlenmesi,” in *2. Ulusal Tasarım İmalat ve AnalizK ongresi,* 2010, pp. 1–9.

[62] E. Nas and S. Akıncıoğlu, “Kriyojenik İşlem Görmüş Nikel Esaslı Süper Alaşımın Elektro- Erozyon İşleme Performansı Optimizasyonu Optimization of Cryogenic Treated Nickel-Based Superalloy in Terms of Electro- Erosion Processing Performance,” *Acad. Platf. J. Eng. Sci.*, vol. 7–1, pp. 115–126, 2019, doi: 10.21541/apjes.412042.

[63] P. A. Gadge, A. C. Waghmare, and R. D. Askhedkar, “Optimization by Grey Relational Analysis (GRA) To Determine the Reverse Osmosis Parameter for Distillery Effluent in ZLD Process,” vol. 7, no. 2, pp. 4413–4419, 2017.

[64] G. Krauss, *S T E E L S Processing, Structure, and Performance*, no. June. 2015.

[65] W. D. Callister, “Materials science and engineering: An introduction (2nd edition),” *Mater. Des.*, 1991, doi: 10.1016/0261-3069(91)90101-9.

[66] ASM, *Metallography and Microstructures*, 9th ed. ASM, 2004.

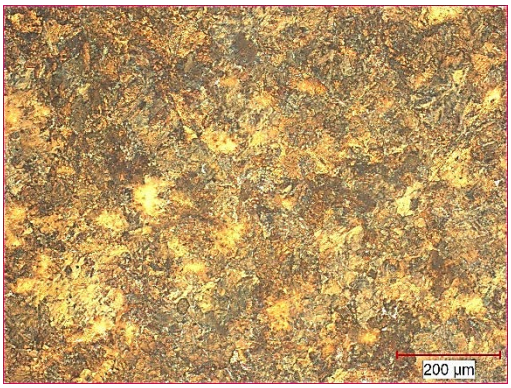
[67] C. García-Mateo and F. G. Caballero, “The role of retained austenite on tensile properties of steels with bainitic microstructures,” *Mater. Trans.*, vol. 46, no. 8, pp. 1839–1846, 2005, doi: 10.2320/matertrans.46.1839.

APPENDICES

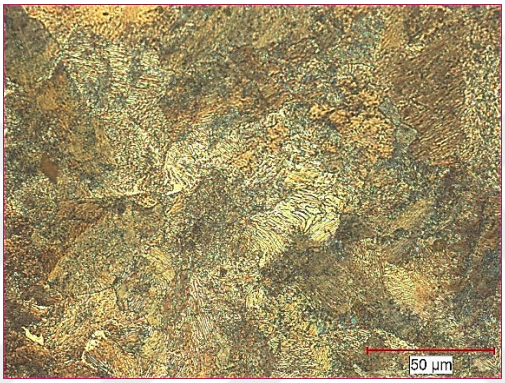
Appendix A: Optical micrographs

Appendix B: Tensile test results

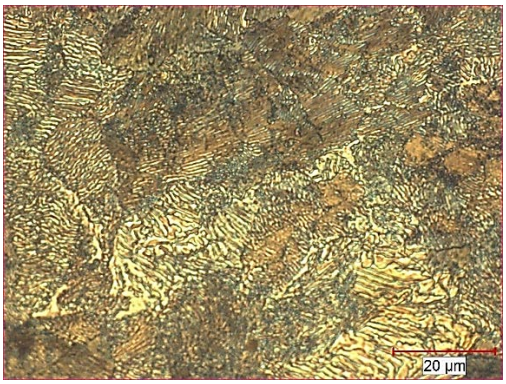
Appendix A: Optical micrographs



(a)



(b)



(c)

Figure A. 1 Conventional R260 rail steel microstructure; (a) 100x, (b) 500x, c) 1000x

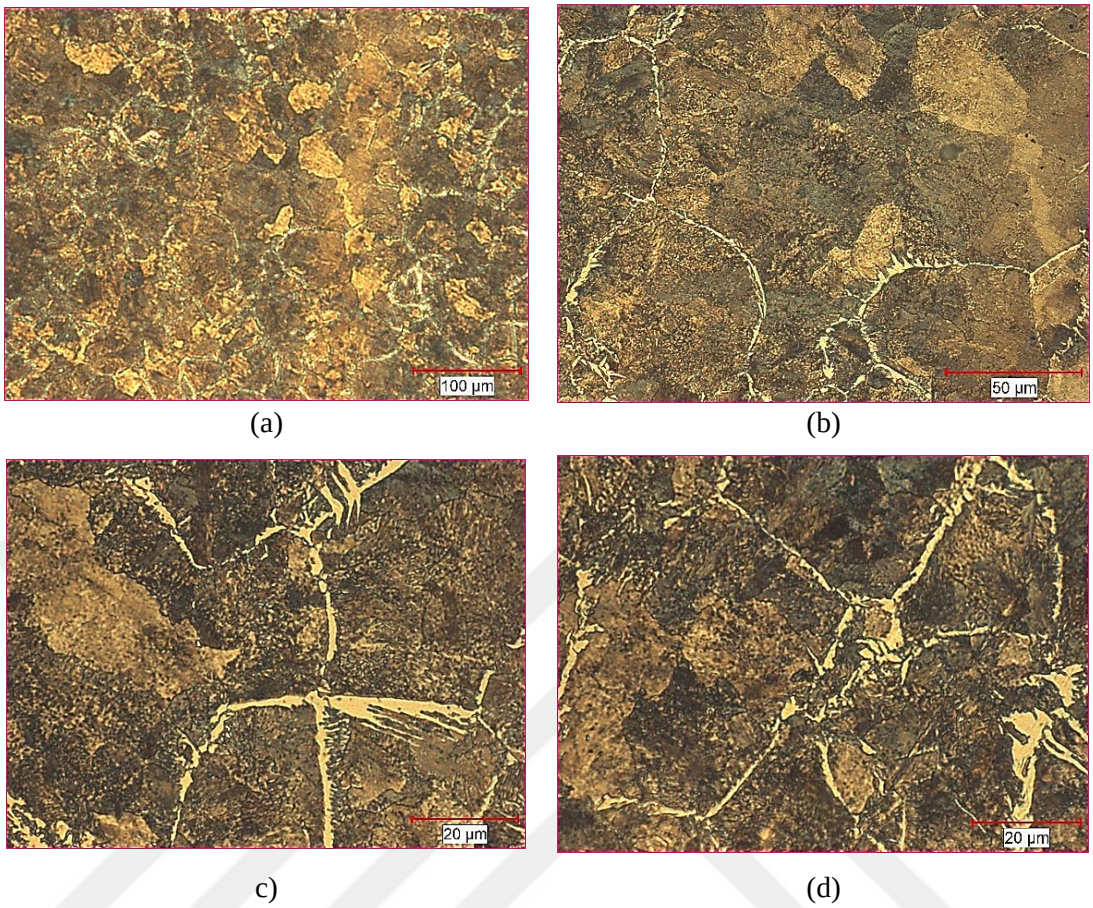


Figure A. 2 Optical microscope images of (1)-A1B1C1 sample; (a) 200x, (b) 500x, c) 1000x-1, (d) 1000x-2

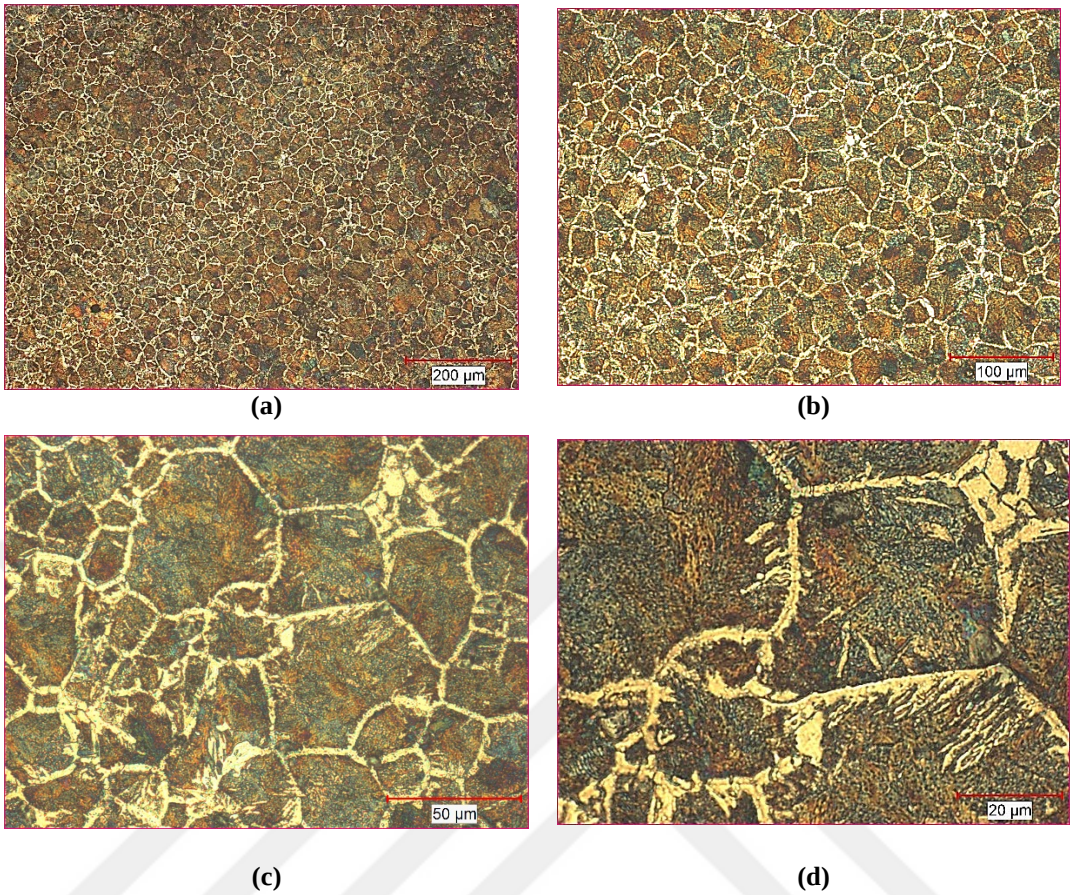


Figure A. 3 Optical microscope images of (2)-A1B2C2 sample; (a) 100x, (b) 200x, (c) 500x, (d) 1000

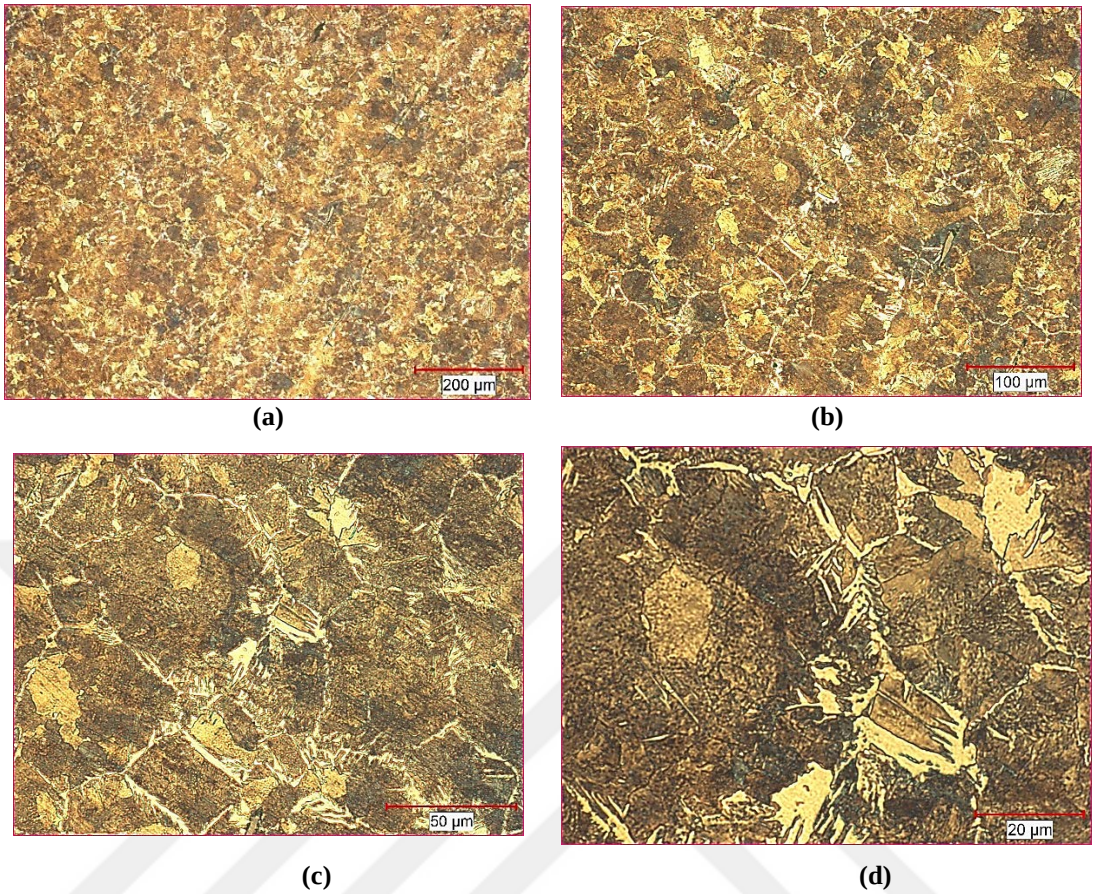
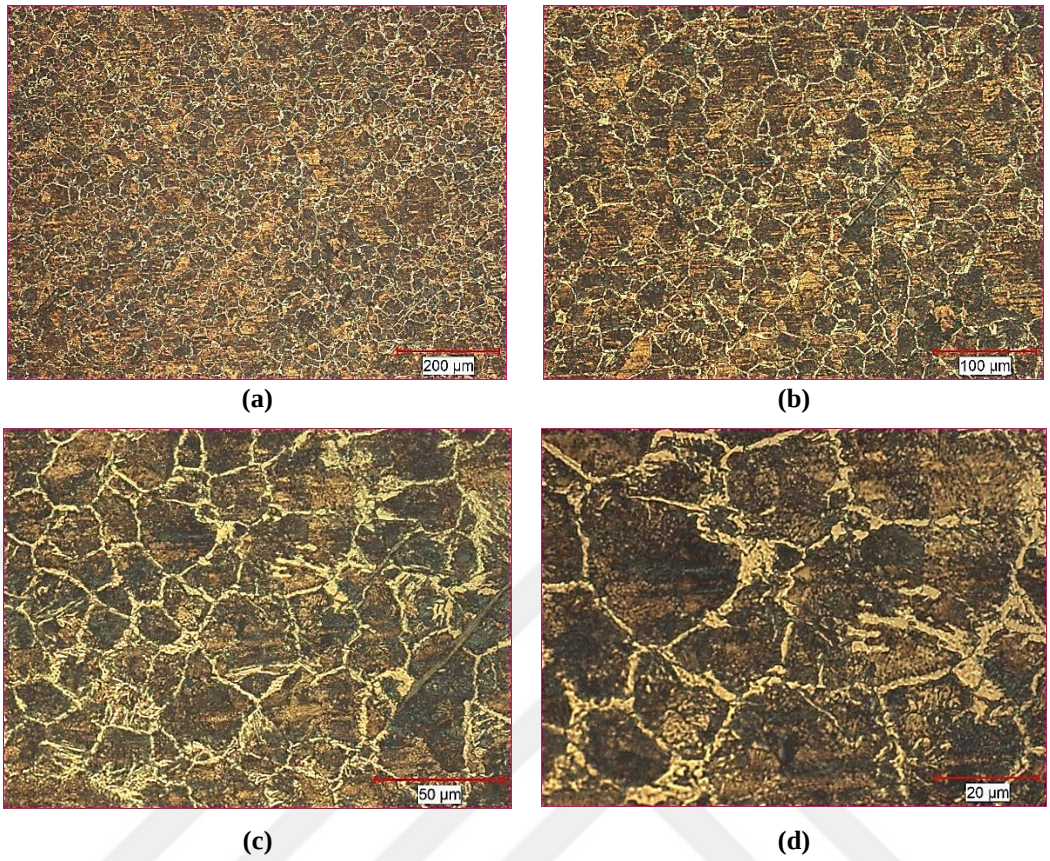


Figure A. 4 Optical microscope images of (3)-A1B3C3 sample; (a) 100x, (b) 200x, (c) 500x, (d) 1000



(a) **(b)**

(c) **(d)**

Figure A. 5 Optical microscope images of (4)-A2B1C2 sample; (a) 100x, (b) 200x, (c) 500x, (d) 1000**x**

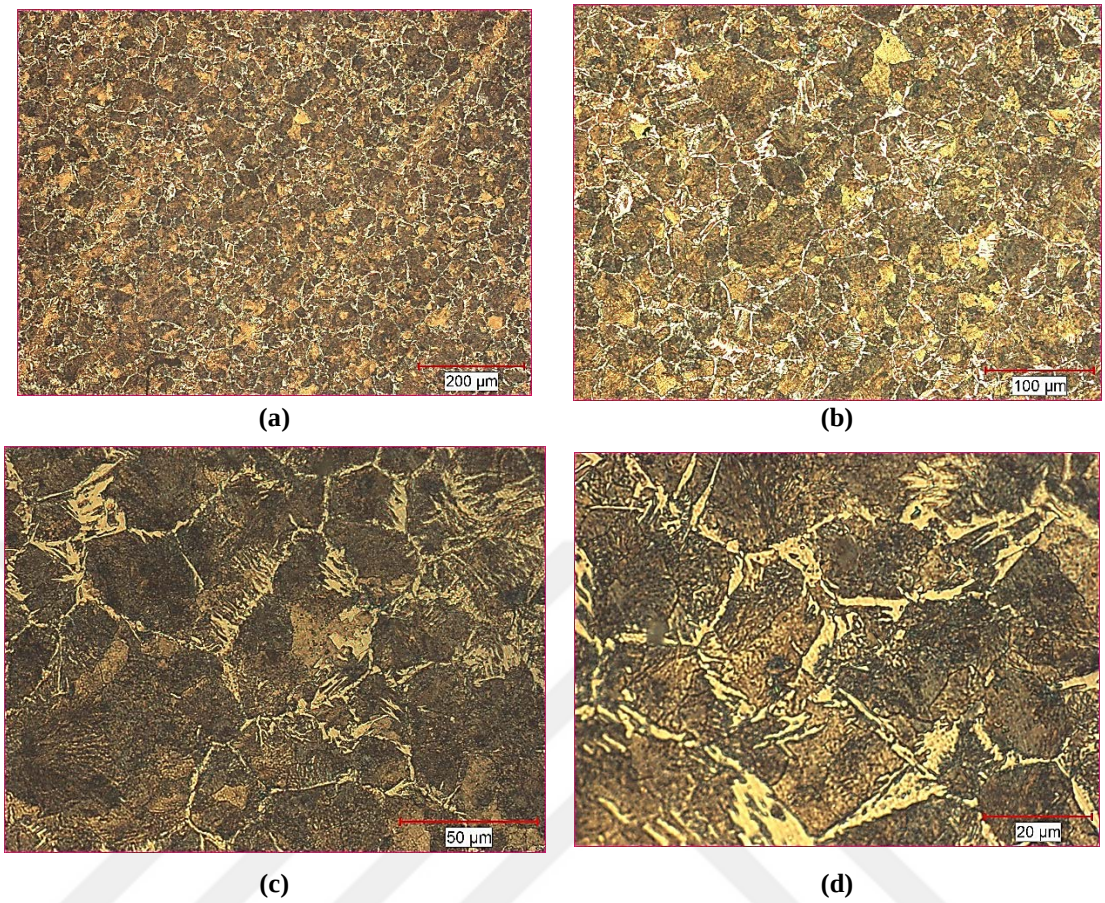


Figure A. 6 Optical microscope images of (5)-A2B2C3 sample; (a) 100x, (b) 200x, (c) 500x, (d) 1000x

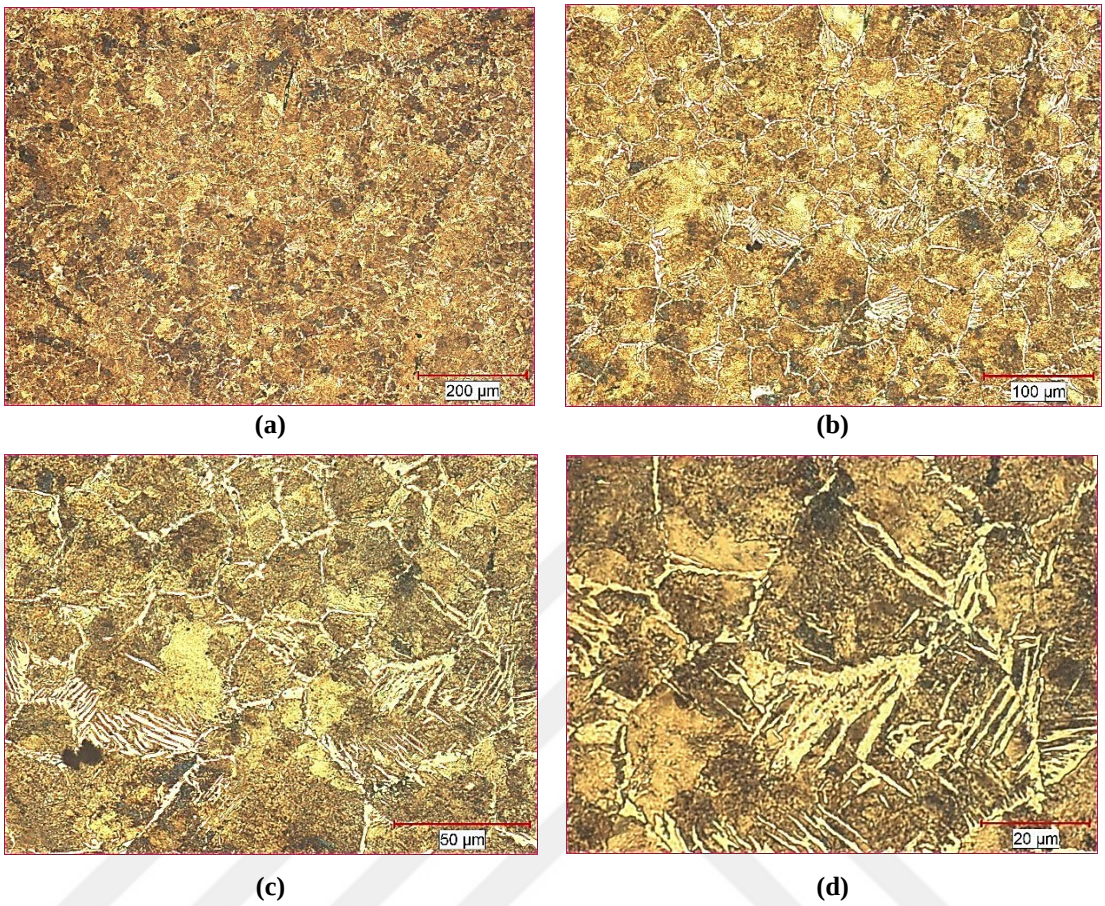


Figure A. 7 Optical microscope images of (6)-A2B3C1 sample; (a) 100x, (b) 200x, (c) 500x, (d) 1000x

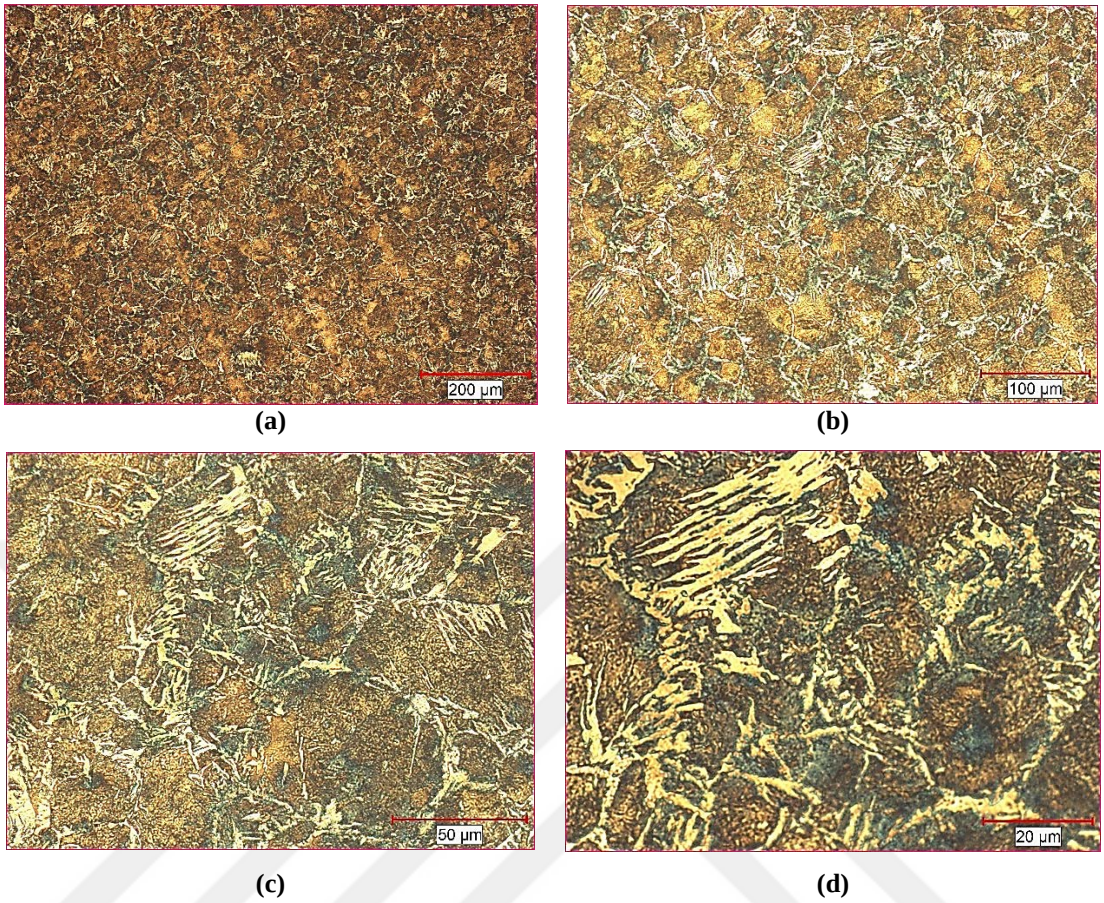
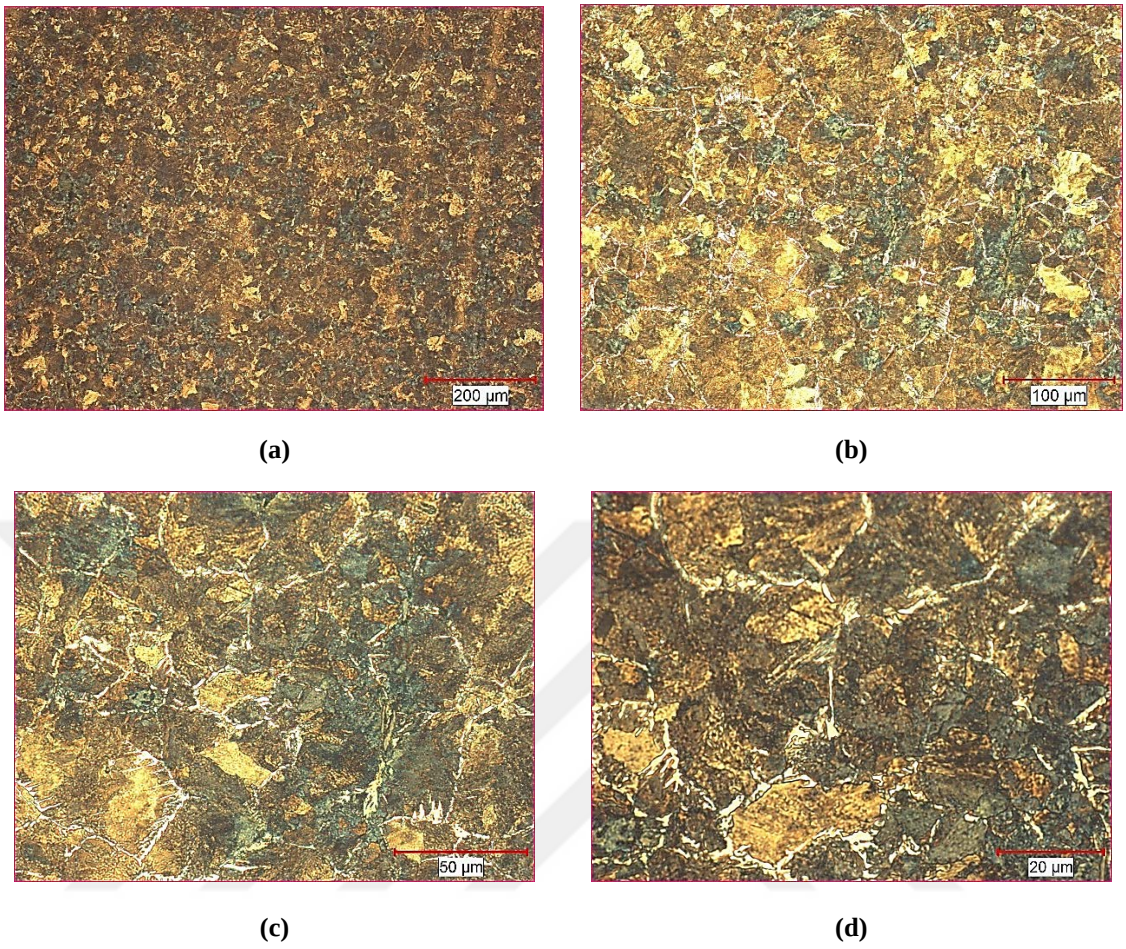


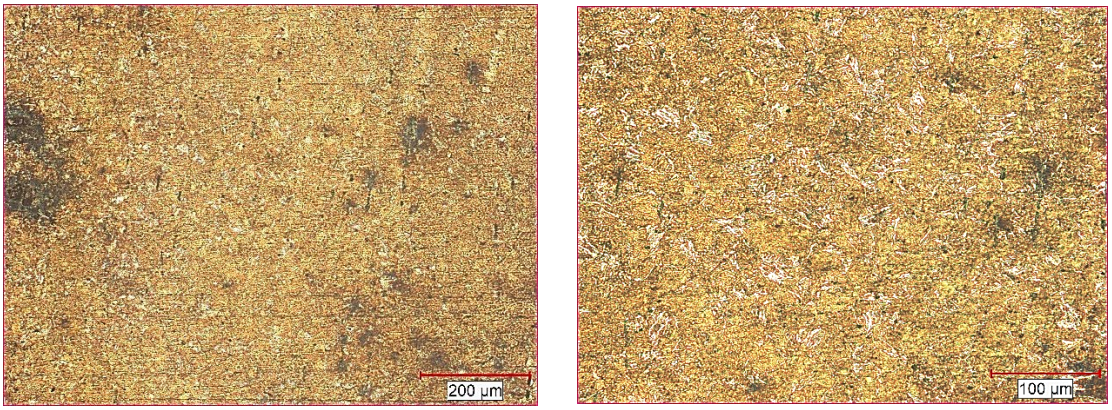
Figure A. 8 Optical microscope images of (7)-A3B1C3 sample; (a) 100x, (b) 200x, (c) 500x, (d) 1000x



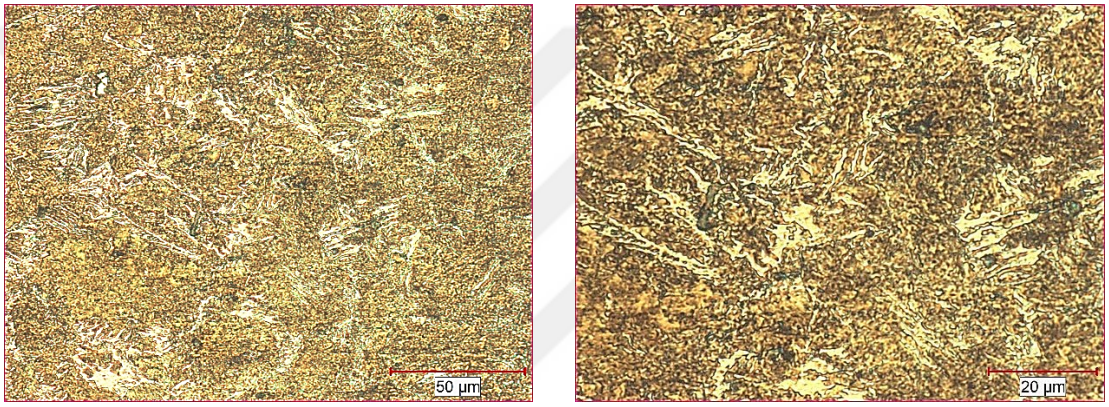
(a) **(b)**

(c) **(d)**

Figure A. 9 Optical microscope images of (8)-A3B2C1 sample; (a) 100x, (b) 200x, (c) 500x, (d) 1000x



(a) **(b)**



(c) **(d)**

Figure A. 10 Optical microscope images of (9)-A3B3C2 sample; (a) 100x, (b) 200x, (c) 500x, (d) 1000x

Appendix B-Tensile test results

MALZEME TEKNOLOJİLERİ MÜDÜRLÜĞÜ

Zwick / Roell

18.06.21

Test report

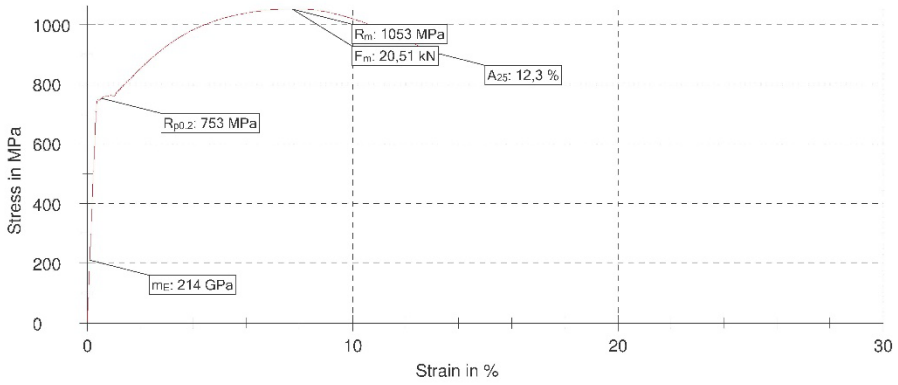
Job no. : 1
Test standard : TS EN ISO 6892-1 (Metod B)
Material : RAY CELIGI
Note :
Machine data : Kullanilan Cihazlar: MT-UST-1,MT-KUM-4,MT-SM-4
Sicaklik: 21,8 °C
Nem: %45,5 RH
Olcülen Numune Capi:4,98 mm

Test speeds	: Method B		Speed, yield point	: 30	MPa/s
Pre-load	: 5	MPa	Speed in the yield range	: 0,00025	1/s
Speed, E-Modulus	: 30	MPa/s	Test speed	: 0,006	1/s

Test results:

No.	m_E GPa	$R_{p0.2}$ MPa	R_{eH} MPa	R_{eL} MPa	R_m MPa	F_m kN	A_{25} %	L_0 mm	S_0 mm²
1	214	753	-	-	1053	20,51	12,3	25,00	19,48

Series graph:



Statistics:

Series n = 1	m_E GPa	$R_{p0.2}$ MPa	R_{eH} MPa	R_{eL} MPa	R_m MPa	F_m kN	A_{25} %	L_0 mm	S_0 mm²
$\bar{x}$	214	753	-	-	1053	20,51	12,3	25,00	19,48
s	-	-	-	-	-	-	-	-	-
v	-	-	-	-	-	-	-	-	-

1.zs2

Page 1/1

Figure B. 1 Tensile test result of A1B1C1

TCDD

MALZEME TEKNOLOJİLERİ MÜDÜRLÜĞÜ

DATEM

Zwick / Roell

18.06.21

Test report

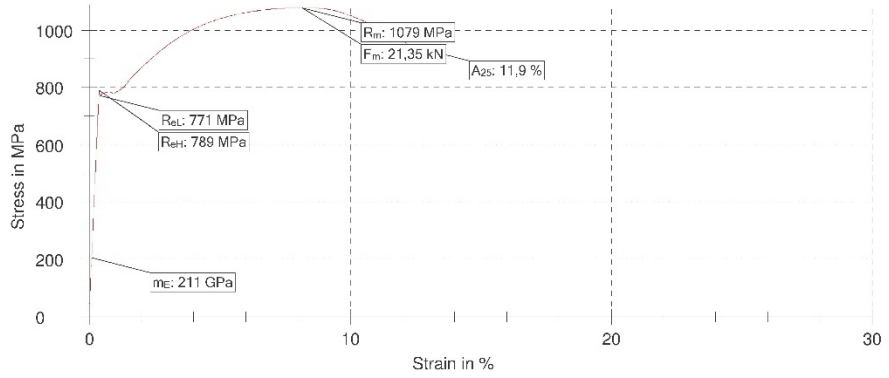
Job no. : 2
Test standard : TS EN ISO 6892-1 (Metod B)
Material : RAY CELIGI
Note :
Machine data : Kullanilan Cihazlar: MT-UST-1,MT-KUM-4,MT-SM-4
Sicaklik: 21,8°C
Nem: %45,5 RH
Olcülen Numune Capi:5,02 mm

Test speeds	: Method B		Speed, yield point	: 30	MPa/s
Pre-load	: 5	MPa	Speed in the yield range	: 0,00025	1/s
Speed, E-Modulus	: 30	MPa/s	Test speed	: 0,006	1/s

Test results:

No.	m_E GPa	$R_{p0.2}$ MPa	R_{eH} MPa	R_{eL} MPa	R_m MPa	F_m kN	A_{25} %	L_0 mm	S_0 mm²
1	211	-	789	771	1079	21,35	11,9	25,00	19,79

Series graph:



Statistics:

Series n = 1	m_E GPa	$R_{p0.2}$ MPa	R_{eH} MPa	R_{eL} MPa	R_m MPa	F_m kN	A_{25} %	L_0 mm	S_0 mm²
$\bar{x}$	211	-	789	771	1079	21,35	11,9	25,00	19,79
s	-	-	-	-	-	-	-	-	-
v	-	-	-	-	-	-	-	-	-

2.zs2

Page 1/1

Figure B. 2 Tensile test result of A1B2C2

MALZEME TEKNOLOJİLERİ MÜDÜRLÜĞÜ

TCDD

DATEM

Zwick / Roell

18.06.21

Test report

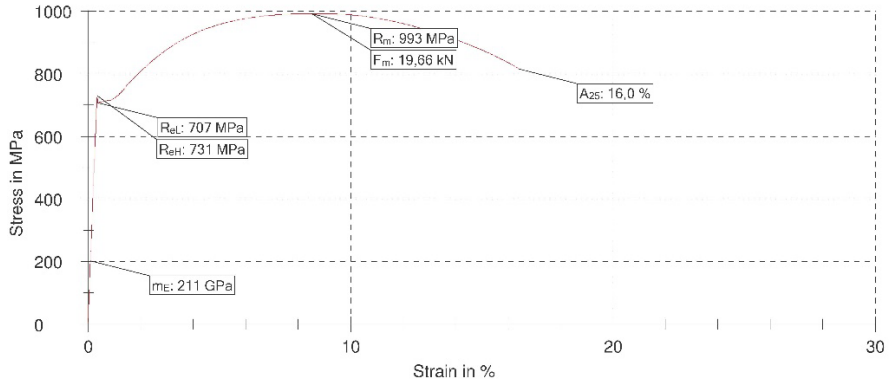
Job no. : 3
Test standard : TS EN ISO 6892-1 (Metod B)
Material : RAY CELIGI
Note :
Machine data : Kullanilan Cihazlar: MT-UST-1,MT-KUM-4,MT-SM-4
Sicaklik: 21,8 °C
Nem: %45,5 RH
Olcülen Numune Capi:5,02 mm

Test speeds	:	Method B		Speed, yield point	:	30	MPa/s
Pre-load	:	5	MPa	Speed in the yield range	:	0,00025	1/s
Speed, E-Modulus	:	30	MPa/s	Test speed	:	0,006	1/s

Test results:

No.	m_E GPa	$R_{p0.2}$ MPa	R_{eH} MPa	R_{eL} MPa	R_m MPa	F_m kN	A_{25} %	L_0 mm	S_0 mm²
1	211	-	731	707	993	19,66	16,0	25,00	19,79

Series graph:



Statistics:

Series n = 1	m_E GPa	$R_{p0.2}$ MPa	R_{eH} MPa	R_{eL} MPa	R_m MPa	F_m kN	A_{25} %	L_0 mm	S_0 mm²
$\bar{x}$	211	-	731	707	993	19,66	16,0	25,00	19,79
s	-	-	-	-	-	-	-	-	-
v	-	-	-	-	-	-	-	-	-

3.zs2

Page 1/1

Figure B. 3 Tensile test result of A1B3C3

MALZEME TEKNOLOJİLERİ MÜDÜRLÜĞÜ

TCDD

DATEM

Zwick / Roell

18.06.21

Test report

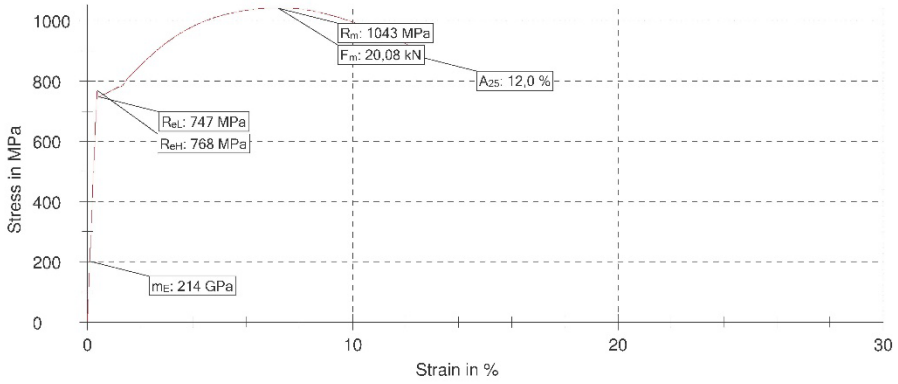
Job no. : 4
Test standard : TS EN ISO 6892-1 (Metod B)
Material : RAY CELIGI
Note :
Machine data : Kullanilan Cihazlar: MT-UST-1,MT-KUM-4,MT-SM-4
Sicaklik: 21,8 °C
Nem: %45,5 RH
Olcülen Numune Capi:4,95 mm

Test speeds	: Method B		Speed, yield point	: 30	MPa/s
Pre-load	: 5	MPa	Speed in the yield range	: 0,00025	1/s
Speed, E-Modulus	: 30	MPa/s	Test speed	: 0,006	1/s

Test results:

No.	m_E GPa	$R_{p0.2}$ MPa	R_{eH} MPa	R_{eL} MPa	R_m MPa	F_m kN	A_{25} %	L_0 mm	S_0 mm²
1	214	-	768	747	1043	20,08	12,0	25,00	19,24

Series graph:



Statistics:

Series n = 1	m_E GPa	$R_{p0.2}$ MPa	R_{eH} MPa	R_{eL} MPa	R_m MPa	F_m kN	A_{25} %	L_0 mm	S_0 mm²
$\bar{x}$	214	-	768	747	1043	20,08	12,0	25,00	19,24
s	-	-	-	-	-	-	-	-	-
V	-	-	-	-	-	-	-	-	-

4.ZP2

Page 1/1

Figure B. 4 Tensile test result of A2B1C2

MALZEME TEKNOLOJİLERİ MÜDÜRLÜĞÜ

TCDD

DATEM

Zwick / Roell

23.06.21

Test report

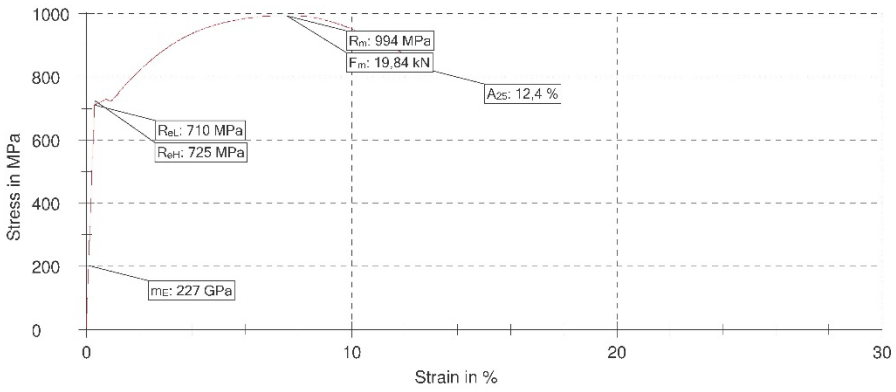
Job no.	:	5
Test standard	:	TS EN ISO 6892-1 (Metod B)
Material	:	RAY CELIGI
Note	:	
Machine data	:	Kullanilan Cihazlar: MT-UST-1,MT-KUM-4,MT-SM-4 Sicaklik: 24,2°C Nem: %42,4 RH Olcülen Numune Capi:5,04 mm

Test speeds	:	Method B		Speed, yield point	: 30	MPa/s
Pre-load	:	5	MPa	Speed in the yield range	: 0,00025	1/s
Speed, E-Modulus	:	30	MPa/s	Test speed	: 0,006	1/s

Test results:

No.	m_E GPa	$R_{p0.2}$ MPa	R_{eH} MPa	R_{eL} MPa	R_m MPa	F_m kN	A_{25} %	L_0 mm	S_0 mm²
1	227	-	725	710	994	19,84	12,4	25,00	19,95

Series graph:



Statistics:

Series n = 1	m_E GPa	$R_{p0.2}$ MPa	R_{eH} MPa	R_{eL} MPa	R_m MPa	F_m kN	A_{25} %	L_0 mm	S_0 mm²
x̄	227	-	725	710	994	19,84	12,4	25,00	19,95
s	-	-	-	-	-	-	-	-	-
v	-	-	-	-	-	-	-	-	-

5.zs2

Page 1/1

Figure B. 5 Tensile test result of A2B2C3

MALZEME TEKNOLOJİLERİ MÜDÜRLÜĞÜ

TCDD

DATEM

Zwick / Roell

23.06.21

Test report

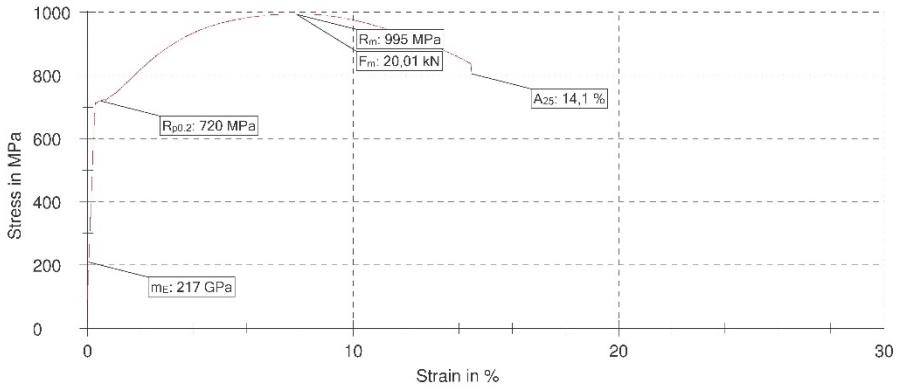
Job no. : 6
Test standard : TS EN ISO 6892-1 (Metod B)
Material : RAY CELIGI
Note :
Machine data : Kullanilan Cihazlar: MT-UST-1,MT-KUM-4,MT-SM-4
Sicaklik: 24,2 °C
Nem: %42,4 RH
Olcülen Numune Capi:5,06 mm

Test speeds	:	Method B		Speed, yield point	:	30	MPa/s
Pre-load	:	5	MPa	Speed in the yield range	:	0,00025	1/s
Speed, E-Modulus	:	30	MPa/s	Test speed	:	0,006	1/s

Test results:

No.	m_E GPa	$R_{p0.2}$ MPa	R_{eH} MPa	R_{eL} MPa	R_m MPa	F_m kN	A_{25} %	L_0 mm	S_0 mm²
1	217	720	-	-	995	20,01	14,1	25,00	20,11

Series graph:



Statistics:

Series n = 1	m_E GPa	$R_{p0.2}$ MPa	R_{eH} MPa	R_{eL} MPa	R_m MPa	F_m kN	A_{25} %	L_0 mm	S_0 mm²
$\bar{x}$	217	720	-	-	995	20,01	14,1	25,00	20,11
s	-	-	-	-	-	-	-	-	-
V	-	-	-	-	-	-	-	-	-

6.zs2

Page 1/1

Figure B. 6 Tensile test result of A2B3C1

MALZEME TEKNOLOJİLERİ MÜDÜRLÜĞÜ

TCDD

DATEM

Zwick / Roell

23.06.21

Test report

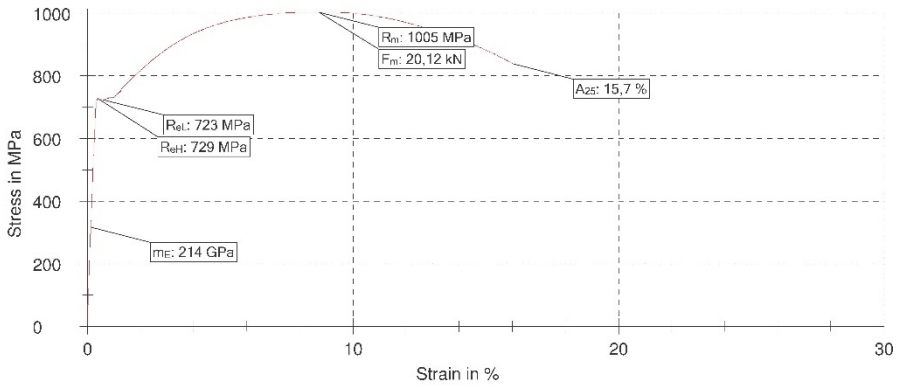
Job no.	:	7
Test standard	:	TS EN ISO 6892-1 (Metod B)
Material	:	RAY CELIGI
Note	:	
Machine data	:	Kullanilan Cihazlar: MT-UST-1,MT-KUM-4,MT-SM-4 Sicaklik: 24,2°C Nem: %42,4 RH Olcülen Numune Capi:5,05 mm

Test speeds	:	Method B		Speed, yield point	:	30	MPa/s
Pre-load	:	5	MPa	Speed in the yield range	:	0,00025	1/s
Speed, E-Modulus	:	30	MPa/s	Test speed	:	0,006	1/s

Test results:

No.	m_E GPa	$R_{p0.2}$ MPa	R_{eH} MPa	R_{eL} MPa	R_m MPa	F_m kN	A_{25} %	L_0 mm	S_0 mm²
1	214	-	729	723	1005	20,12	15,7	25,00	20,03

Series graph:



Statistics:

Series n = 1	m_E GPa	$R_{p0.2}$ MPa	R_{eH} MPa	R_{eL} MPa	R_m MPa	F_m kN	A_{25} %	L_0 mm	S_0 mm²
$\bar{x}$	214	-	729	723	1005	20,12	15,7	25,00	20,03
s	-	-	-	-	-	-	-	-	-
V	-	-	-	-	-	-	-	-	-

7.zs2

Page 1/1

Figure B. 7 Tensile test result of A3B1C3

MALZEME TEKNOLOJİLERİ MÜDÜRLÜĞÜ

TCDD

DATEM

Zwick / Roell

23.06.21

Test report

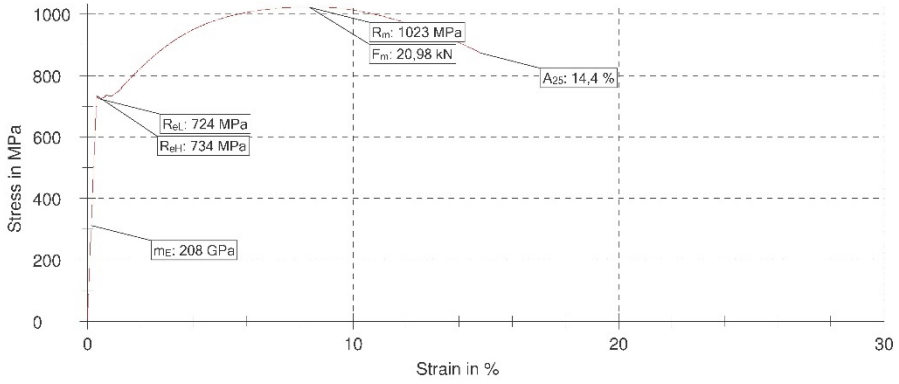
Job no. : 8
Test standard : TS EN ISO 6892-1 (Metod B)
Material : RAY CELIGI
Note :
Machine data : Kullanilan Cihazlar: MT-UST-1,MT-KUM-4,MT-SM-4
Sicaklik: 24,2°C
Nem: %42,4 RH
Olcülen Numune Capi:5,11 mm

Test speeds	: Method B		Speed, yield point	: 30	MPa/s
Pre-load	: 5	MPa	Speed in the yield range	: 0,00025	1/s
Speed, E-Modulus	: 30	MPa/s	Test speed	: 0,006	1/s

Test results:

No.	m_E GPa	$R_{p0.2}$ MPa	R_{eH} MPa	R_{eL} MPa	R_m MPa	F_m kN	A_{25} %	L_0 mm	S_0 mm²
1	208	-	734	724	1023	20,98	14,4	25,00	20,51

Series graph:



Statistics:

Series n = 1	m_E GPa	$R_{p0.2}$ MPa	R_{eH} MPa	R_{eL} MPa	R_m MPa	F_m kN	A_{25} %	L_0 mm	S_0 mm²
$\bar{x}$	208	-	734	724	1023	20,98	14,4	25,00	20,51
s	-	-	-	-	-	-	-	-	-
v	-	-	-	-	-	-	-	-	-

8.zs2

Page 1/1

Figure B. 8 Tensile test result of A3B2C1

MALZEME TEKNOLOJİLERİ MÜDÜRLÜĞÜ

Zwick / Roell

18.06.21

Test report

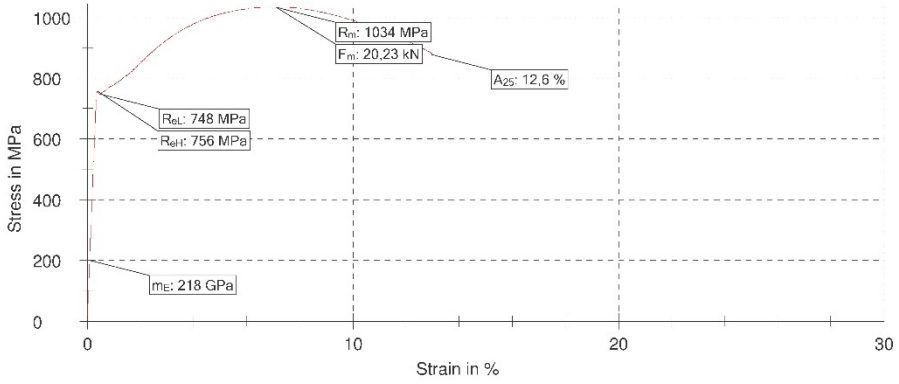
Job no. : 9-1
Test standard : TS EN ISO 6892-1 (Metod B)
Material : RAY CELIGI
Note :
Machine data : Kullanilan Cihazlar: MT-UST-1,MT-KUM-4,MT-SM-4
Sicaklik: 21,8 °C
Nem: %45,5 RH
Olcülen Numune Capi:4,99 mm

Test speeds	: Method B		Speed, yield point	: 30	MPa/s
Pre-load	: 5	MPa	Speed in the yield range	: 0,00025	1/s
Speed, E-Modulus	: 30	MPa/s	Test speed	: 0,006	1/s

Test results:

No.	m_E GPa	$R_{p0.2}$ MPa	R_{eH} MPa	R_{eL} MPa	R_m MPa	F_m kN	A_{25} %	L_0 mm	S_0 mm²
1	218	-	756	748	1034	20,23	12,6	25,00	19,56

Series graph:



Statistics:

Series n = 1	m_E GPa	$R_{p0.2}$ MPa	R_{eH} MPa	R_{eL} MPa	R_m MPa	F_m kN	A_{25} %	L_0 mm	S_0 mm²
$\bar{x}$	218	-	756	748	1034	20,23	12,6	25,00	19,56
s	-	-	-	-	-	-	-	-	-
V	-	-	-	-	-	-	-	-	-

9-1.zs2

Page 1/1

Figure B. 9 Tensile test result of A3B3C2